Exploration and exploitation of the uncommon pH profile of the dynamic covalent interactions between boronic acids and N-acetylneuraminic acids

Peters, Joop A.; Djanashvili, Kristina

DOI
10.1016/j.ccr.2023.215254

Publication date
2023

Document Version
Final published version

Published in
Coordination Chemistry Reviews

Coordination Chemistry Reviews 491 (2023) 215254

Contents lists available at ScienceDirect

Coordination Chemistry Reviews

journal homepage: www.elsevier.com/locate/ccr

Review

Exploration and exploitation of the uncommon pH profile of the dynamic covalent interactions between boronic acids and *N*-acetylneuraminic acids

Joop A. Peters, Kristina Djanashvili

Department of Biotechnology, Delft University of Technology, Van der Maasweg 9, 2629 HZ Delft, The Netherlands

ARTICLE INFO

Keywords:
Boronic acids
Boronic esters
Sialic acids
Drug carriers
Tumor markers
Targeted drug delivery
Targeted tumor therapy

ABSTRACT

In this review, the chemical mechanisms behind the interactions between boronic acids and *N*-acetylneuraminic acids, which have been widely utilized in biomedicine in recent decades, will be examined. It will also be highlighted that the affinity of boronic acids for *N*-acetylneuraminic acids is dependent on pH and is complementary to their affinity for other common monosaccharides found in glycocalyces. Through various examples from the literature, the unique pH profile of the boronic – *N*-acetylneuraminic acids acid interaction and its uses in biomedicine will be illustrated.

1. Introduction

All vertebrate cells are covered by a glycocalyx, a dense layer of glycoproteins and glycolipids, in which the distal parts of the glycans are often terminated by a non-reducing α-linked sialic acid unit [1–3]. Sialic acids (Sias) belong to a family of many differently substituted neuraminic acids. In humans, *N*-acetylneuraminic acid (Neu5Ac) is the most predominant Sia. Its *N*-glycolyl analog (Neu5Gc) is found in most non-human mammals but is absent in normal human cells [4]. From a structural point of view, Neu5Ac is an outlier among the monosaccharides that commonly constitute the polysaccharide chains of the glycocalyx because it has a C_9 rather than a C_5 or C_6 backbone (see Fig. 1) [5]. Since it is the only monosaccharide with an exocyclic glycerol side chain and in addition has an acetamide group, and a negatively charged carboxylate under physiological conditions, it is well suited to function as a target in a myriad of biological processes including cell recognition, cell–cell contact, and structural and protecting effects [6]. The carboxylate groups of terminal Neu5Ac on the glycocalyces of erythrocytes give these a negative zeta potential and thus repulsion between these cells. A decrease in Neu5Ac density during *in vivo* aging has been suggested to trigger their removal from the circulation through phagocytosis [7]. Epithelial surfaces in the eyes, airways, and the gastrointestinal and urogenital tracts are protected by mucins, which are gels composed of highly sialylated glycoproteins.

Diseases are commonly accompanied by alterations in the expression of Sias in glycocalyces. For example, tumor cells often show much higher levels of sialylation than healthy cells due to increased sialyltransferase activity [8–15]. Sia units seem to mask the tumor cells for the immune system [16,17]. An abnormal degree of sialylation of cancerous cells may be associated with aggressiveness and metastatic activity [16–21]. Recently, it was shown that the removal of Neu5Ac in a tumorous environment by an antibody-sialidase conjugate enhances anti-tumor

Abbreviations: APBA, 3-aminomethylphenylboronic acid; ATP, adenosine triphosphate; B-esters, boronic and/or boronate esters; BNCT, boron neutron capture therapy; BODIPY, 4,4-difluoro-4-bora-3a,4a-diaza-*s*-indacene; BPA, 4-Boronophenylalanine; BSA, bovine serum albumin; BzBA, Benzo[*c*][1,2]oxaborol-1(3H)-ol; CAPIR, circulation, accumulation, penetration, internalization, and release; CPT, camptothecin; CRISPR, clustered regularly interspaced short palindromic repeats; DACHPt, dichloro(1,2-diamino-cyclohexane)platinum(II); DFT, density functional theory; DMSO, dimethylsulfoxide; DOX, doxorubicin; EA, D-erythronic acid; EPR, enhanced permeability and retention; FITC, fluorescein isothiocyanate; Fru, D-fructose; Fuc, L-fucose; GA, glycolic acid; Gal, D-galactose; GalA, D-Galacturonic acid; GalNAc, *N*-acetyl-D-galactosamine; Glc, D-glucose; GlcA, D-glucuronic acid; GlcNAc, *N*-acetyl-D-glucose; GSH, glutathione; LAP, laponite; MIP, molecularly imprinted polymer; MRI, magnetic resonance imaging; mRNA, messenger RNA; MW, molecular weight; Neu5Ac, *N*-acetylneuraminic acid; Neu5Gc, *N*-glycolylneuraminic acid; Sia, sialic acid; NIR, near infra-red; NP, nanoparticle; Man, D-mannose; PAPBA, 3-propionamidophenylboronic acid; PBA, phenylboronic acid; PCL, poly(ε-caprolactone); PDA, polydopamine; PDT, photodynamic therapy; pDNA, plasmid DNA; PEG, polyethylene glycol; PEI, polyethyleneimine; PET, positron emission tomography; PicBA, 5-boronopicolinic acid; PGLA, Poly(poly-L-glutamic acid); PTT, photothermal therapy; PTX, paclitaxel; QD, quantum dot; RES, reticuloendothelial system; SERS, surface-enhanced Raman spectroscopy; siRNA, small interfering RNA; SPECT, single-photon emission computerized tomography; VSV, vesicular stomatitis virus; Xyl, D-xylose.

E-mail addresses: j.a.peters@tudelft.nl (J.A. Peters), k.djanashvili@tudelft.nl (K. Djanashvili).

https://doi.org/10.1016/j.ccr.2023.215254
Received 23 March 2023; Accepted 18 May 2023
Available online 2 June 2023

immunity and halts tumor progression in a mouse model [22].

Although Neu5Gc is absent in healthy human cells, high levels of it have been observed in various cancers (ovarian, breast, colon, lung, and prostate) [2,23]. Diseases may also be reflected in abnormal levels of free Neu5Ac in serum, which has been demonstrated for several types of cancer, rheumatoid arthritis, cirrhosis, Crohn's disease, type 2 diabetes, and alcohol abuse [2,21,24–30]. The blood-circulating glycoprotein fetuin also has a terminal Neu5Ac group and abnormal levels of fetuin are indicative of various diseases [31]. Sias probably play an important role in viral infections. For example, mono-sialylated glycolipids have been suggested to facilitate the entry of corona virus 2 (SARS-CoV-2) [32,33].

It can be concluded that both bound and free Neu5Ac are potentially good biomarkers for various diseases and therefore, probes with efficient targeting moieties for Neu5Ac are highly desirable. In nature, immunoglobulin-like lectins (siglecs) are the receptors for sialylated glycans [19,34]. In the human immune system, 13 of these siglecs are found, each differing in selectivity for a distinctive Neu5Ac-containing glycan epitope. The association constants of siglec-Neu5Ac binding are very high, typically log K_{ass}-values in the range 2.5–4 M^{-1} have been reported [35,36]. However, these proteins are less suitable for application as Neu5Ac probes because their availability is limited and modification is difficult. Moreover, their stability *in vivo* is usually poor, and they may exhibit immunogenicity. Synthetic Neu5Ac-receptors may be more appropriate in this respect.

Boronic acids are attractive synthetic lectins because they form reversible covalent esters with carbohydrates and are most likely metabolized in the liver by oxidative de-borylation under formation of boronic acid, which has low toxicity. [37]. Boric acid derivatives are on the rise for pharmaceutical applications. Currently, B-based drugs approved for clinical use are Velcade and Ixazomib (for multiple myeloma), Vaborbactam (an antifungal drug), Tavaborale (an antibacterial drug), and Crisaborole (for psoriasis) (For structures, see Fig. 2) [38,39]. Many other boronic acid derivatives are in clinical trials, including the promising 4-boronophenylalanine for boron neutron-capture therapy (BNCT) [39].

There are many reviews on the interactions of boronic acids and diols and their applications in medicine [19,40–46], but the interactions between boronic acids and α-hydroxycarboxylic acids as in Neu5Ac are usually not discussed, particularly not in a quantitative way. In the present review applications of boronic acids as probes for Neu5Ac, both free and bound in a glycocalyx are discussed with an emphasis on the chemical aspects of the interactions between the functional groups that play a role in the recognition. From fitting of binding data reported during the last decades to the binding model, the stepwise stability constants are estimated and applied to calculate the speciations of the various boronic and boronate esters as a function of the pH. Various possible ways applied to increase the affinity of boronic acids for Neu5Ac and applications of the unique pH profile of boronic acid – Neu5Ac interactions are included.

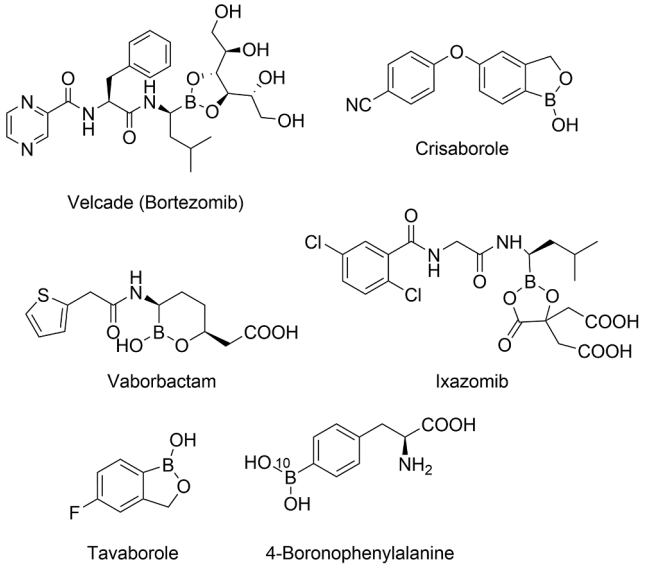

Fig. 2. Chemical structures of clinically applied boronic acid-based therapeutics.

2. The structure of *N*-acetylneuraminic acid

Neu5Ac is a nonulosonic acid, an α-keto sugar acid with a C_9-backbone. An NMR study of the ^{13}C-labeled compound has shown that in an aqueous solution at pH 8, it exists as an equilibrium of the anomeric α- and β-pyranose forms (7.5 and 92.1 %, respectively) and the acyclic keto-forms (0.4 %), see Fig. 3a [47]. At pH < 6, the amount of acyclic anomers slightly increases to 3 % acyclic compounds with decreasing pH, and then in addition to the keto-form, the corresponding enol and hydrated derivatives have been observed. A furanose form is not possible because of the absence of a 5-OH group. The mutarotation rate is slow in D_2O at 298 K and pD 5.4 ($t_{½}$ = 80 min) but very fast at pD 1.3 and 11.7 ($t_{½}$ < 1 min), which indicates that the anomerization is acid- and base-catalyzed [48–50]. The pK_a of the α- and β-pyranose carboxylate function has been determined to be 2.5 and 2.6, respectively. Therefore, the carboxylic acid function is dissociated under physiological conditions.

In glycocalyces, Neu5Ac is usually an exposed end group of a glycan chain, occurring exclusively in the α-pyranose form and commonly connected through an α-glycosidic linkage to either the 3- or the 6-OH of a galactose unit [51]. An α-2,3 glycosidic linkage is for example present in the blood-type tetrasaccharide, sialyl Lewis x (sLe^x), which is an end group of glycoproteins and glycolipids of leukocytes and that is also frequently overexpressed at tumors (see Fig. 3b). It is a common ligand of the three selectins, L-selectin, E-selectin and P-selectin [52]. In polysialic acid (poly-Sia), α-2,8 glycosidic bonds are present between its Neu5Ac units (see Fig. 3c). This highly negatively charged epitope is

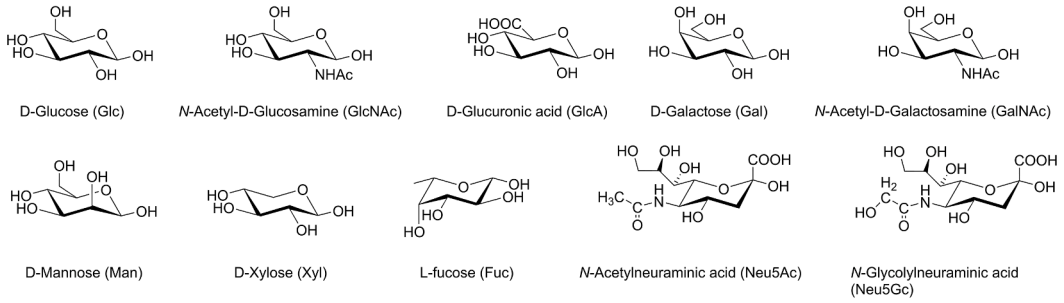

Fig. 1. Monosaccharides occurring in the mammal glycocalyx with their abbreviations.

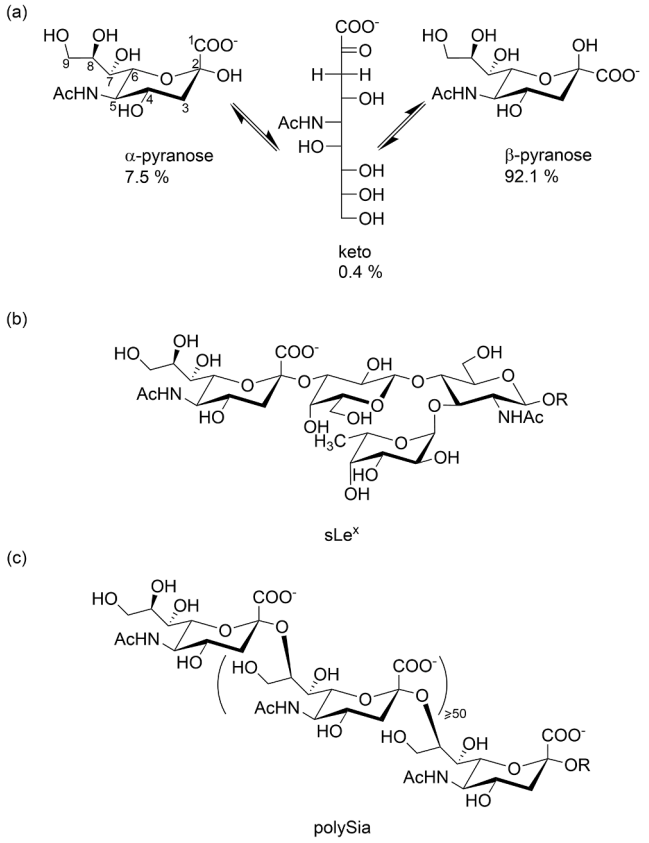

Fig. 3. (a) The anomeric equilibrium of Neu5Ac. (b) The molecular structure of a sLe^x group. (c) The molecular structure of a poly-Sia group. R is a glycoprotein or a glycolipid.

commonly found in the glycocalyces of tumor cells [53].

The negative charge of the carboxylate of Neu5Ac plays a crucial role in the binding to its receptors commonly through a salt bridge between the negatively charged carboxylate and a positively charged arginine unit in the receptor. The OH and amide functions provide various possibilities for H-bridge formation with the receptor and hydrophobic interactions involving the N-CH_3 may reinforce the ligand-receptor binding. This is, for example, illustrated by the crystal structure of a complex between a recombinant fragment of sialoadhesin (a member of the siglec family) and 3′-*N*-acetylneuraminyl-D-lactose, which exhibits

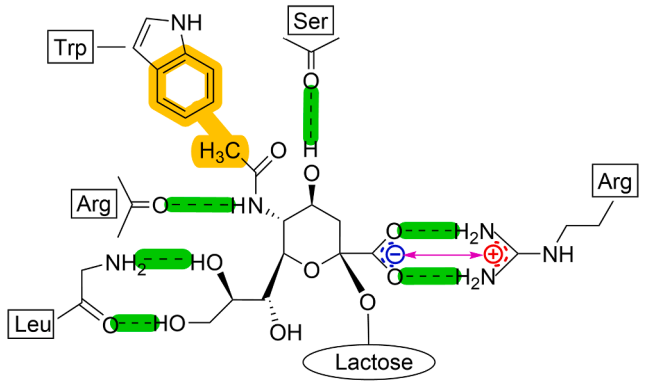

Fig. 4. Schematic representation of the interactions between the Neu5Ac unit of 3′-N-acetylneuraminyl-D-lactose and the N-Terminal Domain of sialoadhesin as observed in the crystal structure. Adapted from ref. [54]. Hydrogen bonds are marked in green, the hydrophobic interaction in orange, and the Coulomb interaction in purple.

each of these modes of interaction (see Fig. 4) [54]. Furthermore, a study of ^{13}C NMR spin–lattice relaxation times has shown that 2-*O*-methyl-Neu5Ac in an aqueous solution is stabilized by various intramolecular H-bonds [55].

3. Interactions between boronic acids and (poly)hydroxy-carboxylic acids

In an aqueous solution, boronic acids and boronates can covalently and reversibly chelate 1,2- or 1,3-diols under the formation of 5- and 6-membered boronic and/or boronate esters, respectively (hereinafter, collectively referred to as B-esters) [46,56]. Boronic esters are neutral species with a planar trigonal sp^2-hybridized B-atom (B^{tri}), whereas boronate esters are negatively charged with a tetrahedral sp^3-hybridized B-atom (B^{tet}), see Fig. 5. The transition from a neutral B^{tri} species to a negatively charged B^{tet} is generally reflected in an increase in hydrophilicity. An α-hydroxycarboxylic acid function contains in its undissociated state also a 1,2-diol function that may form B-esters as well [57]. The possible equilibria involved in the interaction between a boronic acid and a polyhydroxy carboxylic acid (L) are schematically illustrated in Fig. 5. It should be noted that in the presence of endogenous anions such as phosphates and citrate, a more complex situation can arise due to the formation of ternary complexes with the B-esters [45]. These effects will be disregarded in the following discussion. The tetrahedral B-atoms in boronate esters at the carboxylic and diol groups ($B^{tet}L^{ac}$ and $B^{tet}L^{diol}$, respectively) are chiral and therefore, these esters may occur in diastereomeric forms if the ligand in question is chiral as well. For the parent boric acid (Fig. 5, R = OH), an additional set of esters with 1:2 stoichiometry (BL_2) is possible. With compounds having at least three hydroxy functions, boric acids can also form 1:1 esters with the substrate bound in a tridentate fashion, provided that the B-atom can span the respective hydroxy O-atoms [58]. It should be noted that pathways through addition to trigonal boronic acids (B^{tri}) rather than that through substitution of a hydroxyl ion in the tetrahedral boronate anions (B^{tet}) are preferred kinetically [59–62].

Several trends emerge from the reported data on the stability of esters of boronic acids and diols (or polyols) and (poly)hydroxycarboxylates [46]. Generally, the stability constants of esters with phenylboronic acid (R = Ph) are slightly larger than those of 1:1 esters with the parent boric acid (R = OH) [63]. The stabilities of the esters depend on the charge densities at the central B-atom and the same holds for the acidities of the boronic acids. This is nicely demonstrated by linearity in Hammett-type relations for the stability constants of these esters [64]. The electronic properties of both the boronic acid and the diol influence this [65]. Angular strain and steric strain appear also to play a role in determining the stabilities. In the equilibrium between a boronic ester of a 1,2-diol and the corresponding boronate ester (for example, Fig. 5, $B^{tri}L^{diol} \rightleftarrows B^{tet}L^{diol}$), the tension in the 5-membered dioxaborolane ring in the tetrahedral form ($B^{tet}L^{diol}$) is generally lower than in the trigonal form ($B^{tri}L^{diol}$) and therefore the stability of the trigonal compound is usually relatively low, while the opposite is true for esters of 1,3-diols, which have 6-membered dioxaborolane rings.

The stabilities of B-esters of alditols and sugars are also mainly governed by the steric strains induced in the concerning dioxaborolane ring. In other words, the extent of pre-organization for B-ester formation in the constituting diols largely determines the stabilities of the produced esters. In line with this, the following trends in the order of *local* stabilities of borate esters (R = OH) of diol functions in acyclic alditols have been observed: *threo*-1,2 > *erythro*-1,2 and *syn*-1,3 > *anti*-1,3. In saccharides, the order of *local* stabilities is *cis-vic*-diol furanoses ≫ *cis-vic*-diol pyranoses ≫ *trans-vic*-diol pyranoses [57,66–68]. The magnitudes of *local* stabilities of *cis-vic*-diols pyranoses are comparable with those of acyclic *vic*-diols. Boronic esters with high stabilities have been observed for glycolic acid and lactic acid under acidic conditions [57]. Based on these findings, the highest stabilities of B-esters at the common monosaccharide units present in glycocalyces are expected to be the

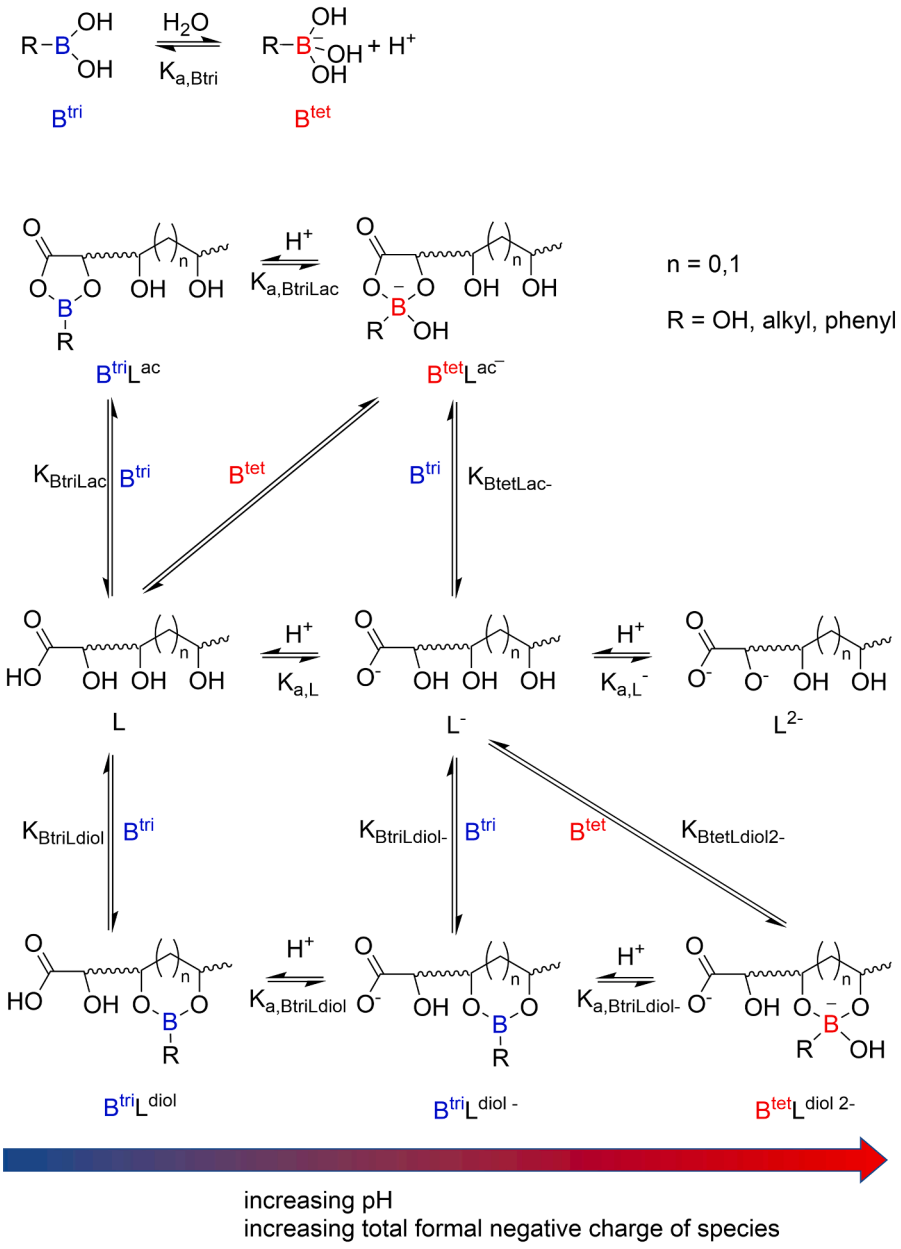

Fig. 5. Possible equilibria in aqueous solutions of a boronic acid and a hydroxycarboxylic acid. The trigonal coordinated B-atoms are in blue and the tetrahedral ones are in red.

exocyclic glycerol tail of Neu5Ac, the 3,4-*cis*-diol groups of Gal, GalNAc, or Fuc, and the 2,3-*cis*-dol group of Man (see Fig. 1). The other monosaccharide units have only *trans-vic*-diol groups, which have much lower affinities for boronic acids. The affinity of free monosaccharides depends on both their anomeric distribution and the above-mentioned orientation of the hydroxyl groups in the various anomers. Generally, the order is Fru > Gal > Man > Glc [66,69].

The overall stability of the complexes between a boronic acid and a hydroxycarboxylic acid at a particular pH can be expressed as the pH-dependent conditional stability constant K_C defined in Eq (1). The abbreviations of the species involved are given in Fig. 5. For a better understanding of the speciation and comparison of stabilities among different ligands, it is more convenient to use pH-independent stepwise stability constants of esters (Eqs (5)–(9). With these stability constants and the pK_a values of the boronic acid and the hydroxycarboxylic acid, the speciation as a function of the pH can be calculated. The second pK_a of the hydroxycarboxylic acid (p$K_{a,L-}$, Eq (4)) is included because, after dissociation of one of the hydroxyl groups, the formation of boronate esters of the resulting dianionic species (L^{2-}) becomes less likely due to the destabilizing anionic repulsion.

$$K_C = \frac{[BL^{tot}]}{[B^{free}][L^{free}]} = \frac{[B^{tri}L^{ac}]+[B^{tet}L^{ac-}]+[B^{tri}L^{diol}]+[B^{tri}L^{diol-}]+[B^{tet}L^{diol2-}]}{([B^{tri}]+[B^{tet}])([L]+[L^-]+[L^{2-}])} \quad (1)$$

$$K_{a,Btri} = \frac{[B^{tet}][H^+]}{[B^{tri}]} \quad (2)$$

$$K_{a,L} = \frac{[L^-][H^+]}{[L]} \quad (3)$$

$$K_{a,L-} = \frac{[L^{2-}][H^+]}{[L^-]} \quad (4)$$

$$K_{\mathrm{BtriLac}} = \frac{[\mathrm{B^{tri}L^{ac}}]}{[\mathrm{B^{tri}}][\mathrm{L}]} \quad (5)$$

$$K_{\mathrm{BtetLac-}} = \frac{[\mathrm{B^{tet}L^{ac-}}]}{[\mathrm{B^{tri}}][\mathrm{L^{-}}]} \quad (6)$$

$$K_{\mathrm{BtriLdiol}} = \frac{[\mathrm{B^{tri}L^{diol}}]}{[\mathrm{B^{tri}}][\mathrm{L}]} \quad (7)$$

$$K_{\mathrm{BtriLdiol-}} = \frac{[\mathrm{B^{tri}L^{diol-}}]}{[\mathrm{B^{tri}}][\mathrm{L^{-}}]} \quad (8)$$

$$K_{\mathrm{BtetLdiol2-}} = \frac{[\mathrm{B^{tet}L^{diol2-}}]}{[\mathrm{B^{tet}}][\mathrm{L^{-}}]} \quad (9)$$

Qualitatively, the speciation as a function of the pH can conveniently be predicted from the charges of the individual species involved: the maximum amount of esters of bor(on)ic acid or bor(on)ate occur at the pH, where the sum of the charges of the free esterifying species is equal to the charge of the B-ester [57]. This rule of thumb has been mathematically substantiated using the concerning equilibrium equations and mass balances [64]. Generally, the order of magnitude of the pK_as is p$K_{a,L}$ < p$K_{a,Btri}$ < p$K_{a,L-}$. Then, three pH regions where the species displayed in Fig. 5 reach their maximum concentrations can be predicted to be (*1*) pH < p$K_{a,L}$: $B^{tri}L^{ac}$ and $B^{tri}L^{diol}$ (B-esters with net charge 0), (*2*) p$K_{a,L}$ < pH < p$K_{a,Btri}$: $B^{tri}L^{diol-}$ and $B^{tet}L^{ac-}$ (B-esters with net charge-1), (*3*) p$K_{a,Btri}$ < pH < p$K_{a,L-}$: $B^{tet}L^{diol\ 2-}$ (B-esters with net charge −2).

It may be noted that the pH regions in which the concentrations of bor(on)ate esters of α-hydroxycarboxyl and *vic*-diol functions are maximal are complementary, the border between these two regions is approximately where the pH is about equal to the pK_a of the bor(on)ic acid concerned (p$K_{a,Btri}$). As a result, B-esters are formed with polyhydroxycarboxylates, including sugar acids, over the whole pH range up to about pH 12, while polyols such as carbohydrates and alditols form in aqueous solution only stable esters at pH values approximately above the pK_a of the bor(on)ic acid (p$K_{a,Btri}$).

Due to the high electrophilicity of trigonal boron, the neutral boronic esters of diol functions ($B^{tri}L^{ac}$, $B^{tri}L^{diol}$, and $B^{tri}L^{diol-}$) are usually not very stable in protic solvents under neutral or basic conditions, they usually hydrolyze rapidly to their tetrahedral conjugated bases. However, in aprotic solvents, these esters are generally stable and can be isolated. For example, the clinically applied Velcade (see Fig. 2) is commercially available in the solid form as the Man ester with a trigonal B-atom ($B^{tri}L^{diol}$).

Another situation arises when the boronic acid or hydroxycarboxylic ligand has additional electron-donating functional groups (such as amino or alcohol groups) that are close enough to interact intramolecularly with the trigonal B-atom to form a dative bond. Such an interaction can convert a trigonal B-atom into a tetrahedral atom without changing the overall charge of the molecule. Those types of interactions exist, for example, in the *o*-(*N*,*N*-dialkylaminomethyl)phenyl and *o*-(hydroxymethyl)phenylboronic acid (which gives BzBA, see Fig. 6) [70]. A detailed study of species occurring in esters of the methylamino

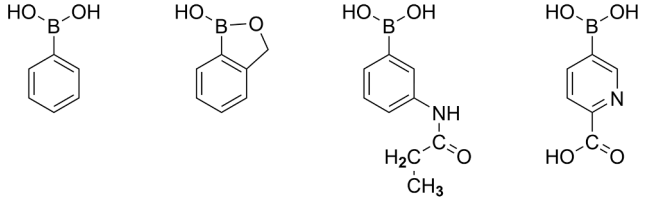

Fig. 6. Molecular structures of boronic acids discussed.

derivatives has shown that in protic solvents also water insertion between the B- and N-atoms can convert a trigonal sp^2 boron into a tetrahedral sp^3 boron [71].

pH-potentiometry cannot discriminate between the individual species $B^{tri}L^{diol-}$ and $B^{tet}L^{ac-}$ in the above-mentioned pH range (*2*), thus at p$K_{a,L}$ < pH < p$K_{a,Btri}$. In those cases, spectroscopic techniques may provide additional details. The ^{11}B NMR chemical shift ranges for tetrahedral and trigonal B nuclei differ significantly [72,73]. The resonances for B^{tet} in bor(on)ate, and bor(on)ate esters with 6-membered boroxolane rings are typically found between 1.2 and 3.5 ppm relative to $BF_3O(C_2H_5)_2$. The B^{tet} nuclei incorporated in 5-membered boroxolane rings of bor(on)ate esters of 1,2-diols typically have chemical shifts around 10 ppm. This probably reflects the relatively large ring strain compared to that of B^{tet} in a 6-membered ring. B^{tri} in bor(on)ic acids usually has chemical shifts of 17–19 ppm. However, B^{tri} in phenylboronic acids (PBAs) has considerably higher chemical shifts (28 ppm), possibly due to the overlap of the B^{tri} sp^2 orbital with the aromatic ring orbitals. Some typical chemical shift ranges are compiled in Table 1. It is noticeable that the exchange between trigonal and tetrahedral B-species often is fast on the NMR time scale when an acid-base equilibrium is involved (rows in Fig. 5) while it is slow when chelation is involved (columns in Fig. 5). It should also be noted that the transverse NMR relaxation is dominated by the quadrupolar mechanism and that consequently, the linewidths of the ^{11}B resonances depend on the rotational correlation time and the electric field gradient asymmetry, which is almost zero for an ideal tetrahedral structure as in $B(OH)_4^-$ and increases strongly when the symmetry deviates from tetrahedral [74]. Consequently, esters with 5-membered boroxolane rings have larger line widths than those with 6-membered ones [67].

4. Interactions between free *N*-acetylneuraminic acids and boronic acids

Each of the anomers of Neu5Ac contains two potential binding sites for bor(on)ates in aqueous media: an α-hydroxycarboxyl group and an exocyclic glycerol chain. The orientation of the latter group is comparable with that of D-erythronic acid (EA). Such an orientation offers bidentate binding capabilities as five-membered boroxolane at the exocyclic *erythro vic*-diol C-7, C-8 and the exocyclic terminal *vic*-diol C-8, C-9. Moreover, binding through a 6-membered ring is possible at the 1,3-diol function C-7, C-9. Each of these diol groups can in principle form both boronic (sp^2 B-atom) and boronate (sp^3 B-atom) esters. In addition, the latter have a chiral B-atom, so that for each functional group two diastereomeric isomers exist. A total of 24 B-esters of Neu5Ac can be considered for the PBA-Neu5Ac system if the acyclic anomer is not taken into account. An ^{11}B and ^{13}C NMR study on 4-vinyl-PBA in DMSO combined with DFT measurements has suggested that the most stable B-esters of this compound are formed with the β-anomer of Neu5Ac [80].

In Fig. 7, the pH profiles of the conditional stability constants (K_C, see Eq, 1) of the B-esters of PBA and Neu5Ac in aqueous solutions as computed from the integrals in ^{11}B NMR spectra [81,82] are compared with those of glycolic acid (GA) and EA. These K_C data and the corresponding ^{11}B NMR chemical shift and integral data were simultaneously fitted to the model displayed in Fig. 5 (Eqs (1)-(9)). The concentrations of the various types of B-esters are assumed to be weighted averages for the anomers and isomers. Good fits were obtained with the best-fit parameters compiled in Table 2. In the ^{11}B NMR spectra (14.1 T), two resonances for B-ester species were observed: one at 7.7 ppm between pH 1.6 and 9.1 and another at 6.2 ppm at pH > 6.3 [82]. These chemical shifts are typical for esters containing tetrahedral B-atoms while resonances for esters with trigonal B-atoms (species $B^{tri}L^{ac}$ and $B^{tri}L^{diol}$) can be expected at 25–40 ppm. At pH > 3, the carboxylic groups are dissociated and thus the concentrations $B^{tri}L^{ac}$ and $B^{tri}L^{diol}$ are expected to be very low. Accordingly, both K_{BtriLac} and $K_{\mathrm{BtriLdiol}}$ were not required to afford a good fit of the data of the B-esters of EA and Neu5Ac.

Table 1
Characteristic ^{11}B chemical shift ranges for selected bor(on)ic and bor(on)ates and their esters with diols in ppm using Et_2O-BF_3 as a reference.[a]

B-compound	B^{tri}	B^{tet}	Ref.
$B(OH)_3$	18.8	1.2	[67]
Esters of $B(OH)_3$ and 1,2-diols	18–18.1[b]	3.9–6.2	[67,75]
Esters of $B(OH)_3$ and 1,3-diols	18.1–18.9[b]	0.2–0.8	[67,75]
Tridentate ester of $B(OH)_3$ and 1,2,3-triols	––	−0.6–0.7	[67]
Esters of $B(OH)_3$ and α-hydroxycarboxylic acids	19.2	6.0–6.9	[57]
$PhB(OH)_2$	28.4–28.8	3.2	[73,75]
Esters of $PhB(OH)_2$ and 1,2-diols	29–34	5.7–6.9	[75–77]
Esters of $PhB(OH)_2$ and 1,3-diols	26–31	1.0–3.2	[75–77]
Esters of $PhB(OH)_3$ and α-hydroxycarboxylic acids	35–36		[75]
Dative N → B in boronic esters		14–16	[71,78]
O → B in boronic 3,6-di-acetamidoPBA		4.1	[79]
O → B in ethylene glycol ester of boronic 3,6-di-acetamidoPBA		8.6	[79]

[a] Chemical shifts reported relative to boric acid were converted by adding 18.8 ppm.
[b] Esters of RO-$B(OH)_2$ where R is an alkyl group.

However, the resonance for the B-esters of GA at pH 2.2 is about 4 ppm downfield relative to the resonances observed at higher pH values (9.0–9.5 ppm). This may be attributed to fast exchange with a very small contribution of $B^{tri}L^{ac}$, which based on literature data is expected to have a chemical shift of about 38.6 ppm [67,73,75]. For the systems of PBA with EA or Neu5Ac, species $B^{tri}L^{diol-}$ and $B^{tet}L^{ac-}$ are both expected to reach their maximum concentration at $pH = 0.5(pK_{a,L} + pK_{a,Btri}) \approx 6.0$ and therefore, discrimination between these two species based on the pH dependency of K_C alone is impossible. Consequently, the fittings gave best fit values for $K_{BtetLac-} + K_{BtriLdiol-}$. But, the ^{11}B chemical shift at pH 6 of the B-esters in each of these systems is in the range 6–8 ppm (see also Fig. 8), which suggests that the values of $K_{BtriLdiol-}$ and hence also the concentrations of $B^{tri}L^{diol-}$ are negligible and that these resonances can be attributed to $B^{tet}L^{ac-}$.

For the B-esters in the system PBA - Neu5Ac, also a single resonance was observed at 7.7 ppm between pH 2 and 6 (see Fig. 8). In this case, an alternative explanation could be that $B^{tri}L^{diol-}$ is converted into a species with a tetrahedral B-atom by a bonding interaction with the *N*-acetyl group (such a species is denoted as B^*L^{diol-} hereafter) as suggested by Otsuka et al. for the PAPBA-Neu5Ac ester [83] (see below). However, this is contradicted by the ^{11}B NMR spectrum of 2-α-O-methyl derivative of Neu5Ac in which the formation of the B-esters at 1,2-position of Neu5Ac ($B^{tri}L^{ac}$ and $B^{tet}L^{ac}$) is blocked. These spectra did not show any resonances for B-esters at $pH < 8$ [81]. Only at $pH > 8$, a resonance at about 9 ppm became visible, which can be assigned to boronate esters at the glycerol tail ($B^{tet}L^{diol2-}$). A very similar result has been reported for the system 4-vinyl-PBA and Neu5Ac in DMSO as the solvent, which also showed an ^{11}B NMR resonance at 8.3 ppm that was not present in the corresponding spectrum with the methyl ester of Neu5Ac where the carboxylate is blocked for B-ester formation [80]. The latter spectrum showed only a resonance for free 4-vinyl-PBA at 28.3 ppm with a very small shoulder at 20 ppm.

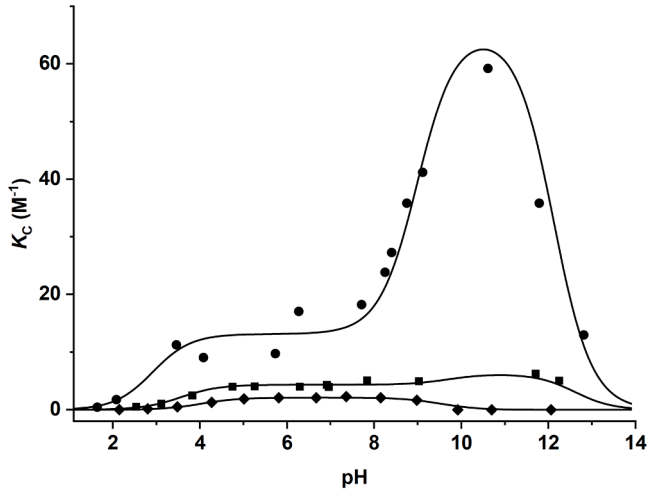

Fig. 7. Comparison of the pH dependence of K_C of PBA-esters of GA (◆), EA (■) in methanol-H_2O (2:1, v/v, 10% D_2O) [81], and of Neu5Ac (●) in H_2O (10% D_2O) as determined from integrals of the resonances in the ^{11}B NMR spectra [82].

The values of K_C of PBA esters of Neu5Ac are considerably higher than those of GA and EA (see Fig. 7), and the stepwise stability constants (Table 2) suggest that both the ester formations at the α-hydroxycarboxylate and the glycerol site contribute. Fig. 8 shows the pH profile of the speciation of the PBA-Neu5Ac system calculated from data obtained by fitting the stepwise stability constants in Table 2 together with the corresponding observed ^{11}B chemical shifts to the model presented in Fig. 5. The signal for ^{11}B NMR B-ester resonance that was observed at $pH > 6.3$ at 6.2 ppm increased in intensity at the expense of the intensity of the resonance at 7.7 ppm (see Fig. 8a and Table 2). The species concerned is dominating at $pH > 9$ and can be attributed to $B^{tet}L^{diol2-}$. Its chemical shift is suggesting that the boronate of this species is bound to a *vic*-diol unit of the glycerol tail of Neu5Ac forming a 5-membered boroxalane ring (compare Table 1). The value of $K_{BtetLdiol2-}$ is much higher than that of other hydroxycarboxylates suggesting that additional stabilizing occurs in this species such as hydrogen bonding(s) or Coulomb interactions.

In the ^1H and ^{13}C NMR spectra of an aqueous sample of PBA and Neu5Ac (59 and 47 mM) at pH 4.7 two sets of 11 resonances were observed, one corresponding to free PBA and the other to the corresponding B-ester ($B^{tet}L^{ac-}$) [82]. Since the tetrahedral B-atom in this ester is chiral two diastereomers can be expected for each anomer of Neu5Ac. Apparently, only one species is present, most likely one of the diastereomers of the β-anomer. However, at high pH, the number of resonances in the spectra increased. For example, at least three N-CH_3 resonances were observed in the ^{13}C NMR spectrum and five in the ^1H NMR spectrum next to the corresponding signals for free Neu5Ac. This indicates that at high pH, the different modes of binding of PBA to the glycerol tail of Neu5Ac coexist in $B^{tet}L^{ac-}$.

Accordingly, resonances for the various possible manners of binding the boronic acids to the glycerol tail of Neu5Ac are all found in the ^{11}B NMR spectrum of a mixture of 2α-O-methyl Neu5Ac and $B(OH)_3$ (1:3 M ratio) in D_2O at pH 11. Two major resonances for the borate esters were observed with chemical shifts at 4.9, and 0.7 ppm and a third minor resonance as a shoulder on the former peak at 5.1 ppm (see Fig. 9). The peaks at 4.9 and 5.1 ppm are typical in the range for a borate group bound to *vic*-diol groups in a bidentate fashion, whereas that at 0.7 ppm is typical for binding of 1,3-diol groups (compare Table 1). From integrals in the deconvoluted spectrum, the corresponding stability constants $K_{BtetLdiol2-}$ were calculated to be 1.2, 4.1, and 2.1 M^{-1} for the peaks at 5.1, 4.9, and 0.7 ppm, respectively. Stepwise stability constants of this order of magnitude are normally found for borate esters of polyol compounds [67]. Molecular modeling with the MM + force field

Table 2
Local stability constants (in M^{-1}), acidity constants, and ^{11}B NMR chemical shifts (in ppm with respect to BF_3OEt_2) of boron species in aqueous mixtures of boronic acids and α-hydroxycarboxylic acids as obtained by fitting the conditional stability constants and ^{11}B NMR chemical shifts as a function of the pH to the model given in Fig. 5.

Boronic acid	PBA	PBA	$B(OH)_3$	PBA	PAPBA	PicBA	PicBA
Ligand	GA	EA	2α-OMe Neu5Ac	Neu5Ac	Neu5Ac	Neu5Ac	Neu5Ac-Me
Solvent	MeOH-H_2O[a]	MeOH-H_2O[a]	D_2O	H_2O[a]	H_2O	H_2O	H_2O
$pK_{a,Btri}$	9.5	9.7	9.0[b]	9.0	8.3[d]	4.2[d]	4.2[b]
$pK_{a,L}$	4.0	3.6	2.5[b]	2.9	2.5[b]	2.5[b]	2.5[b]
$pK_{a,L-}$	13.8[b]	12.6[b]	14.1[b]	12.1	14.1[b]	14.1[b]	14.1[b]
$K_{BtetLac-}$	2.1	4.4[e]	–	13.1	39.7[e]	1.89×10^4	–
$K_{B*Ldiol-}$	–		–[f]			4.5×10^3[c]	4.5×10^3
$K_{BtetLdiol2-}$	–	6.3	1.2, 4.1, 2.1	67.1	18.6	117.0	55.3
$K_{BtriLdiol}$	0.0	0.0	0.0	0.0	0.0	0.0	0.0[b]
δ B^{tri}	28.5	28.6	–[f]	28.5	–[f]	–[f]	–[f]
δ B^{tet}	2.8	3.4	–[f]	2.5	–[f]	–[f]	–[f]
δ $B^{tet}L^{ac-}$	9.0	10.7	–[f]	7.7	–[f]	–[f]	–[f]
δ $B^{tet}L^{diol2-}$	–	8.4	4.6, 5.1, 0.7	6.2	–[f]	–[f]	–[f]
δ $B^{tri}L^{diol-}$	–	30.0[b]	–[f]	–[f]	–[f]	–[f]	–[f]

[a] With 10% D_2O for frequency locking. [b]Fixed value in the fitting. [c]Fixed at the value of the corresponding methyl ester. [d]Determined independently by ^{11}B NMR chemical shifts of free boronic acid in water as a function of the pH [84]. [e]Sum of $K_{BtetLac-}$ and $K_{B*Ldiol-}$. $K_{B*Ldiol-}$ is the borate ester with a tetrahedral B- atom formed by intramolecular interaction of $B^{tri}L^{diol-}$ and an O- or N-atom of Neu5Ac (see text). [f]Not determined.

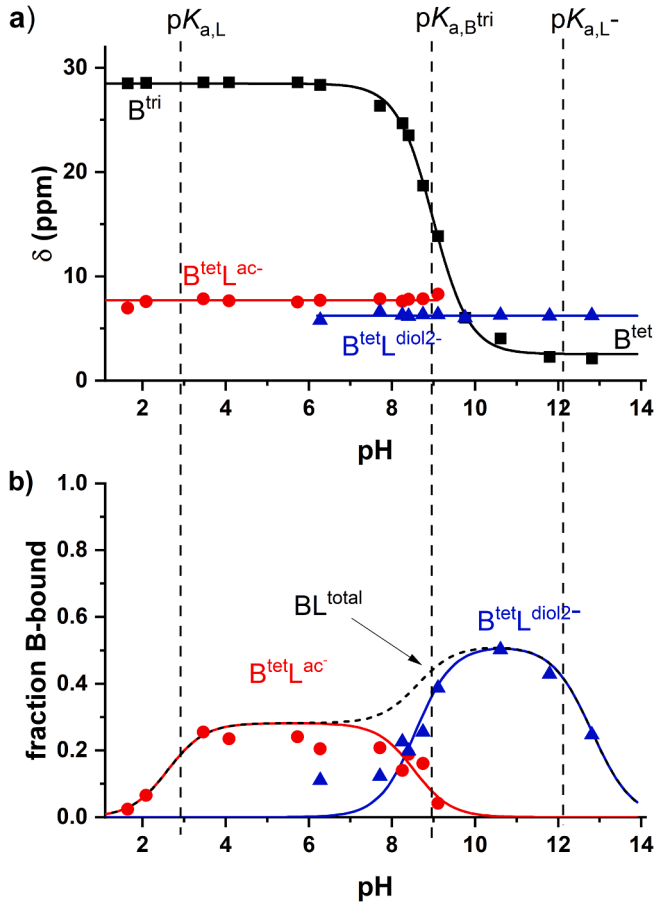

Fig. 8. a)^{11}B NMR chemical shifts of solutions of 0.54 mM PBA and 0.49 mM Neu5Ac in water (10% D_2O). b) Corresponding diagram of the speciation of the B-esters calculated with the parameters given in Table 2.

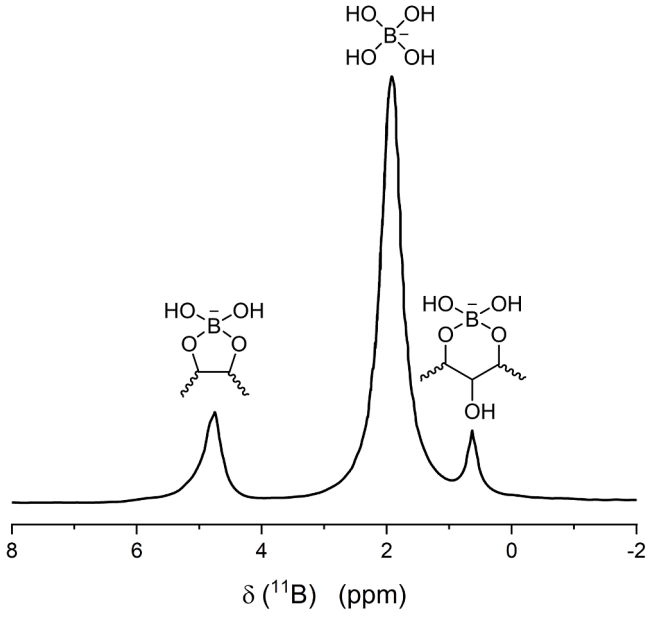

Fig. 9. ^{11}B NMR of a solution of 2α-O-methyl-Neu5Ac (74.8 mM) and H_3BO_3 (0.22 M) in D_2O at pH 11. Redrawn from ref. [81], electronic supporting information. The peak at 4.9 ppm has a small shoulder at 5.1 ppm. The chemical shifts which were reported relative to boric acid were converted into the $BF_3(OEt)_2$ referencing system by adding 18.8 ppm.

suggested that the order of the affinities of the glycerol-binding sites for borate is: C8-C9 > C7-C9 > C7-C8 [81].

Kataoka and coworkers have developed a variety of diagnostic tools and therapeutic agents based on specific Neu5Ac recognition by boronic acids [83–93]. The recognition of Neu5Ac by the 3-propionamido derivative of PBA (PAPBA, see Fig. 6) as a monomeric model for many of these high-molecular-weight systems has been investigated by NMR spectroscopy [83]. The binding sites of Neu5Ac for PAPBA were investigated by ^1H, ^{13}C, ^{11}B, and ^{15}N NMR [83]. In DMSO-d_6 medium, only B-esters of the β-anomer of Neu5Ac were detected. Two isomers were observed, both with minor PAPBA-induced ^1H and ^{13}C NMR shifts of the pyranose ring and relatively large induced shifts in and around the glycerol tail suggesting that in that medium the interaction mainly takes place at the glycerol tail. The amide ^{15}N-resonance of Neu5Ac in the major B-ester species showed an upfield shift of 0.31 ppm, and the ^{11}B resonance of both isomers shifted also upfield from 27.6 ppm to 7.7–8.5 ppm. It was concluded that the PBA binds to C7-C8 (major isomer) and C8-C9 (minor isomer) and that the major B-ester is stabilized by an interaction between the B-atom and the amide function of Neu5Ac [83]. However, the ^{11}B shifts indicate that the B-atoms in both B-esters are tetrahedral (see Table 2) whereas esters of the types $B^{tet}L^{diol-}$ and $B^{tet}L^{diol2-}$ are unlikely in the neutral DMSO medium applied. These

phenomena are reminiscent of the investigations on intramolecular N–B interactions in *o*-aminomethylarylboronic esters system by Anslyn and coworkers in which B-ester species were found with N → B dative bonds and also with water molecules inserted between the N and B-atoms [71,94]. The NMR spectra of Neu5Ac-PAPBA in water as the solvent suggested that similar species occur in DMSO [83]. Fluorescence measurements on the interaction of the conjugate of 3-amino-PBA and a block polymer of PEG and poly-L-glutamic acid with 2-α-*O*-methyl-Neu5Ac showed an increase in K_C from 3.4 to 6.0 M^{-1} with a decrease of the pH from 7.4 to 6.5, also indicating the involvement of $B^{tri}L^{diol-}$ possibly stabilized with a dative bond to a neighboring O- or N-atom (B^*L^{diol}) in this case (see Fig. 10) [90].

More recently, these studies have been extended to a group of 3-pyridylboronic acids (for instance 3-pyridylboronic acid and 5-boronopicolic acid (PicBA). Several members of this series had a much higher affinity for Neu5Ac than PAPBA [84]. Remarkably, the K_C values for the interaction between Neu5Ac with PAPBA or the pyridine derivatives decreased with pH over the range 5–8, while those for PBA with Neu5Ac or the hydroxycarboxylic acids showed the opposite trend (Compare Figs. 7, 11, and 12). Although only a few data points in the pH range 5–8 are available, we fitted these data to Eqs (1)-(9) to provide some insight into the pH-dependent speciation distributions of these systems. The obtained best-fit values of the stepwise stability constants for PicBA/Neu5Ac, and PicBA/Me-ester of Neu5Ac are included in Table 2 and simulated pH dependences of K_C and the species distributions are presented in Fig. 11. Caution is needed with the interpretation of these results because the fittings are based on a few data points over a small pH range. The ^{11}B resonances for the B esters were always found between 2 and 8 ppm over the entire range studied, which indicates that here again exclusively esters with tetrahedral sp^3 B-atoms are observed. The reported value of K_C for the interaction of the methyl ester of Neu5Ac with PicBA is much lower than that of the interaction with the acid Neu5Ac but esters with a tetrahedral B-atom are still present over the whole pH range studied [84]. This indicates that in the system Neu5Ac/PicBA next to $B^{tet}L^{ac-}$ another ester with a tetrahedral B-atom (B^*L^{diol-}) is formed by a dative interaction of $B^{tri}L^{diol-}$ with an N- or O-atom. It may be concluded that in Neu5Ac/PicBA and possibly also in Neu5Ac/PAPBA both $B^{tet}L^{ac-}$ and B^*L^{diol-} are present in significant amounts, whereas in the system Neu5Ac/PBA the amount B^*L^{diol-} seems to be insignificant.

The high K_C values of the B-esters of PAPBA and the pyridine derivatives compared to parent PBA can be attributed to various effects. The local pK_a of the boronic acid function of PAPBA, and the pyridine derivatives are lower than that of PBA [61,84,95], which probably can mainly be explained by the electron-withdrawing effects of the propionamido and pyridine group that increase the positive charge density at the B-atoms of these compounds relative to PBA. This effect is very large for the pyridineboronic acids, in which the N-atom is protonated at physiological pH ($pK_{a,N} \approx 8$) [61,95]. The electron-withdrawing effects will not only lower the pK_a of the boronic acid (B^{tri}), but also those of its boronic esters ($B^{tri}L^{ac}$, $B^{tri}L^{diol}$ and $B^{tri}L^{diol-}$) albeit to a lesser extent. From Eqs (1)-(9) can be deduced that $K_{BtriLdiol-}/K_{BtetLdiol2-} = pK_{a,BtriLdiol2-} - pK_{a,Btri}$. This implies that the electron-withdrawing effects will increase $pK_{a,BtriLdiol2-} - pK_{a,Btri}$ and thus increase the stability of $B^{tri}L^{diol-}$ compared to $B^{tet}L^{diol2-}$. When $B^{tri}L^{diol-}$ can form a dative bond to afford B^*L^{diol-}, this effect will be reinforced.

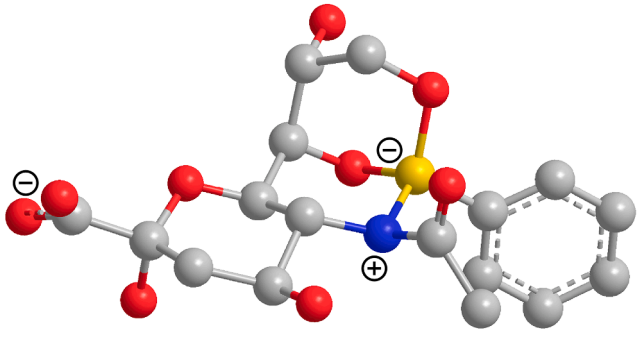

Fig. 10. Molecular model of a B^*L^{diol-} ester of PBA on the 7,9-diol function of Neu5Ac having a dative B-N bond. Since the tetrahedral B-atom is chiral, two diastereomers are possible, the one with an *R*-B-atom is shown. C, gray; O, red; N blue, B, yellow; hydrogen atoms are hidden for clarity.

With the decrease of the pK_a of the boronic acids going from PBA to PAPBA to PicBA the maximum concentration of ($B^{tet}L^{ac-} + B^*L^{diol-}$) shifts to lower pH (see Figs. 8 and 11) [46]. At the same time the ratio $K_{BtriLdiol-}/K_{BtetLdiol2-}$ increases. As a result, the total amount of boric acid bound by Neu5Ac increases relatively steeply as the pH decreases from physiological value to that of the more acidic hypoxic microenvironment of tumors (typically in the range of pH 6.4–7). This behavior is unique for Neu5Ac, the other common saccharides show generally only significant interaction with boronic acids at pH > 9). This gives these boric acid esters potential for targeting tumors in diagnostic and therapeutic applications.

Wellington et al. have reported that the system isoquinoline-4-boronic acid – Neu5Ac in the presence of phosphate at pH 3 has a K_C value that is a factor 65 greater than at pH 7 [96]. Based on the presence of a resonance at 19.8 ppm in the ^{11}B NMR spectrum, these authors suggested that the formation of a ternary complex with phosphate is mediating the high stability. However, it cannot be excluded that this resonance is due to the presence of a B-N dative bond in the B-esters (see Table 2). Unfortunately, no comparison with data for the system in the absence of phosphate was reported.

5. Interactions between boronic acids and *N*-acetylneuraminic acid end groups in glycocalyces

From Figs. 7 and 8, it can be concluded that boronic acids producing high concentrations of $B^{tet}L^{ac-} + B^*L^{diol-}$ in the presence of free Neu5Ac around physiological pH are favorable if high sensitivity is desired. Fortunately, the maximum concentration of these species is reached at $pH = 0.5(pK_{a,L} + pK_{a,Btri})$, which is generally at pH < 7. Since the intratumoral pH often is slightly acidic (pH 6.7–7.1) [97], the B-esters may reach their maximal concentration in the vicinity of tumors. However, the anomeric hydroxyl group of Neu5Ac on cell surfaces is always connected to a D-galactose or another monosaccharide and therefore the hydroxy carboxylate group is not available for B-ester formation, only the glycerol tail (forming B^*L^{diol-}) remains available for that purpose. The affinity of boric acids for glycerol is rather low and comparable with that for other diol groups on monosaccharides [63,67], particularly at physiological pH. Moreover, Neu5Ac in a glycocalyx is fixed into the α-anomeric pyranose form, which is less favorable than the β-anomer for B-ester formation [80].

Compounds with a blocked hydroxycarboxylate, 2-α-OMe-Neu5Ac [81] and the Me-ester of Neu5Ac [43], have been used as low-molecular-weight (low-MW) models to study the interactions with PBA and PicBA, respectively (see above). Although these Neu5Ac derivatives only have the exocyclic glycerol chain available for B-ester formation, they have still a considerable affinity for boronic esters, particularly at pH < 7, see Table 2 and Fig. 11. Generally, polyhydroxy compounds such as glycerol have almost no affinity for boric acids at low pH, underscoring the importance of stabilization of $B^{tri}L^{diol}$ esters by interaction with the 5-NHAc function to form tetrahedral esters (B^*L^{diol}) of Neu5Ac in glycocalyces. This is confirmed by many examples of B-ester formation on cell surfaces with Neu5Ac-terminated glycocalyces. The pH dependence of the affinity of PBA-Neu5Ac has also been demonstrated on a submicrometer resolution by atomic force microscopy (AFM) of the blood-circulating glycoproteins fetuin and asialofetuin using a cantilever installed with PBA through PEG-linkers [98]. The force curves revealed that the strength of interaction depends on the amount of (bound) Neu5Ac in the substrate and increased with decreasing pH

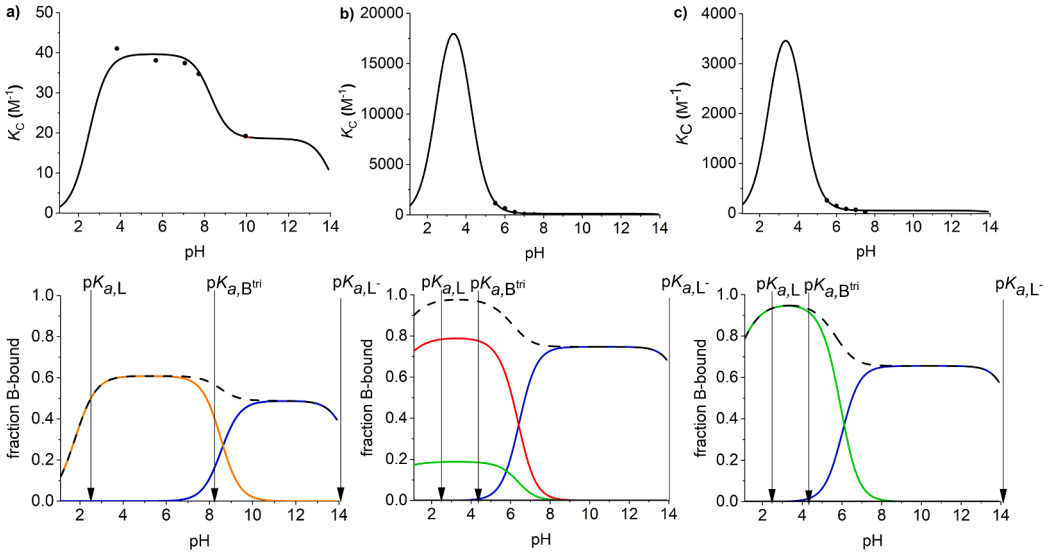

Fig. 11. Simulations of K_C (top) and speciation distributions (bottom) as a function of the pH for mixtures of a boronic acid (0.1 M) and either Neu5Ac or its methyl ester (0.1 M) in D_2O using the parameters given in Table 2. The dots are the experimental data from ref. [84]. Orange curve: $B^{tet}L^{ac-} + B^*L^{diol-}$, Red curve: $B^{tet}L^{ac-}$, green curve: B^*L^{diol-}, blue curve: $B^{tet}L^{diol2-}$, dashed black curve: total of BL-esters. (a) PAPBA/Neu5Ac. (b) PicBA/Neu5Ac. (c) PicBA/Neu5Ac-methyl ester.

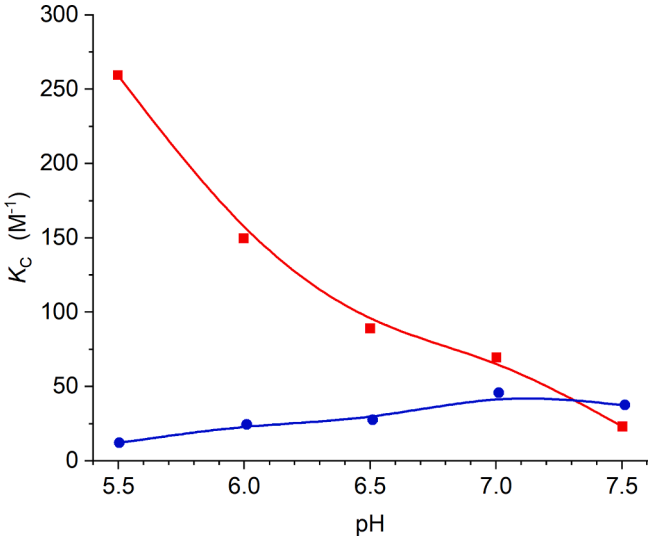

Fig. 12. Conditional stability constants K_C of PicBA-esters of Neu5Ac (■) and Glc (●) as a function of the pH. Experimental data from [84]. The curves are guides to the eye.

between 7.4 and 5.5. This technique allowed the mapping of Neu5Ac on the surface of MCF7 and NHDF cell lines.

6. Competition to B-ester formation of *N*-acetylneuraminic acids by other endogenous compounds

As mentioned above, relatively high stabilities of B-esters at monosaccharide units other than Neu5Ac may be expected at the 3,4-*cis*-diol groups of Gal, GalNAc, or Fuc, and the 2,3-*cis*-diol group of Man (see Fig. 1). The other monosaccharide units have only trans *vic*-diol groups, which have much lower affinities for boronic acids. Due to a stabilizing effect through its 5-N-Ac function, Neu5Ac is the only monosaccharide unit that shows optimal binding affinity at physiological pH. All other monosaccharides only form significant amounts of B-esters under basic conditions (at pH > $pK_{a,Btri}$).

However, in the blood and serum of healthy humans, the total amount of Neu5Ac (free and bound) is 1.58–2.22 mmol L^{-1} and free Neu5Ac is only 0.5–3 μmol L^{-1} [28]. Free Glc, glucosamine, and Fru are dominant sugars with concentrations of 3.3–5.6 mmol L^{-1} (serum after fasting), 4.2–6.2 mmol L^{-1} (serum, plasma), and 0.03–0.3 mmol L^{-1} (whole blood) [99], respectively, and can therefore compete with Neu5Ac (free or in a glycocalyx) for binding to boronic acids. The free monosaccharides all have furanose anomers, which are well-preorganized for B-ester formation. Fortunately, these monosaccharides form almost exclusively $B^{tet}L^{diol}$ esters with a maximal concentration at pH = 0.5($pK_{a,Btri}$ + $pK_{a,Ldiol}$), which is usually at pH > 8. Therefore, the concentrations of their B-esters are relatively low at physiological pH compared to those of Neu5Ac. Table 3 compares the conditional stability constants (K_Cs) of the B-esters of some monosaccharides under physiological conditions. The K_Cs of B-esters of Neu5Ac increase with decreasing pH, whereas those of other monosaccharides show the opposite trend. Fig. 12 illustrates that for the interaction of PicBA with Neu5Ac and glucose [84]. The same trend in the pH-dependent interaction of PicBA has also been observed with pancreatic epithelioid carcinoma cells (PANC 1); when pH was decreased from 7.4 to 6.5, the labeling of the cells with PicBA increased significantly [84].

These special pH effects were exploited, for example, in the design of an HPLC column consisting of silica conjugated with PicBA via a PEG linker [106]. At pH 7.5, Glc and Man had long retention times while Neu5Ac was immediately eluted. At pH 5.0, the reverse occurred:

Table 3
Conditional stability constants (in M^{-1}) of the esters of some PBA derivatives with Neu5Ac and Glc.

	solvent	pH	Neu5Ac	Glc	ref.
PBA	H_2O	7.4	21	4.6	[100]
PAPBA	H_2O	7.4	37.6	5.1	[83]
BzPA	H_2O	7.4	160	21	[101]
2d[a]	H_2O	7.4	50.4	15.9	[102]
2e[a]	H_2O	7.4	3.3	1.7	[102]
11[b]	H_2O-CH_3OH (1:2)	8	200	<10	[103]
12b[b]	H_2O	7.4	151	12.3	[104]
14[b]	H_2O	7.4	135	31	[105]

[a] The structures of compounds **2d** and **2e** are given in Fig. 13. The two boronic functions present in the B-esters were regarded as independent and the K_C value is based on mol boronic acid.
[b] The structures of compounds **11**–**14** are given in Fig. 16.

Neu5Ac was retained and Man and Glc eluted immediately. Similar behavior was observed with polysaccharides and glycoproteins.

It should be noted that the above reasoning considers the thermodynamically controlled situation. B-ester formation is usually very fast, it takes only a few minutes. However, the conversion of one sugar anomer to another can be very slow and could kinetically control B-ester formation [40,105,107]. Therefore, the formation of highly stable B-esters of the furanose anomers probably does not play a significant role *in vivo*. Nevertheless, with the large excess of weakly binding sugars in the blood, it is surprising that PBA derivatives are successful in reaching tumors and labeling them, as has been shown in several *in vivo* studies [108]. In fact, the PBA derivatives can be temporarily protected by B-ester formation with Glc (possibly in the pyranose form). As outlined by Deshayes et al., the concentration of Glc in tumors decreases due to the enhanced metabolism, and concomitantly the pH decreases [90]. The lower pH leads to a decrease in the K_C for the B-ester of Glc and an increase for that of Neu5Ac. Moreover, the amount of Neu5Ac in for example B16F10 melanoma is 1100 nmol/10^9 cells, which is significantly more than in erythrocytes (20 nmol/10^9 cells). Consequently, "*trans*-B-esterification" of the PBA-Glc B-esters into PBA-Neu5Ac B-esters can be expected to take place in the intra-tumoral space.

Ribose is perfectly preorganized for B-ester formation. Accordingly, it has a very high affinity to PBA. Although the highest affinity may be expected at pH > 9, its K_C at pH 7.4 is still high (21 M^{-1}) and comparable with that of Neu5Ac [100]. The ribonucleotide adenosine triphosphate (ATP) has a very low extracellular concentration (1–10 nM), but the intracellular concentration is orders of magnitude higher (5–10 mM) and the extracellular concentration in tumor tissue may also be elevated [109–111]. Therefore, ATP can compete with Neu5Ac for B-ester formation inside cells and perhaps also in tumorous tissue.

The competition of Glc, Fru, and other compounds with diol moieties that are well-preorganized for B-ester formation can be exploited in *trans* B-esterifications to release Neu5Ac. Thus, Fru by competition reduces the labeling capacity of Neu5Ac on the surface of vesicular stomatitis virus (VSV) by quantum dots (QDs) with attached PBA targeting groups. Consequently, Fru can be applied to release the free virus from this VSV-QD adduct [112]. The difference in pH dependence of K_C for B-esterification of PBA between Neu5Ac and Glc has been exploited in the construction of a dual pH/Glc sensitive cell-capturing system for Neu5Ac-overexpressing cells by attaching poly(acrylamidophenylboronic acid) to aligned silicon nanowires [113] and by the incorporation of PBA groups into an oxime-based PEG hydrogel [114]. In the absence of Glc at pH 6.8, Neu5Ac over-expressing cancer cells were effectively bound and at pH 7.8 and in the presence of 70 mM Glc they were almost completely released. The cycle of switching between binding and release was reproducible at least 5 times, while the cells remained their viability.

7. Increasing the affinity and selectivity of boronic probes for *N*-accetylneuraminic acids

The binding constants of PBA-esters of Neu5Ac (see section 4) are very low compared to lectin–oligosaccharide binding, which typically has binding constants of 10^3-10^4 M^{-1} [115]. Therefore, higher binding constants are especially desirable for synthetic probes for biomedical applications in therapies and diagnosis where Neu5Ac is used as a biomarker for disease.

7.1. Electronic effects on the affinity of the boronic group for N-neuraminic acids

The primary binding of synthetic Neu5Ac probes is the reversible B-ester formation. As shown above, an increase in the positive charge density at the B-atom by electron-withdrawing substituents is an important tool to achieve higher affinities. For example, F substituents have been introduced in PBA for this purpose [116–118]. Also the very high affinity of PicBA [84] (see Table 2) can be attributed to the strong electron-withdrawing effect of its pyridinium function. Many of the Neu5Ac probes described in the literature employ conjugates of PBA. An amide or an ester substituent on the phenyl group of PBA is often used as the anchor for an attached group. These anchoring functions have an electron-withdrawing effect on the B-atom. This is illustrated by the higher affinity of the model compound PAPBA as compared to PBA (see Table 2). Electron-withdrawing moieties not only increase the affinity of PBA derivatives for saccharide moieties and widen the plateaus of maximum affinity, but they also lower the pHs where the maximum affinities occur (see section 4). Therefore, tuning for optimal performance at pH 7.4 or slightly lower (in the case of targeting cancer markers) may be desirable when it comes to biomedical applications. To the best of our knowledge, no systematic study has been made on the effect of electronegative substituents on the affinity of PBA for Neu5Ac.

It has been shown that BzBA has a greater affinity for Neu5Ac than PBA (see Table 3), but also a greater affinity for 3,4 *cis*-diol moieties of other saccharides. The p$K_{a,Btri}$ is lower than that of PBA as well, which may indicate that the electron-withdrawing effect of the CH_2-O group plays a role, but possibly also the reduction of the ring strain in the conversion of a trigonal to a tetrahedral B-atom contributes to the increased stability of the B-esters [70,101,119]. Since BzBA also has selectivity for Neu5Ac compared to the other common monosaccharides at pH 7.4, it is likely that the interaction between the 5-acetyl group and the boron group also plays a role here.

7.2. Increasing the affinity for N-acetylneuraminic acids by molecular imprinting

Syntheses carried out in polymeric matrices with template-shaped cavities may produce compounds with a predetermined selectivity and high affinity [120,121]. The reversibility of the Neu5Ac-boronic acid ester formation is ideal for the construction of such molecularly imprinted polymers (MIPs) [121]. For this purpose, polymerization of a boronic acid containing monomer is carried out in the presence of Neu5Ac, after which the Neu5Ac is removed. The resulting MIPs show enhanced affinity and selectivity for Neu5Ac. One of the first examples in the field of Neu5Ac was a poly(4-vinylbenzeneboronic acid) that was cross-linked with ethylene glycol dimethyl acrylate in the presence of Neu5Ac. The obtained MIPs were successfully applied as stationary phase in HPLC: the retention time of Neu5Ac as compared to the corresponding non-templated adsorbent material increased with pH between pH 8.1 and 11.5, but the selectivity for Neu5Ac over Man, Glc, and methyl glucoside decreased at the same time [122]. This system was improved by attaching trimethyl ammonium cations groups to the MIPS that can enhance the affinity for Neu5Ac by electrostatic interaction with its carboxylate (see below) [123–125]. A further enhancement of the affinity was achieved by also introducing urea moieties into the MIPS for additional hydrogen bonding [126]. High affinities and selectivities for free Neu5Ac were achieved and cells with Neu5Ac overexpression (prostate cancer cell lines DU145 and PC3) were stained with similar nanoparticles (NPs). These NPs had a 1000-fold higher affinity with the cells than with free Neu5Ac due to multivalent interactions. A hollow double-layered NO-delivery system has been constructed that had a Neu5Ac imprinted shell, which consisted of a complex block-copolymer with PBA and *S*-nitosothiol functions [127].

Another Neu5Ac-printed nanoparticulate material was prepared with poly(fluorene-alt-benzothiadiazole) and provided with additional trimethylammonium groups to enhance Neu5Ac bonding [128]. The fluorescent NPs selectively labeled DU-145 cell lines for prostate cancer, while HeLa cells, which have lower levels of Neu5Ac overexpression, were not recognized. Electrochemical polymerization of 3-amino-PBA affords poly(aniline boronic acid). By carrying out this polymerization in the presence of Neu5Ac, MIPs were obtained that have been applied as a film on glassy carbon and carbon cloth for the potentiometric determination of Neu5Ac in blood [129–131].

Several silica-based MIPs have been reported. For example, silica was deposited on 4-formyl-PBA linked to Raman-sensitive Ag particles in the presence of Neu5Ac. Removal of the Neu5Ac afforded MIPs, which were used for SERS imaging of human hepatoma carcinoma cells (HepG-2). A fluorescent MIP system was prepared by coating a core of fluorescein isothiocyanate (FITC) doped silica with a Neu5Ac-imprinted silica layer. With the obtained NPs, free Neu5Ac, human hepatoma carcinoma cells (HepG-2), and breast cancer cells (MCF-7) were labeled specifically as compared to the corresponding normal cells (respectively, L-02 and MCF-10A) [132]. QDs with three different fluorescence emission wavelengths and bearing 3-amino-PBA groups were imprinted by coating them with silica in the presence of Neu5Ac, Fuc, and Man as the template, respectively. Using these QDs, multiplexed imaging of various cell lines allowed discrimination between normal and cancerous cell lines as well as the characterization of various types of cancer cells [133,134]. Molecularly imprinted silica core–shell materials have been prepared from highly porous microspheres (5.5 μm) on which a shell of Neu5Ac or Neu5Gc molecularly imprinted co-polymer was applied. The polymerization mixture consisted of 3-dimethylaminopropylmethacrylamide (DMAPM), ethylene dimethacrylate (EDMA), and 4-vinyl-PBA (VPBA). The resulting MIP was successfully used for the selective extraction and enrichment of Neu5Ac and Neu5Gc from complex biological samples [135].

The above-described MIPs were synthesized using monosaccharide Neu5Ac as a template. Most likely, the β-anomer was the actual template in these cases, whereas the α-anomer always is present in glycocalyces. Nevertheless, these MIPs appeared to perform well with Neu5Ac on cancer cell surfaces.

A system for the recognition of poly-Sia residues has been fabricated by attaching 4-formyl-PBA to silica NPs with amino functions at the surface. The boronic groups were reacted with a short oligo-Sia chain (4–10 Sia units) and then these chains were covered with a layer of

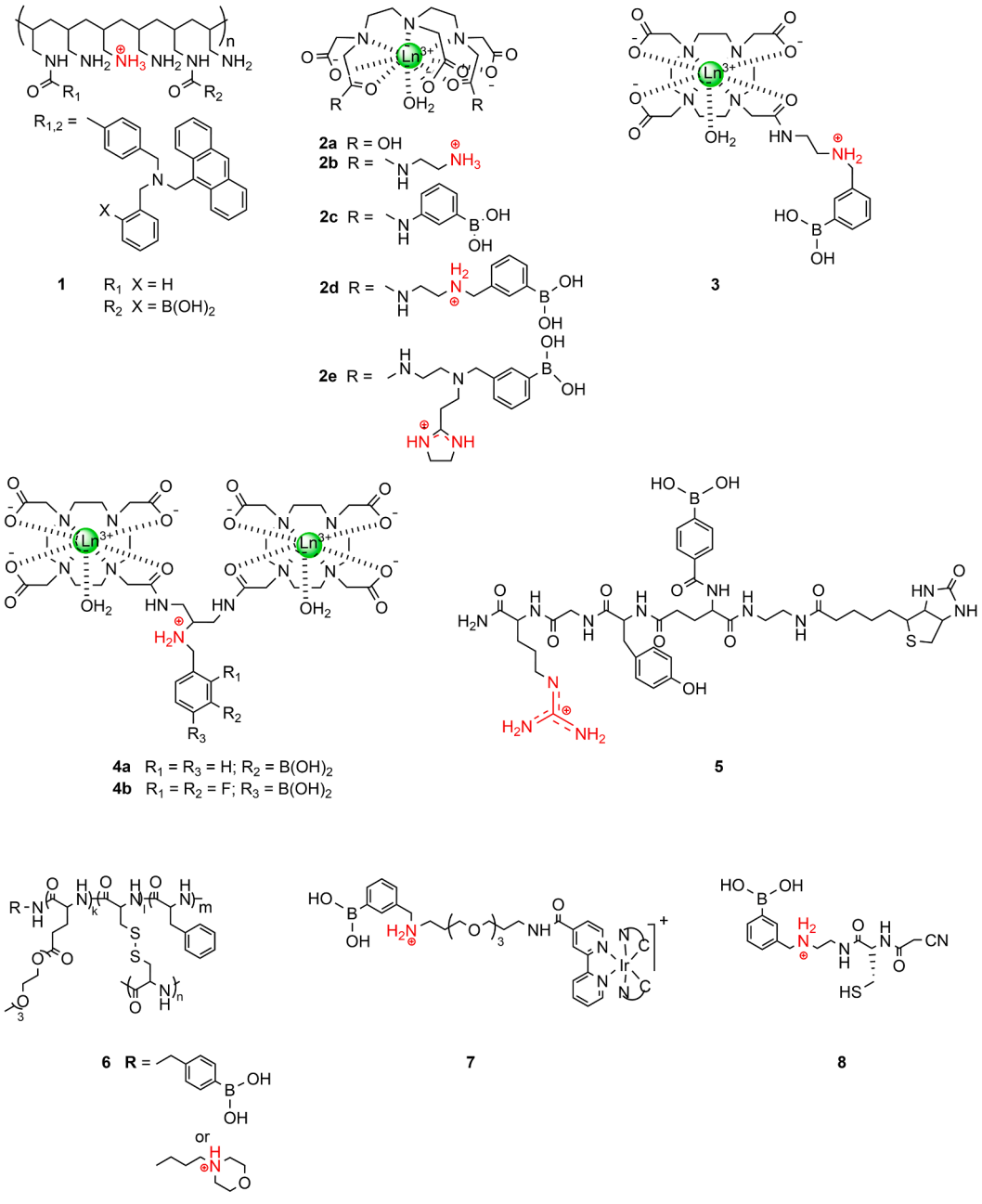

Fig. 13. Examples of structures of Neu5Ac targeting agents with amine functions as secondary binding sites (in red).

silica. After the removal of the oligo-Sia, the resulting MIP showed increased affinity and selectivity for poly-Sia residues as demonstrated by *in vivo* and *in vitro* tests [136]. Loading these NPs with an NIR fluorescent dye afforded a theranostic for image-guided photothermal therapy (PTT).

7.3. Enhanced affinity and selectivity by increased valency of the boronic acid – N-acetylneuraminic acid interactions

7.3.1. Ammonium or guanidinium groups as secondary binding sites

The affinity and selectivity of B-based probes for Neu5Ac can be boosted by the introduction of additional Neu5Ac-binding moieties. In nature, a salt bridge between the carboxylate group of Neu5Ac and a guanidinium group of arginine is always the principal bond (see Fig. 4). For the design of synthetic B-based probes, adding a cationic group to form a salt bridge with the carboxylate group of Neu5Ac is an obvious choice to increase the affinity. Since other common saccharides in glycocalyces lack carboxylate groups, the introduction of cationic binding sites can also increase selectivity over other monosaccharide units.

An early example of the application of ammonium functions is given by Patterson et al. who designed a luminescence reporter (compound **1**, see Fig. 13) conjugated with a fluorescent PBA derivative that has been attached to poly(allylamine) (degree of substitution 2 mol%). The material exhibited a larger response for Neu5Ac than for Glc or Fru, which can be ascribed to the binding of the Neu5Ac-glycerol chains by the PBA and cooperative electrostatic interaction between its carboxylate functions and the ammonium groups on the poly(allylamine)chain [137].

Potential PBA-based MRI contrast agents with protonated amine functions at physiological pH have been constructed by conjugating 3-amino-PBAs with $Gd(DTPA)^{2-}$ or $Gd(DOTA)^{-}$ using ethylene diamine as a bridging group (**2–4,** Ln = Gd) [102,108,116,138–141]. Compound **2d** has a larger affinity for Neu5Ac than PBA and PAPBA as demonstrated by the conditional stability constants in comparison to those of Glc as a typical representant of the usual monosaccharides in glycocalyces (see Table 3). Although boronic acid derivative **2e** is endowed also with positively charged guanidinium groups, it has a low affinity and specificity for Neu5Ac probably for steric reasons [102]. Cell studies with radioactive **2d** (Ln = ^{153}Sm) have shown that a significant amount of it is retained on the surface of C6 Glioma rat cells. The simultaneous binding of ammonium and boronic groups of **2d** (Ln = ^{170}Tb) was supported by kinetic studies with human glioma brain tumor cells (U-251 MG), in which interaction kinetics of the cells with **2d** were compared with those of analogous complexes lacking an ethylenediamine group, a PBA group, or both (**2a-c**) [102]. These studies showed that the removal of either of these groups resulted in a significant decrease of adsorbed DTPA-complex

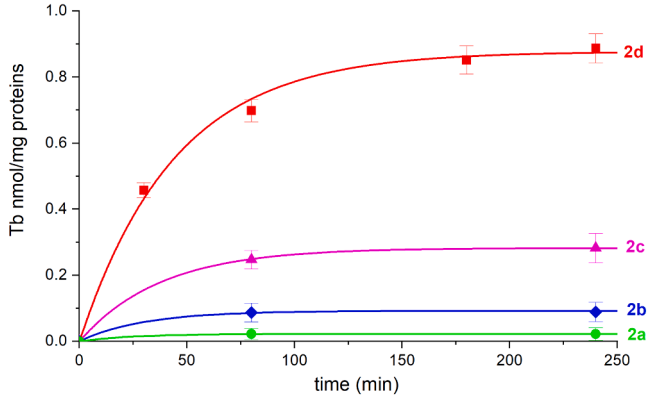

Fig. 14. The amount of Tb-complex on the cell surfaces as a function of the time after incubation of 0.1 mM solutions of 2a-d (for structures, see Fig. 13) with 2.5×10^5 human glioma brain tumor cells (U-251 MG) for 4 h at 37 °C in PBS medium. The amount of Neu5Ac available is about 1.2 nmol/mg protein [138].

(see Fig. 14). The saturation level for complex **2d** corresponds with a molar ratio **2d**/Neu5Ac, which is somewhat higher than 0.5, suggesting that the binding occurs predominantly through both PBA units of **2d**. Almost no internalization of the intact complex was observed but at the cell surface, some demetallation occurred.

A similar approach to enhance the affinity of PBA for Neu5Ac (free or in glycocalyces) used the guanidinium function of arginine in the tetrapeptide EYGR to establish a stabilizing Coulomb interaction with the carboxylate of Neu5Ac (compound **5**, see Fig. 13) [142]. Additional stabilization of the concerning B-ester was possibly obtained by CH-π interaction between the tyrosine and the pyranoside group. The compound also featured a biotin function available for coupling luminescent streptavidin. The affinity of **5** for free Neu5Ac is about three orders higher than for Man, Gal, or Fuc, whereas the corresponding isomer with a *meta* boronic function showed almost no selectivity for Neu5Ac compared to these monosaccharides. MM2 calculations demonstrated that this is due to the distance between the COO^- of Neu5Ac and the guanidinium group, which is too large in the latter B-ester. Confocal microscopy studies on cancer cell lines (HeLa and MDA-MB-231) incubated with the F-streptavidin conjugate **5** demonstrated that it has also a high and selective affinity for highly sialylated glycocalyces.

Chen et al. have designed a polypeptide nanogel (NPs with a diameter of 40 nm) consisting of PEGylated arginine, cysteine, and phenylalanine with PBA and morpholine end groups (6)[143]. The morpholine groups protonated at about pH 7 and as a result, the zeta potential changed from − 1.3 to + 7.8 mV between pH 6 and 7.4. Therefore, the interaction between the gel and Neu5Ac in the more acidic tumor tissue is enhanced by the increased affinity and selectivity of both the boronic and morpholine groups and enhanced cell uptake. The nanogel can be applied as a drug carrier and then the cysteine functions act to take care of reductive responsive disintegration of the gel by glutathione (GSH) present at high concentrations inside the cell. The nanogel was demonstrated *in vitro* and *in vivo* with highly metastatic B16F10 cells.

Following the same approach of simultaneously binding Neu5Ac by a boronic and an ammonium group, a luminescent probe **7** was constructed by connecting 3-aminomethyl-PBA to a cyclometalated Ir(III)-bipyridine luminescent reporter through a triethylene glycol linker [144]. The stability constants of B-esters in these probes at pH 7.4 followed the order Neu5Ac > Gal ≈ Man > Glc. Confocal microscopy showed that these materials were internalized into HepG2 cells at a rate corresponding to the lipophilicity.

A SERS probe (**8**) has been designed for the visualization of Neu5Ac on cells. It consisted of an SH function to bind it to the surface of a metal (Ag NPs), a PBA moiety for selective Neu5Ac recognition, an ethylenediamine for additional binding of the carboxylate of Neu5Ac through an ammonium group, and a CN function as a reporter, exhibiting a single and sharp SERS peak in the cellular Raman silent region, leading to background-free detection [145].

Matsumoto et al. have hypothesized that the involvement of the pyridinium NH in an intramolecular hydrogen bond with the Neu5Ac

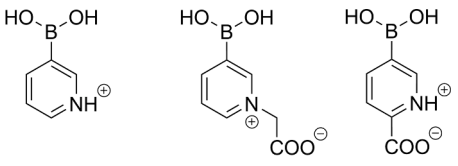

	9	**10**	**PicBA**
$pK_{a,Btri}$	4.4	4.4	4.2
K_C (M^{-1})	182	61	645

Fig. 15. $pK_{a,Btri}$ and K_C values for borate ester formation with Neu5Ac (at pH 6) of some pyridinylboronic acids [84].

carboxyl group plays also a role in stabilizing its B-esters with Neu5Ac. This was supported by a drastic reduction in K_C upon steric blocking that site in **9** by carboxymethylation to **10**, whereas the carboxymethylation did not affect the pK_a of the boronic group (see Fig. 15) [84].

7.3.2. Secondary binding by coordination of the N-acetylneuraminic acid carboxylate to a metal cation

Another example of 2-site binding taking advantage of the negatively charged carboxylate group in Neu5Ac is a fluorescent sensor consisting of a conjugate of a Zn^{2+}-phenanthroline complex and *o*-aminomethyl-PBA (**11,** see Fig. 16) that simultaneously binds the Neu5Ac-carboxylate through coordination to the Zn^{2+}- chelate and Neu5Ac-glycerol chain through ester formation with the PBA moiety. In the absence of Zn^{2+}, this ligand has almost no affinity to Neu5Ac [103,146]. The binding of the carboxylate function of Neu5Ac can also be accomplished by the lanthanide ions in complexes with a DOTA-type ligand (**12**) [104]. ^{13}C NMR showed that the borate function of compound **12b** binds its glycerol tail while the Ln^{3+} coordinates its carboxylate. Luminescence on the Tb^{3+} complex, NMRD measurements, and DFT calculations on the Gd^{3+} complex indicate that the coordination of the Neu5Ac-carboxylate is accompanied by a reduction of the number of Ln-bound water molecules. Once again, this divalent binding increases the affinity and the selectivity for Neu5Ac over other sugars (see Table 3), whereas also the 2α-OMe derivative of Neu5Ac still has an appreciable affinity (K_C = 79 M^{-1}). In the absence of Neu5Ac, compound **12a** exhibits intramolecular coordination of its boronate group to the Ln^{3+} cation, which is reflected in a decrease of its pK_a to 4.6, and the absence of Ln^{3+}-coordinated water molecules ($q = 0$). Consequently, the affinity of this complex for Neu5Ac is negligible [104]. In methanol as solvent, NOTA complex **13** was found to have a very high affinity to Neu5Ac (log $K_C > 5.3$). Based on the results of circularly polarized luminescence spectroscopy and DFT calculations, the binding of Neu5Ac by the Eu^{3+} complex of NOTA derivative **13** was hypothesized to occur through combined B-ester formation of the glycerol tail and Eu^{3+}-binding of the 5-*N*-acetyl group of Neu5Ac [147]. Remarkably, La(DTPA)-derivative **14** showed a higher affinity for Glc than for Neu5Ac [105] (see Table 3). Possibly, this can be attributed to repulsion between the negatively charged La(DTPA) moiety and the carboxylate of Neu5Ac.

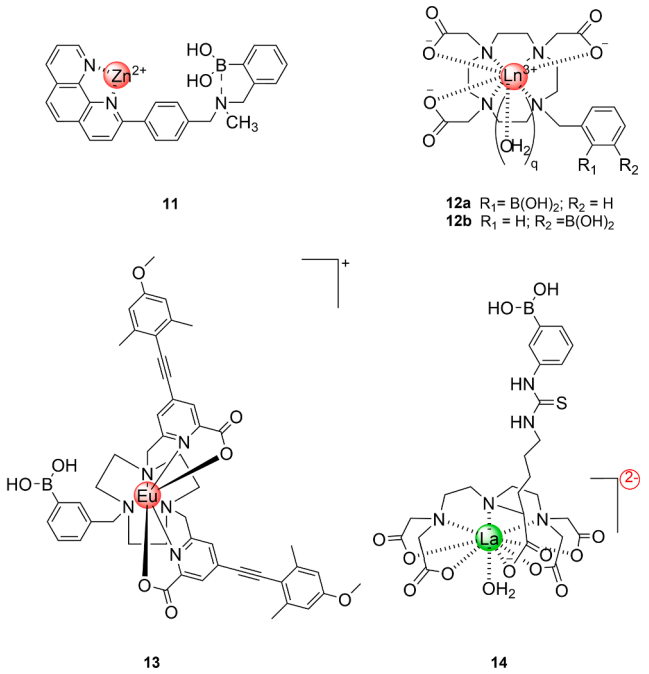

Fig. 16. Molecular structures of complexes **11**–**14**.

7.3.3. Probes with two boronic functions

Sensors with two boronic acid functions may also have increased affinity and specificity as a result of covalent binding of the second boronic binding site to diol functions in another Neu5Ac unit or a *cis*-diol function of Fuc, Gal, GalNAc, or Man. Weaker contributions to the stability may be afforded by covalent bonds to other hydroxyl groups, hydrogen bonds, and hydrophobic interactions. Covalent bonds to *trans*-diol functions, including those in Glc (in the glycocalyx) are unlikely because they are sterically unfavorable. The high affinity of compound **2d** for Neu5Ac may be partly caused by its two boronic groups.

A library of 26 bis-boronic acid compounds characterized by two fluorescent anthracene units linked by different groups has been screened to identify sensors of sLe^x (structure, see Fig. 3b) [148,149]. A compound with a phenyl linker was found to have optimal affinity and specificity (Compound **15**, see Fig. 17, R = H). It was also effective on a HEPG2 cancer cell line that expressed sLe^x. Removal of either Neu5Ac or fucose from the cell surfaces with neuraminidase or fucosidase, respectively, inhibited the recognition, showing that both monosaccharides are essential for effective binding. Since generally B-esters of *cis-vic*-diols are considerably more stable than *trans* ones [66], the exocyclic glycerol of Neu5Ac and the *cis*-3,4-diol of fucose are most likely the binding sites for this bis-boronic acid. Decoration of the central phenyl in **15** with a reporter group (R) for MALDI imaging mass spectrometry enabled the specific detection of tumors overexpressing sLe^x in a tissue sample [150]. Linking of **15** with a fluorophore afforded a very sensitive probe for the fluorescent imaging of sLe^x-expressing tumors (HEPG2 and COLO205) implanted in mice [151]. The importance of the spatial rearrangement of the two boronic functions was also demonstrated with another series of similar fluorescent anthracene-containing compounds now with an alkyl linker, -$(CH_2)_n$, where n = 6, 7, or 8 (**16**) [152]. High affinities and selectivities for Glc and Fruc were observed for n = 7 or 8, whereas the compound with a hexamethylene spacer recognized sLe^x and stained HEPG2 cells at a concentration as low as 1 μmol L^{-1}.

Since Neu5Ac has two potential sites for B-ester formation, the glycerol tail and the α-hydroxycarboxylate, also a divalent binding of a bis-boronate is possible. Fluorescence and mass spectral data have suggested that a divalent ester of **17** is formed selectively with Neu5Ac at pH 6.2 but at pH 7.8 other monosaccharides bind as well. Probably, at pH 6.2, esters of both types $B^{tet}L^{ac-}$ and $B^{tet}L^{diol2-}$ occur, which allows divalent binding, whereas, at pH 7.8, the monovalently bound $B^{tet}L^{diol2-}$ ester dominates [153]. Obviously, such binding is much weaker and no longer specific to Neu5Ac. Possibly, the aminomethyl groups in the divalent complex at pH 6.2 are protonated, which may provide additional stabilization.

7.3.4. Hydrogen bonds for enhanced binding

The importance of hydrogen bonding as a secondary effect to increase the stability of PBA-Neu5Ac in DMSO solution has been demonstrated with derivatives having urea and thiourea groups [154] A library of boronated octapeptides showed K_C values between 53.1 and 166.5 M^{-1} at pH 7.4 [155]. These variations can be ascribed to the combination of the effects of covalent B-ester formation and varying non-bonding interactions depending on the geometry of the peptide under study.

7.3.5. Multivalent boronic acid - N-acetylneuraminic acid interactions

The pH dependency of PBA-Neu5Ac interactions is harnessed in a great variety of disciplines, including those of chromatography, synthetic lectins, sensors, diagnostics, theranostics, and drug carriers. One of the first examples of the application of a PBA-conjugated polymer is reported by Kataoka and coworkers who demonstrated that a co-polymer of 3-acrylamidophenylboronic acid and *N*,*N*-dimethyl acrylamide acts as an artificial selectin by inducing the proliferation of lymphocytes, particularly tumoricidal ones [85]. This effect may be related to the relatively strong and selective affinity of the PBA functions

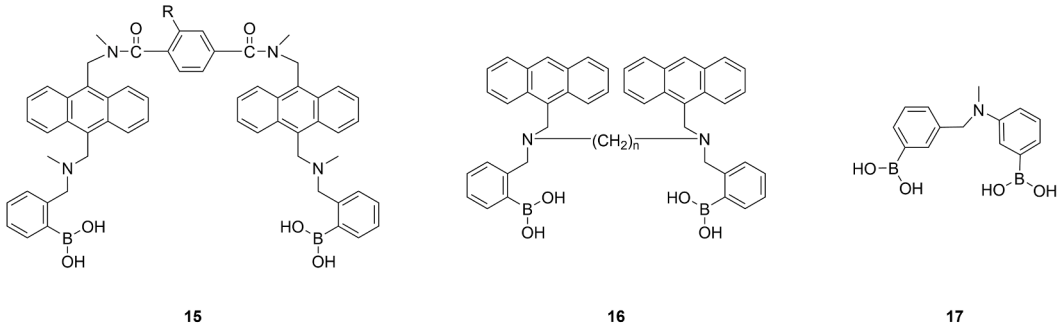

Fig. 17. The molecular structure of the bis-boronic acid compounds **15**–**17**. R = H or a reporter group for either MALDI mass spectrometry imaging or a fluorophore.

for Neu5Ac on the cell surfaces of this copolymer under physiological conditions. The *N*,*N*-dimethylacetamide groups in the resin possibly stabilize the boronate esters by an intramolecular interaction.

After that many other multivalent boronic acids have been synthesized, usually by attachment of 3- and 4-substituted PBA derivatives directly or via linkers to dendrimers [156–160], micelles [90,161–167], liposomes [139,168,169], other natural and synthetic organic polymeric systems [170–184], metal–organic frameworks [185,186], silica NPs [187–190], silicon nanowires[190,191], glass slides [192], ZnO NPs [193,194], graphene oxide [195], carbon nanotubes [196,197], carbon dots [198,199], glassy carbon [131,200,201], pencil graphite electrodes [202], QDs [112,203–208], and Au- and Ag-NPs and electrodes [30,31,87–89,209–228].

If multiple PBA moieties interact simultaneously with Neu5Ac groups on cell surfaces, the binding affinity and selectivity may be greater than for an individual PBA-Neu5Ac interaction due to multivalency effects. Thermodynamic models have been developed to describe these interactions [229–232]. Parameters such as receptor and ligand density, and linker flexibility are of importance. Multivalency can provide "ultra-sensitivity" to external triggers such as pH, temperature, and receptor density [233]. The adsorption of multivalent ligands may display a steep response to the receptor density (see Fig. 18).

The importance of dynamic multivalent interactions was nicely demonstrated in a study of the interaction between Neu5Ac at the surface of human erythrocytes and 1D fibers of benzene-1,3,5-tricarboxamide to which BzBA moieties were appended via amphiphilic linkers [234]. A 1000-fold excess of free Neu5Ac compared to the amount of BzBA on the fibers was needed to detach the fibers from the cell surface, while the K_C value of the B-ester between monomeric BzBA and free Neu5Ac is only 160 M^{-1}. Interestingly, the multivalent interactions could be visualized in real-time using total internal reflection fluorescence microscopy.

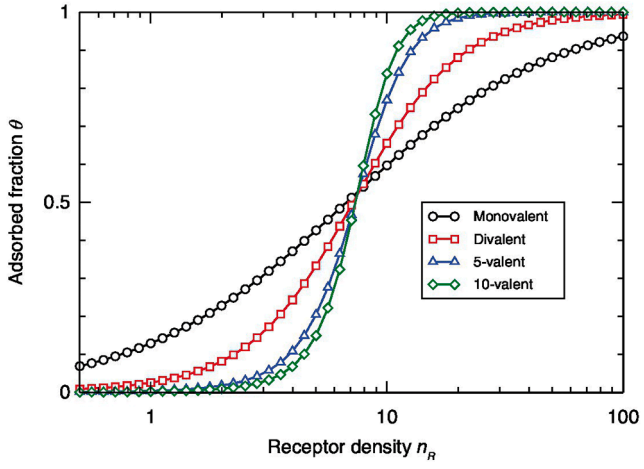

Fig. 18. Computed adsorption profiles of monovalent and multivalent particles. Monovalent adsorption (circles) yields the familiar Langmuir isotherm. In contrast, multivalent particles show a steep, sigmoidal response. Reproduced with permission from ref. [233]. Copyright 2018 John Wiley & Sons Ltd.

A conjugate prepared by amidation of 7.5 of the 11 carboxylate groups of bovine pancreatic ribonuclease (RNase A) with 5-amino-BzBA has a 440-fold greater association constant with GD3 ganglioside liposomes than the free boronic acid, demonstrating that a multivalent interaction is involved with the two Neu5Ac residues of this ganglioside [119]. Fru inhibits the interaction. Moreover, cell experiments indicate that this conjugate mediates the delivery of the protein into the cytosol.

As described above, the boronic acids recognize Neu5Ac usually selectively at or below physiological pH, whereas interaction with most other monosaccharides is optimal at pH > 8. In addition to the multivalency effect, diagnostic agents and sensors often use an amplification effect to increase the signal intensity of the reporter. Here, we will describe only a few typical examples.

Gold electrodes with 3-amino-PBA attached to the surface through a C_{10}-chain allowed direct potentiometric detection of free and cell-bound Neu5Ac in cell suspensions [87–89]. As expected, the highest sensitivity and selectivity for Neu5Ac compared to other monosaccharides was obtained at pH < 8. The gold surface of a thermal biosensor was modified similarly and then used to quantify the amount of Neu5Ac on erythrocytes through the heat developed upon the interaction of the Neu5Ac end groups with the PBA groups at the electrode [223]. More recently, Au-electrodes to which the same probes were attached via a PEG-linker were used for potentiometry of fetuin and asiolofetuin [31]. The Neu5Ac groups of these glycoproteins were detected selectively at pH 5.5, whereas at pH 7.4, the electrode was no longer selective for Neu5Ac but also interacted with other saccharides. With another Au-probe, now with PicBA linked through ethylthiol, the sensitivity for detection of Neu5Ac was increased to a submicromolar level [235]. With this probe, the Neu5Ac-binding reduced dramatically with an increase in pH from 5 to 7, and at pH 9, most of the Neu5Ac was released.

7.3.6. Examples of enhanced affinity and selectivity by dual receptor targeted strategies

An enhancement in stability and specificity for sLe^x was obtained with a bis(boronic acid) similar to compound **15** but with a peptide chain containing an RGD peptide sequence as a linker between the two anthracene units [236]. This compound is capable of simultaneously targeting sLe^x and integrins at cell surfaces. The association constant on the cell surface of HepG2 cancer cells was more than threefold that of free sLe^x in an aqueous solution.

NPs consisting of poly(3-acrylamido-PBA) and bovine serum albumin (BSA) have been exploited for the Neu5Ac-targeted delivery of doxorubicin (DOX) to hepatic H22 tumor cells [237]. The pharmacokinetics and the biodistribution were improved by coating these NP with a copolymer of PEG and polyethyleneimine, whereas additional attachment of cRGD was applied to enhance the tumor selectivity [238].

NPs constructed by attachment of 3-aminomethylphenylboronic acid

(APBA) attached to a chondroitin sulfate A–deoxycholic acid conjugate has been used as a drug carrier of DOX [239]. The simultaneous interactions of APBA with Neu5Ac and of chondroitin sulfate A with CD44 receptors resulted in efficient delivery and cell penetration of DOX in lung carcinoma epithelial cells (A549). Another PBA-based system with an additional CD44 receptor targeting function was obtained by coupling APBA to hyaluronic acid ceramide. These NPs (diameter 239 nm) were fabricated for encapsulation of the anti-cancer drug manassantin B [240].

An electrochemical biosensor for Neu5c has been constructed by linking PBA to an Au-electrode through an aptamer that is capable of capturing Neu5Gc [241]. The affinity of PBA directly bound to the Au-surface for both Neu5Ac and Neu5Gc showed a pH profile similar to Fig. 12, i.e. decreasing affinity between pH 3 and 10. With the aptamer as link the opposite trend was observed, increasing affinity with pH until pH 9 where a plateau was reached. Consequently, the sensor captures both Neu5Ac and Neu5Gc at low pH, by binding to the boronic unit and at higher pH values, Neu5Gc moved to the aptamer linker whereas Neu5Ac remained released.

8. Oxidation of boronic esters

Boronic esters are susceptible to oxidative decomposition to phenols (see Fig. 19). This has been exploited in the design of various fluorescent sensors for H_2O_2 in living systems [242–244]. If an electron-withdrawing group is present at the phenyl ring, a 1,6-elimination reaction can subsequently take place that yields a quinone methide.

Oxidative deborylation has been exploited for the design of a fluorescence imaging probe [245]. Multiple targeting to enhance its selectivity was achieved by including (1) octreotide as a synthetic peptide ligand of somatostatin receptors, which are over-expressed in many tumors, (2) an H_2O_2-responsive PBA group, (3) a dipeptide substrate for cathepsin B, which is also usually over-expressed in tumors, and (4) a NIR fluorophore. The octreotide is responsible for somatostatin receptor-mediated endocytosis. The intact probe is only weakly NIR-fluorescent, but by the combined action of H_2O_2 and cathepsin B inside the tumor cells, the probe disassembles and the NIR-fluorophore is deprotected resulting in a large increase in its fluorescence. The success of this approach was demonstrated *in vitro* and with cancer cell lines. This type of reaction may also be applied in drug delivery (see below).

9. Applications of the boronic acid –*N*-acetylneuraminic acid interactions in drug design

The unique pH profile of the interaction between boronic acids and Neu5Ac as compared to that of other monosaccharides has found many applications in analytic chemical methods including chromatography, potentiometry, spectroscopy, sensors, cell labeling, and drug design. Several reviews on this topic have been published recently [2,38,43,92,121,246–250]. Here, the focus will be on the applications in drug delivery. Because relatively high densities of Neu5Ac occur in mucins and tumors, these are the most commonly used Neu5Ac targets.

9.1. Drug delivery to mucins in the eyes, genitourinary tract, and lungs

Neu5Ac residues are abundant in the mucous tissue of the eye. Therefore, PBA has been exploited as a targeting function in the formulation of drug delivery systems for pharmaceuticals for ocular diseases such as dry eye disease [251]. For example, NPs consisting of block-polymers of polylactic acid and dextran or polymethacrylate were functionalized with 3-amino-PBA and have been successfully applied as mucoadhesive for the encapsulation, delivery, and sustained release of dry eye therapeutic cyclosporin A [252–254]. Another dry eye therapeutic, dexamethasone, has been encapsulated into chondroitin sulfate, which was conjugated with APBA [255]. The feasibility of using PBA derivatives as lubricants for the treatment of dry eye disease has been demonstrated with PEG that had on one terminus a FITC fluorescent group and on the other terminus a 2-hydroxymethyl-PBA group for the anchoring onto the Neu5Ac of the mucous membrane of the eye [256].

Nanoparticles prepared from a copolymer of 3-acrylamido-PBA and N-maleated glucosamine have been applied to encapsulate insulin. The strong multivalent dynamic covalent binding of the boronic acid groups with Neu5Ac groups was exploited to mediate nasal delivery of insulin across the mucin barrier and cellular lipid bilayers [257]. The boronic groups also inhibited the enzymatic biodegradation of the insulin. Nasal drug delivery can be antagonized by several defense mechanisms in the mucus. Therefore, it may be advantageous to find ways to prolong the residence times of these formulations in the nasal cavity. Attachment of a 3-amino-PBA to a glycopolymer composed of 2-lactobionamidoethyl methacrylate and 3-acrylamidophenylboronic acid (AAPBA) has been suggested to achieve this [182]. A library of micelles of these PBA-grafted copolymers with various compositions has been tested for the ocular delivery of cyclosporin A as a treatment for serious dry eye disease [254].

Mucoadhesive NPs for vaginal delivery of pharmaceuticals have been prepared by NPs consisting of an Ag core covered with a PBA-rich shell obtained by polymerization of 4-vinyl-PBA with ethyleneglycol dimethylacrylate, and *N,N'*-methylenebisacrylamide [258]. The long-term aggregation of these NPs could be avoided by adding 4-vinylphenylsulfonate to the polymerization mixture [259]. These NPs were loaded with interferon by adsorption. The release was dependent on the mucin concentration.

9.2. Drug delivery to tumors

For optimal efficiency of diagnostics, chemotherapeutics, or theranostics, it is important to deliver these agents at the target site with optimal selectivity and sufficient concentration. Several low-MW conjugates of PBA derivatives and anti-cancer drugs have been investigated for drug delivery [260], but these systems can only deliver a small amount of drug per targeting group to a tumor. A maximum amount of an injected anti-tumor drug must reach the tumor to reduce toxic and side effects to healthy cells. Multidrug resistance is a major obstacle to clinical chemotherapy for tumors, which can be caused by inadequate drug retention due to overexpression of efflux transporters [261–266].

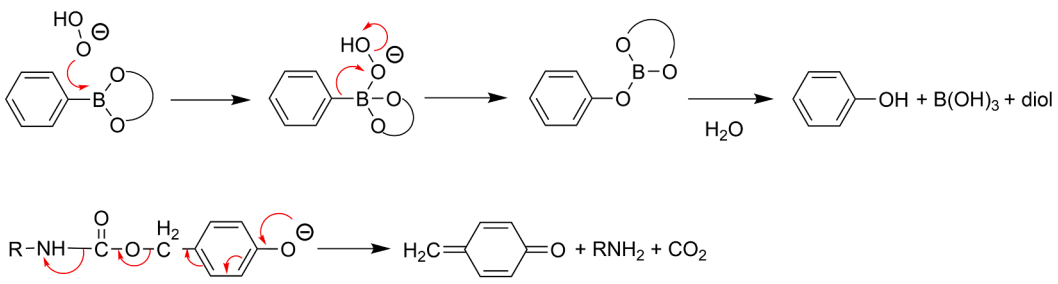

Fig. 19. Oxidative deborylation of a boronic ester of a diol and an example of a subsequent 1,6-elimination.

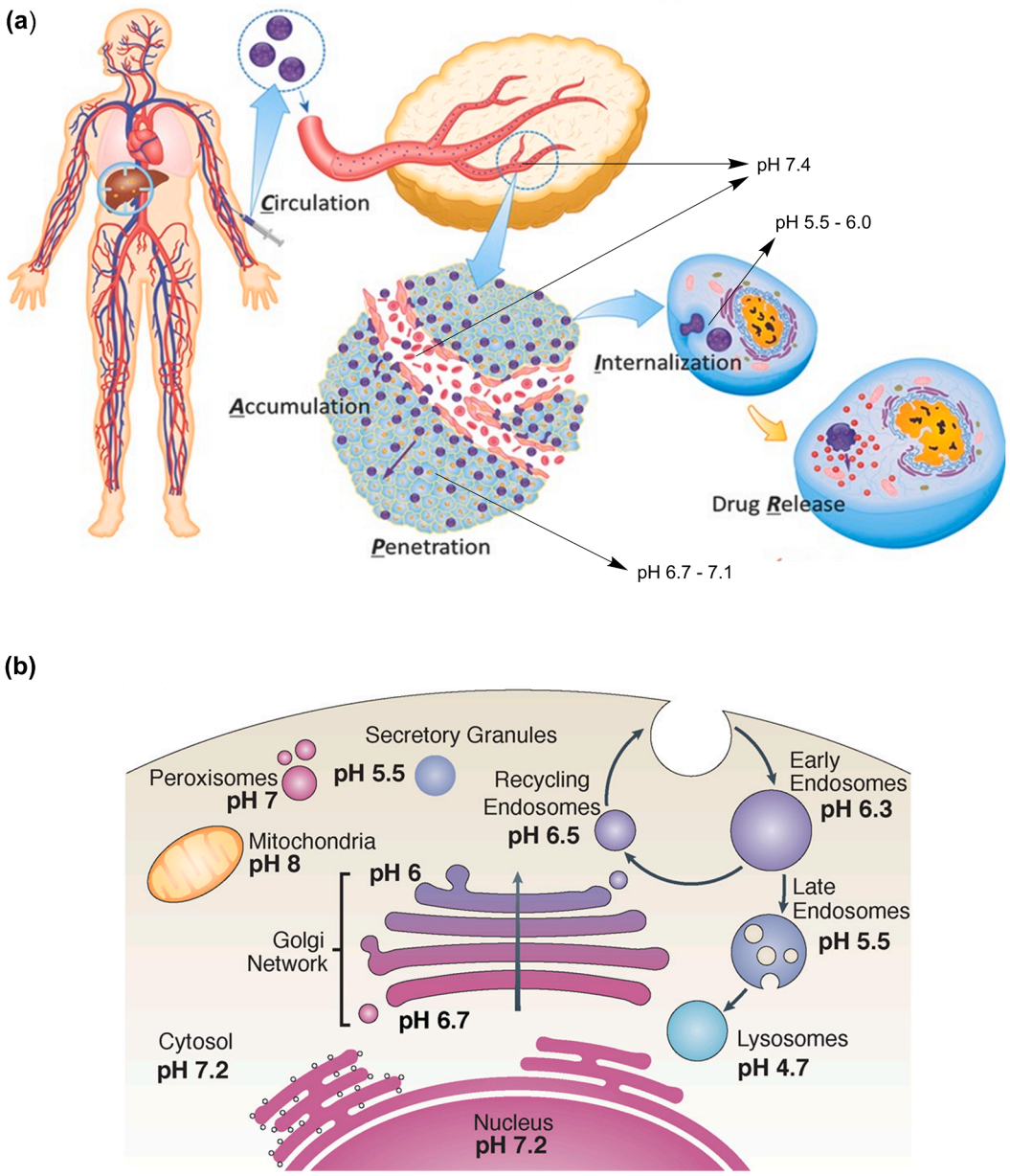

Fig. 20. (a) Schematic representation of CAPIR cascade of drug delivery to tumors. Adapted with permission from ref. [288]. Copyright 2014, Wiley-VCH Verlag GmbH. (b) pH of the different subcellular compartments. Copied with permission from ref. [284]. Copyright 2010, MacMillan Publishers Ltd.

Nanocarriers with attached boronic functions for Neu5Ac-targeting are attractive for the delivery of drugs to tumors. To reach a tumor cell, an injected nano-system has to go through the so-called CAPIR cascade: (i) circulation, (ii) accumulation, (iii) penetration, (iv) internalization, and (v) drug release (see Fig. 20) [267]. The efficiency of each of these steps is essential for the success of the overall process, which can only be achieved by fine-tuning of the various physicochemical parameters that control them: size and surface chemistry are the most important. Obviously, a drug carrier must be biocompatible and remain intact all the way from injection to arrival in the tumor cell. Anti-cancer agents such as DOX, paclitaxel (PTX), and camptothecin (CPT) are often hydrophobic and therefore, amphiphilic materials are the favorite materials for the construction of nanocarriers. The binding inside the carrier sometimes is reinforced by chemical binding to the carrier material through a linker that is stable extracellularly but not intracellularly, for example, an S-S linker that breaks under the influence of intracellular GSH [268–272]. The blood-circulation time of the nanocarriers must be long enough to allow efficient accumulation, which implies that the particle size should be above the renal clearance threshold (5–6 nm) [273]. Larger particles will be opsonized after injection and cleared by the reticuloendothelial system (RES). To avoid this generally, PEGylation is applied, which however may hamper the endocytosis. Nanoparticulate systems may benefit from additional passive targeting by the enhanced permeability and retention (EPR) effect due to leaky vasculature and poor lymphatic drainage [267,274–278]. Efficient penetration is required to allow homogeneous accumulation of the drug over the tumor. For high penetration efficiency diameters of less than 30 nm are preferable [279]. The pH control is disregulated in tumors; the extracellular pH (6.7–7.1) usually is lower than that of healthy cells (7.4) [97,280–282]. Although the opposite trend is observed for the average intercellular pH, the endosomes and lysosomes inside both tumor and healthy cells are assumed to have relatively low pH (4.5–6.5) [283,284]. Furthermore, Glc concentrations are usually low in a tumor microenvironment, whereas the intracellular concentrations of GSH and ATP are

relatively high. Therefore, pH and the concentrations of ATP and GSH are attractive endogenous triggers in drug delivery processes [92,111,285,286]. The anti-cancer drug DOX has a 1,3-diol function, which can be applied to bind DOX in drug carriers by B-ester formation [117,179,287]. At the low pH of endosomes and lysosomes, the stability of these DOX B-esters decreases. Moreover, the high concentration of ATP competes, resulting in the release of DOX [117,179,287].

In a seminal study on the use of the PBA-Neu5Ac interaction for drug carriers, Deshayes et al. have created micellar nanocarriers with 3-amino-PBA end groups around the anti-tumor agent dichloro(1,2-diamino-cyclohexane)platinum(II) (DACHPt) by self-assembly of the bio-compatible block-copolymer PBA-PEG-*b*-PLGA (PGLA = poly-L-glutamic acid) [90]. The PEG enlarges the residence time in blood by suppressing the recognition by macrophages and the carboxylate groups of PGLA are utilized to coordinate the DACHPt. The particle size was tuned at about 30 nm to ensure optimal EPR and penetration efficiency [289]. These investigations also confirmed that the boronic acid-Neu5Ac interaction decreases significantly with increasing pH between pH 6.5 and 7.4, whereas other saccharides show the opposite trend (see Table 4). The high affinity of the PBA groups for Neu5Ac in the slightly acidic micro-environment of a tumor afforded an enhanced cellular uptake in tumor cells resulting in an improved anti-tumor effect of the cargo DACHPt. The efficiency of these micelles was demonstrated both *in vitro* and *in vivo* using a B16F10 murine melanoma cell line. Similar micellar nanocarriers were more recently constructed with PicBA as a Neu5Ac targeting group [93]. An *in vitro* and *in vivo* study using an orthotopic head and neck tumor model with the HSC2 cell line demonstrated that the micelles with PicBA-targeting groups performed significantly better in the slightly acidic micro-environment of a tumor (pH 6.5) than those with PBA-targeting groups, while the interaction with normal cells in the bloodstream at pH 7.4 is not significant. An additional study on pancreatic cancer stem cells with the fluorescent dye rhodamine conjugated to PicBA through a hexanediamine linker showed that this compound was taken up by different epitopes (CD44 and CD133) [290]. The recognition between boronic acid and Neu5Ac is solely dependent on the amount of Neu5Ac on the surface of the stem cells, whereas antibodies would be specific for a single epitope.

To avoid undesired interactions of the boronic groups during the blood circulation, it can be useful to protect temporarily them with an acid-labile diol. This may be achieved by pre-organized diols that usually bind boronic acids strongly in basic media (between the pK_as of the boronic acid and the diol), whereas they are rather labile in acidic media. At the slightly acidic pH in the micro-environment of tumor cells, *trans*-B-esterification can take place with Neu5Ac if their density at the cell membrane is sufficient. Protective alcohols that have been used for that purpose include derivatives of dopamine and other catechols [268,272,291,292], pinacol [293], Fru [294–296], and cyclodextrin. PEG derivatives of these compounds have often been used and then the protective group and the PEG chain are simultaneously removed from the NPs in the slightly acidic extracellular tumoral environment, which facilities cell uptake.

A typical example of such an approach is the design of a sequential delivery system for cisplatin that was composed by co-polymerization of some acrylates (see Fig. 21) [293]. The PEG groups prolong the blood circulation of the resulting nanogels, but because they may hamper cell uptake, they were attached through an acid-labile *ortho*-ester group. The EPR favors the uptake of the 160 nm nanogel particles in tumorous tissue where the slightly acidic conditions resulted in detachment of the PEG groups by hydrolysis of the ortho ester group and of the pinacol B-ester. The exposed PBA functions facilitate cell uptake and the reductive intracellular medium triggers the breaking of the Pt(IV)-crosslinks liberating Pt(II). Inside the cells, furthermore, oxidative deborylation can occur under the influence of H_2O_2 (see Fig. 19), followed by 1,6-elimination of the acrylate ester of 4-HO-CH2-PBA (see Fig. 21, purple component) to produce *p*-quinone methide. The latter reduces the intracellular GSH concentration resulting in the enhanced anti-tumor effect of cisplatin.

Table 4
Conditional stability constants of PBA-PEG-*b*-PLGA and some monosaccharides (in M^{-1}) at pH 7.4 and 6.5 [90].

	K_C (pH 6.5)	K_C (pH 7.4)
2α-OMe-Neu5Ac	6.00	3.40
Neu5Ac	12.7	12.3
Glc	0.39	1.71
Man	0.70	3.95
Gal	1.11	5.11

The clinically applied proteasome inhibitor Velcade (see Fig. 2) has low aqueous solubility in water [297]. Therefore, it is usually supplied as the B-ester of Man, which has a much higher solubility. The B-ester is in the $B^{tri}L$ form because it is prepared in t-butanol as solvent. Prior to administration, the solid B-ester is dissolved in 0.9 % aqueous NaCl, which provides the $B^{tet}L$ ester in equilibrium with free Velcade and Man. Mannitol has two *threo*-diol functions and therefore has a high affinity to Velcade, but optimal stability is at high pH (>9). Nevertheless, it has been suggested that the interaction of Velcade with mannitol reduces its toxic effects on healthy cells, but that the free compound is exposed in the acidic micro-environment of tumors [298]. Using Neu5Ac instead of Man to B-esterify Velcade afforded a prodrug that showed improved targetability and less toxicity. In this case, the Neu5Ac probably targets over-expressed selectins.

Alternatively, boronic functions on the surface of NPs can be protected by multivalent interactions with polysaccharide chains on the surface of the NP. This is illustrated by a multifunctional platform assembled by: (1) a glutaminic-acid-based dendrimeric core, (2) PBA units for Neu5Ac recognition, (3) a porphyrin Pp IX (compound **15**) photosensitizer for photodynamic therapy (PDT), (4) S-S functions for crosslinking of the assemblies, and (5) a coating of the polysaccharide lentinan (bound through PBA-diol bonds) (see Fig. 22) [299]. After cross-linking NPs with a diameter of 110 nm were obtained that were loaded with PTX. These NPs accumulated in tumoral tissue through the EPR effect. The lentinan coat served to shield the PBA functions to avoid binding of the NPs to Neu5Ac in blood or other healthy cells. Upon arrival in the acidic environment of the tumor cells, PBA-lentinan bonds destabilized so that the PBA functions could recognize the Neu5Ac groups and facilitate the uptake into the tumor cells. There the NPs disassembled and released PTX in response to GSH or H_2O_2.

A third strategy to protect boric acid is to use micelles that have two different chains in each NP, one with boron groups and a second with a diol group. In neutral media, the boronic and the diol moiety then form B-esters protecting each other against interactions with components in the bloodstream. In the slightly acidic tumor micro-environment, these B-esters hydrolyze, liberating the boronic functions that then can form stable B-esters with Neu5Ac under these conditions [300,301]. For example, such a system has been made by self-assembling two different amphiphilic chains of poly(ethyleneglycol)-*b*-poly(ε-caprolactone), one with PBA end groups (PBA-PEG-PCL) and the other with Gal end groups (Gal-PEG- PCL) [300]. At pH 7.8, the PBA and the Gal at the surface of the micelles formed mutually B-esters but after entering the slightly acidic tumorous tissue (pH 6.8) these were more labile and the PBA preferred esterification of the Neu5Ac groups at the tumor cell surface, whereas the Gal groups are deshielded and thus available for the recognition of asialoglycoprotein receptors, which are generally over-expressed on tumor cells, leading to increased cellular uptake. Moreover, the mutual protection-deprotection is reversible, and therefore, this system exhibited prolonged blood circulation due to reduced RES capture.

The mutual protection strategy has also been applied in the design of the oral veterinary medicine diclazuril, which is used to treat poultry with coccidiosis, an infection that mainly affects the cecum section and causes severe damage to the intestinal epithelium. Chitosan has been

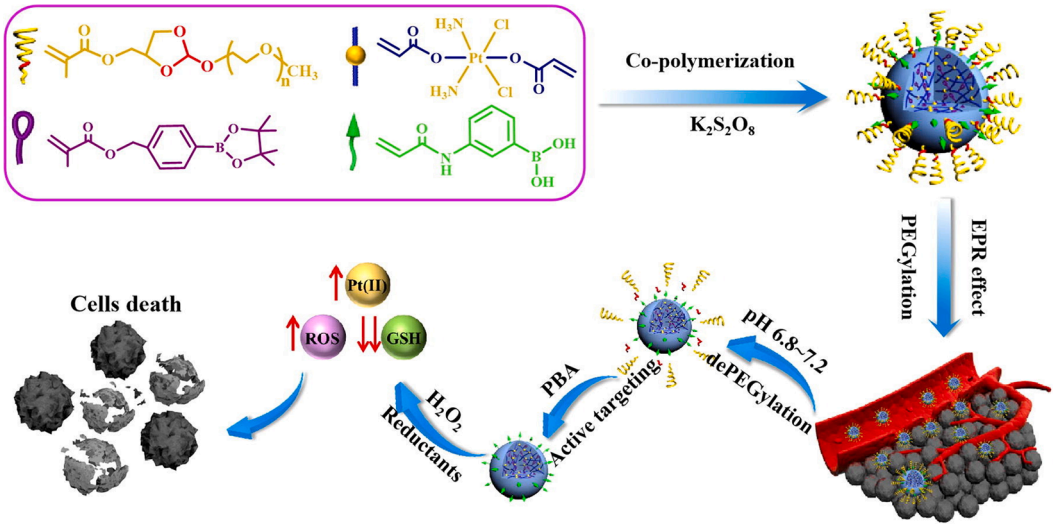

Fig. 21. Schematic representation of the *in vivo* drug delivery of a Pt(IV) cross-linked nanogel. Copied with permission from [293]. Copyright 2021 Elsevier Inc.

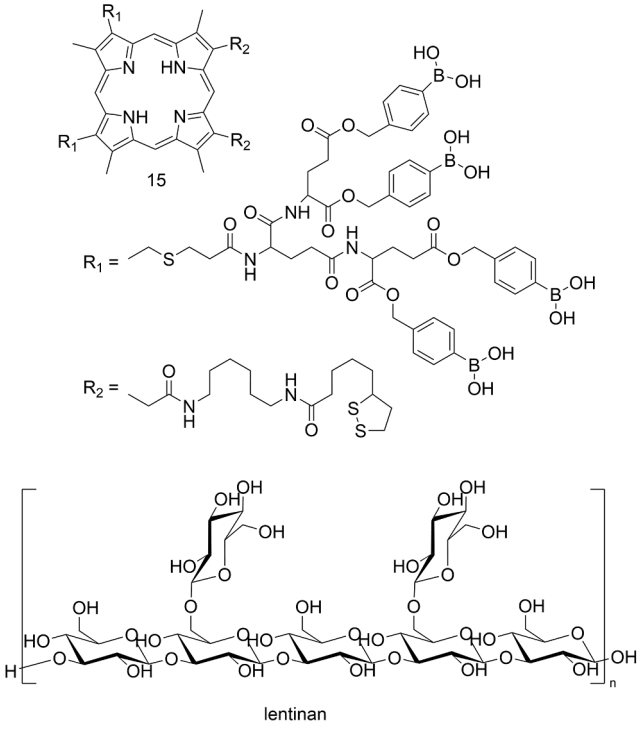

Fig. 22. The chemical structures of dendrimeric NPs for synergistic chemo-PDT [299].

conjugated with both 3-COOH-PBA and Neu5Ac through amide bonding with each of these compounds. B-ester formation between the PBA moieties and the diol functions of Neu5Ac resulted in self-assembly into micelles in an acidic medium [302]. These micelles were utilized as drug carriers of the diclazuril. The micelles are highly stable under the acidic conditions in the upper intestinal tract, but upon reaching the cecum region, the pH increases and the concentration of Glc is relatively high, leading to *trans*-esterification of the Neu5Ac-B esters to Glc-B-esters and thus to destabilization of the micelles and release of the drug.

An external trigger strategy for drug delivery used encapsulation of compound **3** (Ln = Tb, see Fig. 13) and the fluorescent dye calcein in thermosensitive PEGylated liposomes having a gel-liquid phase transition of 41.4 °C [139]. The PEGylated liposomes ensure a long blood circulation time as well as an uptake in tumors utilizing the EPR effect. Mild hyperthermia at the tumor sites triggered rapid release of **3**, which is bound to Neu5Ac at the tumor cell surface. The great efficiency of this strategy was demonstrated on mice with implanted a human BLM melanoma tumor.

A local application of the PBA-Neu5Ac interaction has been demonstrated by a hydrogel prepared from the tumor cell-penetrating peptide 9-fluorenyl methoxycarbonyl (Fmoc)–KCRGDK conjugated to PBA. The PBA moiety has been used in a surgical bed to target Neu5Ac residue tumors to deliver an autologous tumor cell vaccine that locally mobilizes antitumor immunity to inhibit tumor relapse [303].

9.3. Intramolecular delivery of genes, siRNA, or mRNA

Transfection of nuclear material into cells requires good protection against degradation by nucleases during transport, but in the cytosol, the carrier must be degraded to release the transfected material. The differences in pH profiles of the stabilities of PBA-esters of Neu5Ac as compared to those of other diols were exploited in the design of an architecture of a dual stimuli-responsive carrier for gene transfection in tumor therapy [117]. Low-MW polyethyleneimine (PEI) was grafted with 3-fluoro-4-carboxy-PBA (PEI-PBA), or galacturonic acid (PEI-GalA) through amidation. Both polymers were PEGylated. Mixing of the resulting two low-MW polymers gave a crosslinked high-MW polymer as a result of multivalent PEI-PBA-GalA-PEI B-ester formations and thus protecting the boronic functions. This high-MW polymer has a high cationic charge at physiological pH which was applied to bind anionic plasmid DNA (pDNA) through multivalent electrostatic interactions. In the slightly acidic tumor environment, some PBA-GalA esters were hydrolyzed to expose PBA moieties for targeting Neu5Ac at cancer cells to promote cellular uptake. At the low pH and the relatively very high ATP concentration inside the tumor cells, the high-MW polymer was disassembled because the PEI-PBA-GalA-PEI ester bonds were broken due to competing PEI-PBA-ATP interactions. This resulted in the release of the pDNA because the cationic charges of the two low-MW fragments (PEI-PBA-ATP and PBA-GalA) were too low to maintain the electrostatic binding of pDNA. In an analogous gene therapy procedure but now with PEGylated catechol instead of GalA, siRNA was delivered to tumor cells [304]. Several other studies using similar strategies have been reported for the transfection of siRNAs [305,306].

The dendrimer poly(amidoamine) (PAMAM) has also been utilized as a cationic carrier in cancer gene therapy. To this aim, it was linked to 3-S-PBA through a PEG_{5k}-chain. This carrier has been employed for the transfection of siRNAs Bcl-3 [307], and microRNA miR-34a [158].

Direct attachment of 4-carboxy-PBA (by amidation) to PAMAM has been applied in the construction of other carriers for gene therapy, now with short guanine-cytosine rich DNA [157] or the DNA-based enzyme Dz13 [159]. It should be noted that B-ester formation between PBA and the *cis*-diol moieties of RNA may tighten the binding to the PAMAM carrier.

The PBA-Neu5Ac interaction has also been applied for the selective delivery of mRNA (tumor suppressor p53 mRNA or Cas9 mRNA) to cancer cells in gene therapy and genome editing [308]. To this end, PBA was conjugated to a cationic lipid (PBA-BADP, see Fig. 23) followed by self-assembly into NPs through electrostatic interactions. These NPs had PBA at the surface, which facilitated cell uptake (see Fig. 23).

Recently, a polyplex formulation has been devised for oral delivery of CRISPR. Oral delivery requires protection of the plasmid against degradation in the intestinal tract [118]. A low MW chitosan-PEI copolymer was grafted with 3-fluoro-4-carboxy-PBA. The PBA moiety is hydrophobic at low pH and thus protects the encapsulated plasmid. In the intestine, PBA-SA interactions facilitate transport across the mucus layer, and upon arrival in the target cells, PBA forms B-esters with ATP in late endosomes (pH 5.5), which promotes plasmid release, partly due to the hydrophobicity of ATP-PBA at this relatively low pH [309].

9.4. Boron neutron capture therapy agents

4-Boronophenylalanine (BPA) is frequently clinically employed for the treatment of gliomas and cutaneous melanoma with BNCT [310]. The alanine residue in this compound is recognized by amino acid transporters that are usually over-expressed on cancer cells. The boronic function serves as a carrier of ^{10}B for electron capture. To increase the solubility, this agent is commonly administered after esterification of the boronic function with Fru or another saccharide. A disadvantage of BPA is that it is readily pumped out of the cell by an antiport mechanism. Therefore, micellar NPs (10 nm diameter) fabricated of PBA-PEG-*b*-PLA have been proposed as an alternative [311]. Selective accumulation thereof in cancer cells is facilitated by EPR combined with active targeting of Neu5Ac by the boronic functions on the surface of the micelles. A Gd^{3+}-conjugate of Gd-DTPA and BPA (**16**, see Fig. 24) has been proposed as a theranostic agent for combined MRI and neutron-capture therapy through ^{10}B and ^{157}Gd [312].

9.5. Image-guided therapy and multimodal therapy

Many of the investigations on Neu5Ac-PBA interactions have used imaging techniques by attaching reporter groups to the NPs involved [249,250]. Fluorescence imaging, MRI, PET, SPECT, and SERS are applied as detection techniques, frequently in cell studies, but

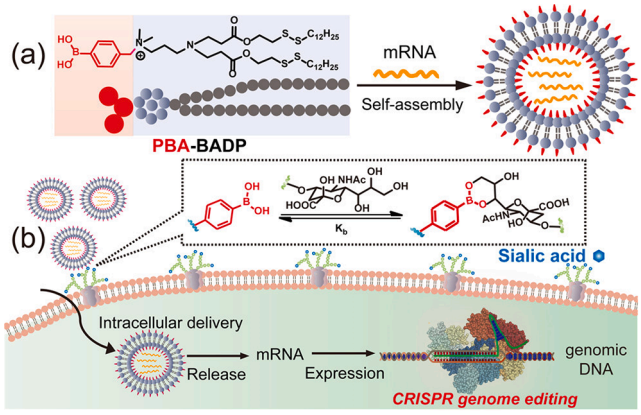

Fig. 23. (a) The self-assembly of PBA–BADP and mRNA into NPs. (b) PBA and Neu5Ac-promoted endocytosis of PBA–BADP/mRNA NPs for cancer cell-selective genome editing. Copied with permission from [308]. Copyright 2019 American Chemical Society.

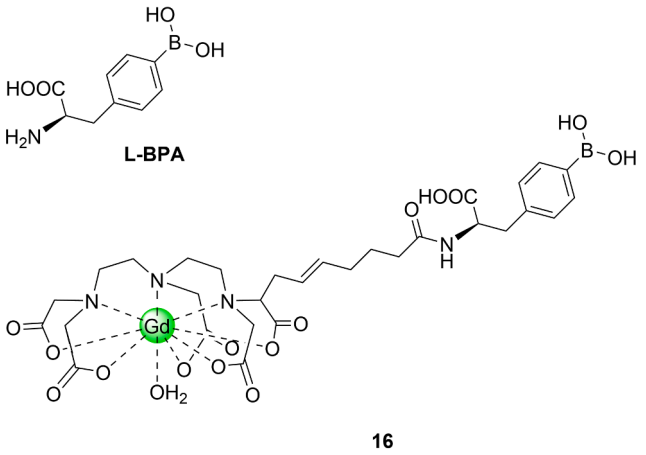

Fig. 24. Schematic representation of structures of the BNCT agent L-BPA and the BNCT-MRI agent **16**. The charges in **16** have been omitted for clarity.

sometimes also *in vivo*. Combinations of chemotherapy with other therapeutic techniques are often designed to tackle the problem of multi-drug resistance.

A platform for image-guided therapy has been developed by dispersing Fe_3O_4 NPs in the synthetic nanoclay laponite (LAP) [313]. These NPs were coated with polydopamine (PDA) whose catechol groups were exploited to anchor SH-PEG-CONH-PBA. The obtained NPs (LAP-Fe_3O_4@PDA-PEG-PBA) have a high transverse NMR relaxivity (r_2 = 266 $s^{-1}mM^{-1}$), making them suitable as a negative contrast agent in T_2-weighted MRI, while also showing efficiency as a photoacoustic imaging agent. Moreover, in addition, they can be used in PTT with NIR absorption. A somewhat similar approach was followed by Cao et al. in the design of a multimodal theranostic. Au-bipyramids (AuBP) were covered with a PDA coat [314]. The catechol groups of this coat were exploited to anchor PBA-conjugated with the fluorescent dye BODIPY. The construct AuBP@PDA@PBA-BODIPY did not show fluorescence or development of reactive oxygen species due to the quenching effect of the AuBP@PDA moiety, but in the presence of Neu5Ac at pH 7.4, the Neu5Ac displaced the Au@PDA turning on the fluorescence and photoactivity of PBA-BODIPY. The accompanying alteration of the Au surface was monitored by SERS.

Another Neu5Ac-targeting MRI-fluorescence agent was prepared by conjugating polylysine with Gd-DTPA, PBA, and rhodamine [315]. To reduce the cytotoxicity, the remaining unconjugated amino groups were reacted with 3,4,5,6-tetrahydrophtalic anhydride which resulted in the reversal of the molecular charge from positive to negative. At pH 5, the zeta potential became positive again suggesting that the tetrahydrophtalic anhydride group splits off in the slightly acidic tumor environment, which will facilitate the tumor cell uptake. However, confocal microscopy on HepG2 cancer cells showed that most of this agent was accumulated on the cell surface. Glc did not affect the affinity of the contrast agent for Neu5Ac.

Peptide nanotubes (diameter 50 nm, length optimized 200 nm) with 4-carboxy-PBA functions on the surface for multivalent PBS-Neu5Ac interactions have been loaded with the anticancer drug 7-ethyl-10-hydroxycamptothecin (SN38), and the NIR-activated photosensitizer indocyanine green for combined chemotherapy and PDT [177]. Another example of an agent for chemo-PDT is the dendrimeric system depicted in Fig. 22. [299]. Carbon nanotubes loaded with superparamagnetic iron oxide NPs, porphyrin, and a PEG_{5000} derivative with 4 PBA groups as Neu5Ac-targeting functions have been employed for combined T_2-weighted MRI, fluorescence imaging, and PDT [296].

A platform for combined fluorescence imaging and PDT has been constructed from 4-(4-(pyren-1-yl)butyramido)phenylboronic acid as a building block for self-assembling into hydrophilic nanorods that were

applied for PDT [316]. Cell studies indicated that the cell uptake was rather slow, and the imaging agent predominantly was found on the cell surface. It was suggested that this might be due to the larger average curvature radius of non-spherical particles, the hydrophilicity, as well as the electronegativity. Therefore, these NPs have been suggested to be suitable to study the sialylation on cell surfaces.

Multimodal and multi-drug delivery systems have been constructed by decorating NPs with PEG to increase the blood circulation time, PBA for Neu5Ac-recognition, QDs for PDT and fluorescence imaging, and ^{99m}Te-DTPA for SPECT [165,181].

10. Conclusions

In an aqueous solution, boronic acids bind Neu5Ac with optimal affinity through the two of its exocyclic O-atoms. The resulting B-ester group is neutral and has a tetrahedral B-atom, indicating that another O- or N-atom must form a dative bond with the B-atom. The exact structure of these B-esters is not yet known, but most likely the B-atom has a dative bond with the N- or O-atom of the 5-N-Ac group. A complicated series of equilibria exists among the various B-containing species that are pH-dependent. The affinity between boronic acids and Neu5Ac generally increases with a decrease in pH and the ester formation is completely reversible and has a pH profile that can be tuned by substituents in the boronic acid. The pH-dependent interactions between Neu5Ac and the other monosaccharides present in glycocalyces are complementary, the other monosaccharides form negatively charged B-ester moieties with optimal stability at pH $>$ 9, while the stability of these B-esters is very low at physiological pH. Only diols that are highly pre-organized for B-ester formation can compete with Neu5Ac at physiological pH. Diols of this type include the ribose moiety of ATP and the catechol moiety of dopamine. B-esters of these alcohols have very high stabilities at pH $>$ 8 and decreasing stabilities at lower pH, but at physiological pH, the stabilities of their B-esters are still high enough to compete with Neu5Ac at physiological pH. These properties make boronic acids ideal targeting groups for Neu5Ac groups that occur in high densities as the end group of glycocalyces in mucins and tumors. For the latter applications, NPs with multiple boronic acids are very suitable, since multivalent interactions between the probe and the cell surface enhance the affinity and make the pH effects steeper. Often, the pH in the micro-environment of tumors is slightly acidic, as well as in endosomes and lysosomes. Consequently, pH is a suitable endogenous trigger in drug delivery with NPs facilitated by boronic acid - Neu5Ac mediated endocytosis. Other parameters including the concentrations of Glc, ATP, and GSH may differ substantially between the extra- and intracellular environments of tumor cells and can also serve as endogenous triggers. Surprisingly, almost exclusively agents based on PBA and pyridine boronic acids are studied. It may be expected that including existing B-based clinical pharmaceuticals in nanoparticulate drug carriers will increase their selectivity for tumors and decrease harmful side effects on healthy tissues.

Declaration of Competing Interest

The authors declare that they have no known competing financial interests or personal relationships that could have appeared to influence the work reported in this paper.

Data availability

Data will be made available on request.

References

[1] D.B. Werz, R. Ranzinger, S. Herget, A. Adibekian, C.-W. von der Lieth, P. H. Seeberger, Exploring the structural diversity of mammalian carbohydrates ("glycospace") by statistical databank analysis, ACS Chem. Biol. 2 (2007) 685–691, https://doi.org/10.1021/cb700178s.

[2] S.K. Guin, T. Velasco-Torrijos, E. Dempsey, Explorations in a galaxy of sialic acids: a review of sensing horizons, motivated by emerging biomedical and nutritional relevance, Sens. Diagn. 1 (2022) 10–70, https://doi.org/10.1039/D1SD00023C.

[3] A.L. Lewis, X. Chen, R.L. Schnaar, A. Varki, Sialic acids and other nonulosonic acids., in: A. Varki, R.D. Cummings, J.D. Esko, P. Stanley, G.W. Hart, M. Aebi, D. Mohnen, T. Kinoshita, N.H. Packer, J.H. Prestegard, R.L. Schnaar, P.H. Seeberger (Eds.) Essentials of Glycobiology [Internet], Cold Spring Harbor Laboratory Press, Cold Spring Harbor (NY), 2022, doi:10.1101/glycobiology.4e.015.

[4] A. Varki, Multiple changes in sialic acid biology during human evolution, Glycoconjugate J. 26 (2009) 231–245, https://doi.org/10.1007/s10719-008-9183-z.

[5] P.H. Seeberger, Monosaccharide diversity, in: A. Varki, R.D. Cummings, J.D. Esko, P. Stanley, G.W. Hart, M. Aebi, D. Mohnen, T. Kinoshita, N.H. Packer, J.H. Prestegard, R.L. Schnaar, P.H. Seeberger (Eds.) Essentials of Glycobiology [Internet], Cold Spring Harbor Laboratory Press, Cold Spring Harbor (NY), 2022, doi:10.1101/glycobiology.4e.002.

[6] A. Varki, R.L. Schnaar, R. Schauer, Sialic acids and other nonulosonic acids, in: A. Varki, R.D. Cummings, J.D. Esko, P. Stanley, G.W. Hart, M. Aebi, A.G. Darvill, T. Kinoshita, N.H. Packer, J.H. Prestegard, R.L. Schnaar, P.H. Seeberger (Eds.) Essentials of Glycobiology [Internet], Cold Spring Harbor Laboratory Press, Cold Spring Harbor (NY), 2017, doi:10.1101/glycobiology.3e.015.

[7] T. Shinozuka, Changes in human red blood cells during aging in vivo, Keio J. Med. 43 (1994) 155–163, https://doi.org/10.2302/kjm.43.155.

[8] A. Varki, R. Kannagi, B.P. Toole, Glycosylation changes in cancer, in: A. Varki, R. D. Cummings, J.D. Esko, H.H. Freeze, P. Stanley, C.R. Bertozzi, G.W. Hart, M.E. Etzler (Eds.) Essentials of Glycobiology, Cold Spring Harbor Laboratory Press, Cold Spring Harbor (NY), 2017, doi:10.1101/glycobiology.3e.047.

[9] B.N. Vajaria, K.R. Patel, R. Begum, P.S. Patel, Sialylation: An avenue to target cancer cells, Pathol. Oncol. Res. 22 (2016) 443–447, https://doi.org/10.1007/s12253-015-0033-6.

[10] A. Harduin-Lepers, M.-A. Krzewinski-Recchi, F. Colomb, F. Foulquier, S. Groux-Degroote, P. Delannoy, Sialyltransferases functions in cancers, Front. Biosci., Elite Ed., 4 (2012) 499–515, https://doi.org/10.2741/e396.

[11] M.M. Fuster, J.D. Esko, The sweet and sour of cancer: glycans as novel therapeutic targets, Nat. Rev. Cancer 5 (2005) 526–542, https://doi.org/10.1038/nrc1649.

[12] D.H. Dube, C.R. Bertozzi, Glycans in cancer and inflammation — potential for therapeutics and diagnostics, Nat. Rev. Drug Discovery 4 (2005) 477–488, https://doi.org/10.1038/nrd1751.

[13] A. Varki, Sialic acids in human health and disease, Trends Mol. Med. 14 (2008) 351–360, https://doi.org/10.1016/j.molmed.2008.06.002.

[14] O.M.T. Pearce, H. Läubli, Sialic acids in cancer biology and immunity, Glycobiology 26 (2015) 111–128, https://doi.org/10.1093/glycob/cwv097.

[15] S.S. Pinho, C.A. Reis, Glycosylation in cancer: mechanisms and clinical implications, Nat. Rev. Cancer 15 (2015) 540–555, https://doi.org/10.1038/nrc3982.

[16] C. Büll, M.H. den Brok, G.J. Adema, Sweet escape: Sialic acids in tumor immune evasion, Biochim. Biophys. Acta, Rev. Cancer 1846 (2014) 238–246, https://doi.org/10.1016/j.bbcan.2014.07.005.

[17] C. Büll, M.A. Stoel, M.H. den Brok, G.J. Adema, Sialic acids sweeten a tumor's life, Cancer Res., 74 (2014) 3199-3204, doi:10.1158/0008-5472.Can-14-0728.

[18] A. Cazet, S. Julien, M. Bobowski, M.-A. Krzewinski-Recchi, A. Harduin-Lepers, S. Groux-Degroote, P. Delannoy, Consequences of the expression of sialylated antigens in breast cancer, Carbohydr. Res. 345 (2010) 1377–1383, https://doi.org/10.1016/j.carres.2010.01.024.

[19] I. Martinez-Duncker, R. Salinas-Marin, C. Martinez-Duncker, Towards *in vivo* imaging of cancer sialylation, Int. J. Mol. Imaging 2011 (2011), 283497, https://doi.org/10.1155/2011/283497.

[20] B. Adamczyk, T. Tharmalingam, P.M. Rudd, Glycans as cancer biomarkers, Biochim. Biophys. Acta Gen. Subj. 2012 (1820) 1347–1353, https://doi.org/10.1016/j.bbagen.2011.12.001.

[21] A. Laganà, B. Pardo-Martínez, A. Marino, G. Fago, M. Bizzarri, Determination of serum total lipid and free N-acetylneuraminic acid in genitourinary malignancies by fluorimetric high performance liquid chromatography. Relevance of free N-acetylneuraminic acid as tumour marker, Clin. Chim. Acta 243 (1995) 165–179, https://doi.org/10.1016/0009-8981(95)06165-7.

[22] M.A. Stanczak, N. Rodrigues Mantuano, N. Kirchhammer, D.E. Sanin, F. Jacob, R. Coelho, A.V. Everest-Dass, J. Wang, M.P. Trefny, G. Monaco, A. Bärenwaldt, M. A. Gray, A. Petrone, A.S. Kashyap, K. Glatz, B. Kasenda, K. Normington, J. Broderick, L.i. Peng, O.M.T. Pearce, E.L. Pearce, C.R. Bertozzi, A. Zippelius, H. Läubli, Targeting cancer glycosylation repolarizes tumor-associated macrophages allowing effective immune checkpoint blockade, Sci. Transl. Med. 14 (669) (2022), https://doi.org/10.1126/scitranslmed.abj1270.

[23] C. Dhar, A. Sasmal, A. Varki, From serum sickness to xenosialitis: Past, present, and future significance of the non-human sialic acid Neu5Gc, Front. Immunol. 10 (2019), https://doi.org/10.3389/fimmu.2019.00807.

[24] F.J. Krolikowski, K. Reuter, T.P. Waalkes, S.M. Sieber, R.H. Adamson, Serum sialic acid levels in lung cancer patients, Pharmacology 14 (1976) 47–51, https://doi.org/10.1159/000136578.

[25] G.N. Raval, L.J. Parekh, D.D. Patel, F.P. Jha, R.N. Sainger, P.S. Patel, Clinical usefulness of alterations in sialic acid, sialyl transferase and sialoproteins in breast cancer, Indian J. Clin. Biochem. 19 (2004) 60–71, https://doi.org/10.1007/bf02894259.

[26] M.A. Crook, P. Tutt, H. Simpson, J.C. Pickup, Serum sialic acid and acute phase proteins in type 1 and type 2 diabetes mellitus, Clin. Chim. Acta 219 (1993) 131–138, https://doi.org/10.1016/0009-8981(93)90204-H.

[27] L. Chrostek, B. Cylwik, W. Korcz, A. Krawiec, A. Koput, Z. Supronowicz, M. Szmitkowski, Serum free sialic acid as a marker of alcohol abuse, Alcohol: Clin. Exp. Res. 31 (6) (2007) 996–1001, https://doi.org/10.1111/j.1530-0277.2007.00392.x.

[28] P. Sillanaukee, M. Pönniö, I.P. Jääskeläinen, Occurrence of sialic acids in healthy humans and different disorders, Eur. J. Clin. Invest. 29 (1999) 413–425, https://doi.org/10.1046/j.1365-2362.1999.00485.x.

[29] A. Carter, N.H. Martin, Serum sialic acid levels in health and disease, J. Clin. Pathol. 15 (1962) 69–72, https://doi.org/10.1136/jcp.15.1.69.

[30] C. Yi, J.-H. Lee, B.S. Kwak, M.X. Lin, H.O. Kim, H.-I. Jung, Diagnosis of diabetes mellitus using sialic acid expression of erythrocyte and a microfluidic resistive temperature detector (micro-RTD), Sens. Actuators, B 191 (2014) 305–312, https://doi.org/10.1016/j.snb.2013.10.004.

[31] A. Matsumoto, S. Osawa, T. Arai, Y. Maejima, H. Otsuka, Y. Miyahara, Potentiometric determination of circulating glycoproteins by boronic acid end-functionalized poly(ethylene glycol)-modified electrode, Bioconjugate Chem. 32 (2021) 239–244, https://doi.org/10.1021/acs.bioconjchem.0c00657.

[32] L. Nguyen, K.A. McCord, D.T. Bui, K.M. Bouwman, E.N. Kitova, M. Elaish, D. Kumawat, G.C. Daskhan, I. Tomris, L. Han, P. Chopra, T.J. Yang, S.D. Willows, A.L. Mason, L.K. Mahal, T.L. Lowary, L.J. West, S.D. Hsu, T. Hobman, S. M. Tompkins, G.J. Boons, R.P. de Vries, M.S. Macauley, J.S. Klassen, Sialic acid-containing glycolipids mediate binding and viral entry of SARS-CoV-2, Nat. Chem. Biol. 18 (2022) 81–90, https://doi.org/10.1038/s41589-021-00924-1.

[33] R. Uraki, Y. Kawaoka, Host glycolipids in SARS-CoV-2 entry, Nat. Chem. Biol. 18 (2022) 6–7, https://doi.org/10.1038/s41589-021-00923-2.

[34] A. Gonzalez-Gil, R.L. Schnaar, Siglec ligands, Cells 10 (2021) 1260, https://doi.org/10.3390/cells10051260.

[35] R.N. Knibbs, S.E. Osborne, G.D. Glick, I.J. Goldstein, Binding determinants of the sialic acid-specific lectin from the slug Limax flavus, J. Biol. Chem. 268 (1993) 18524–18531, https://doi.org/10.1016/S0021-9258(17)46659-2.

[36] P.R. Crocker, J.C. Paulson, A. Varki, Siglecs and their roles in the immune system, Nat. Rev. Immunol. 7 (2007) 255–266, https://doi.org/10.1038/nri2056.

[37] T.M. Altamore, P.J. Duggan, G.Y. Krippner, Improving the membrane permeability of sialic acid derivatives, Bioorg. Med. Chem. 14 (2006) 1126–1133, https://doi.org/10.1016/j.bmc.2005.09.028.

[38] B.C. Das, M. Adil Shareef, S. Das, N.K. Nandwana, Y. Das, M. Saito, L.M. Weiss, Boron-Containing heterocycles as promising pharmacological agents, Bioorg. Med. Chem. 63 (2022) 116748, https://doi.org/10.1016/j.bmc.2022.116748.

[39] K. Messner, B. Vuong, G.K. Tranmer, The boron advantage: the evolution and diversification of boron's applications in medicinal chemistry, Pharmaceuticals 15 (2022) 264, https://doi.org/10.3390/ph15030264.

[40] J. Boeseken, The use of boric acid for the determination of the configuration of carbohydrates, Adv. Carbohydr. Chem. 4 (1949) 189–210, https://doi.org/10.1016/S0096-5332(08)60049-1.

[41] S.D. Bull, M.G. Davidson, J.M.H. van den Elsen, J.S. Fossey, A.T.A. Jenkins, Y.-B. Jiang, Y. Kubo, F. Marken, K. Sakurai, J. Zhao, T.D. James, Exploiting the reversible covalent bonding of boronic acids: recognition, sensing, and assembly, Acc. Chem. Res. 46 (2013) 312–326, https://doi.org/10.1021/ar300130w.

[42] W. Zhai, X. Sun, T.D. James, J.S. Fossey, Boronic acid-based carbohydrate sensing, Chem. - Asian J. 10 (2015) 1836–1848, https://doi.org/10.1002/asia.201500444.

[43] A. Matsumoto, Y. Miyahara, A. Matsumoto, 'Borono-lectin' based engineering as a versatile platform for biomedical applications, Sci. Technol. Adv. Mater. 19 (2018) 18–30, https://doi.org/10.1080/14686996.2017.1411143.

[44] J.P.M. António, R. Russo, C.P. Carvalho, P.M.S.D. Cal, P.M.P. Gois, Boronic acids as building blocks for the construction of therapeutically useful bioconjugates, Chem. Soc. Rev. 48 (2019) 3513–3536, https://doi.org/10.1039/C9CS00184K.

[45] L.I. Bosch, T.M. Fyles, T.D. James, Binary and ternary phenylboronic acid complexes with saccharides and Lewis bases, Tetrahedron 60 (2004) 11175–11190, https://doi.org/10.1016/j.tet.2004.08.046.

[46] J.A. Peters, Interactions between boric acid derivatives and saccharides in aqueous media: Structures and stabilities of resulting esters, Coord. Chem. Rev. 268 (2014) 1–22, https://doi.org/10.1016/j.ccr.2014.01.016.

[47] T. Klepach, I. Carmichael, A.S. Serianni, ^{13}C-labeled N-acetyl-neuraminic acid in aqueous solution: detection and quantification of acyclic keto, keto hydrate, and enol forms by ^{13}C NMR spectroscopy, J. Am. Chem. Soc. 130 (2008) 11892–11900, https://doi.org/10.1021/ja077565g.

[48] H. Friebolin, M. Supp, R. Brossmer, G. Keilich, D. Ziegler, Proton NMR studies on the mutarotation of N-acetyl-D-neuraminic acid, Angew. Chem., Int. Ed. Engl. 19 (1980) 208–209, https://doi.org/10.1002/anie.198002081.

[49] S.W. Fesik, W.E. Kohlbrenner, R.T. Gampe, E.T. Olejniczak, Interconversion rates of tautomers of 3-deoxy-d-manno-octulosonic acid (KDO) from a quantitative analysis of two-dimensional n.m.r. exchange data, Carbohydr. Res. 153 (1) (1986) 136–140, https://doi.org/10.1016/S0008-6215(00)90203-9.

[50] H. Friebolin, P. Kunzelmann, M. Supp, R. Brossmer, G. Keilich, D. Ziegler, Proton NMR spectroscopic study of the mutarotation of N-acetyl-D-neuraminic acid. The pH-dependence of the mutarotation rate, Tetrahedron Lett 22 (1981) 1383–1386, https://doi.org/10.1016/S0040-4039(01)90327-2.

[51] P. Stanley, R.D. Cummings, Structures common to different glycans, in: A. Varki, R.D. Cummings, J.D. Esko, P. Stanley, G.W. Hart, M. Aebi, A.G. Darvill, T. Kinoshita, N.H. Packer, J.H. Prestegard, R.L. Schnaar, P.H. Seeberger (Eds.) Essentials of Glycobiology [Internet]. Cold Spring Harbor Laboratory Press, Cold Spring Harbor (NY), 2017, doi:10.1101/glycobiology.3e.014.

[52] F. Jin, F. Wang, The physiological and pathological roles and applications of sialyl Lewis x, a common carbohydrate ligand of the three selectins, Glycoconj. J. 37 (2020) 277–291, https://doi.org/10.1007/s10719-020-09912-4.

[53] C. Sato, K. Kitajima, Polysialylation and disease, Mol. Aspects Med. 79 (2021), 100892, https://doi.org/10.1016/j.mam.2020.100892.

[54] A.P. May, R.C. Robinson, M. Vinson, P.R. Crocker, E.Y. Jones, Crystal structure of the n-terminal domain of sialoadhesin in complex with 3′ sialyllactose at 1.85 Å resolution, Mol. Cell 1 (1998) 719–728, https://doi.org/10.1016/S1097-2765(00)80071-4.

[55] M.F. Czarniecki, E.R. Thornton, Carbon-13 nuclear magnetic resonance spin-lattice relaxation in the N-acylneuraminic acids. Probes for internal dynamics and conformational analysis, J. Am. Chem. Soc. 99 (1977) 8273–8279, https://doi.org/10.1021/ja00467a025.

[56] D.G. Hall, Editor, Boronic Acids, volume 1: Preparation and Applications in Organic Synthesis, Medicine and Materials, Second Completely Revised Edition, Wiley-VCH Verlag GmbH & Co. KGaA, 2011.

[57] M. Van Duin, J.A. Peters, A.P.G. Kieboom, H. Van Bekkum, Studies on borate esters. I. The pH dependence of the stability of esters of boric acid and borate in aqueous medium as studied by boron-11 NMR, Tetrahedron 40 (1984) 2901–2911, https://doi.org/10.1016/S0040-4020(01)91300-6.

[58] J.C. Norrild, H. Eggert, Evidence for mono- and bisdentate boronate complexes of glucose in the furanose form. Application of $^{1}J_{C\text{-}C}$ coupling constants as a structural probe, J. Am. Chem. Soc. 117 (1995) 1479–1484, https://doi.org/10.1021/ja00110a003.

[59] M. Rietjens, P.A. Steenbergen, Crosslinking mechanism of boric acid with diols revisited, Eur. J. Inorg. Chem. 2005 (2005) 1162–1174, https://doi.org/10.1002/ejic.200400674.

[60] S. Iwatsuki, S. Nakajima, M. Inamo, H.D. Takagi, K. Ishihara, Which is reactive in alkaline solution, boronate ion or boronic acid? Kinetic evidence for reactive trigonal boronic acid in an alkaline solution, Inorg. Chem. 46 (2007) 354–356, https://doi.org/10.1021/ic0615372.

[61] S. Iwatsuki, Y. Kanamitsu, H. Ohara, E. Watanabe, K. Ishihara, Higher reactivity of 3-pyridinium boronic acid compared with 3-pyridinium boronate ion toward 4-isopropyltropolone in acidic aqueous solution: fundamental reaction analyses for an effective organoboron-based chemosensor, J. Phys. Org. Chem. 25 (2012) 760–768, https://doi.org/10.1002/poc.2915.

[62] J.W. Tomsho, S.J. Benkovic, Elucidation of the mechanism of the reaction between phenylboronic acid and a model diol, alizarin red s, J. Org. Chem. 77 (2012) 2098–2106, https://doi.org/10.1021/jo202250d.

[63] J.P. Lorand, J.O. Edwards, Polyol complexes and structure of the benzeneboronate ion, J. Org. Chem. 24 (1959) 769–774, https://doi.org/10.1021/jo01088a011.

[64] M.A. Martínez-Aguirre, R. Villamil-Ramos, J.A. Guerrero-Alvarez, A. K. Yatsimirsky, Substituent effects and pH profiles for stability constants of arylboronic acid diol esters, J. Org. Chem. 78 (2013) 4674–4684, https://doi.org/10.1021/jo400617j.

[65] M.A. Martínez-Aguirre, F. Medrano, S. Ramírez-Rave, A.K. Yatsimirsky, Analysis of the relative stability of trigonal and tetrahedral boronate cyclic esters in terms of boronic acid and diol acidities and the strain release effect, J. Phys. Org. Chem. (2022) e4425, https://doi.org/10.1002/poc.4425.

[66] R. van den Berg, J.A. Peters, H. van Bekkum, The structure and (local) stability-constants of borate esters of monosacchharides and disaccharides as studied by B-11 and C-13 NMR-spectroscopy, Carbohydr. Res. 253 (1994) 1–12, https://doi.org/10.1016/0008-6215(94)80050-2.

[67] M. Van Duin, J.A. Peters, A.P.G. Kieboom, H. Van Bekkum, Studies on borate esters. II. Structure and stability of borate esters of polyhydroxycarboxylates and related polyols in aqueous alkaline media as studied by boron-11 NMR, Tetrahedron 41 (1985) 3411–3421, https://doi.org/10.1016/S0040-4020(01)96693-1.

[68] K. Oshima, H. Toi, Y. Aoyama, Complexation of phenylboronic acid with alkyl glycopyranosides and related polyols as studied by 11B NMR spectroscopy, Carbohydr. Lett. 1 (1995) 223–230.

[69] X. Wu, Z. Li, X.-X. Chen, J.S. Fossey, T.D. James, Y.-B. Jiang, Selective sensing of saccharides using simple boronic acids and their aggregates, Chem. Soc. Rev. 42 (2013) 8032–8048, https://doi.org/10.1039/C3CS60148J.

[70] M. Bérubé, M. Dowlut, D.G. Hall, Benzoboroxoles as efficient glycopyranoside-binding agents in physiological conditions: Structure and selectivity of complex formation, J. Org. Chem. 73 (2008) 6471–6479, https://doi.org/10.1021/jo800788s.

[71] L. Zhu, S.H. Shabbir, M. Gray, V.M. Lynch, S. Sorey, E.V. Anslyn, A structural investigation of the N−B interaction in an o-(N, N-dialkylaminomethyl) arylboronate system, J. Am. Chem. Soc. 128 (2006) 1222–1232, https://doi.org/10.1021/ja055817c.

[72] H. Nöth, H. Vahrenkamp, Kernresonanzuntersuchungen an Bor-Verbindungen, I. 11B-Kernresonanzspektren von Boranen mit Substituenten aus der ersten Achterperiode des Periodensystems, Chem. Ber. 99 (1966) 1049–1067, https://doi.org/10.1002/cber.19660990347.

[73] B. Wrackmeyer, Nuclear magnetic resonance spectroscopy of boron compounds containing two-, three- and four-coordinate boron, Annu. Rep. NMR Spectrosc. 20 (1988) 61–203, https://doi.org/10.1016/S0066-4103(08)60170-2.

[74] J.W. Akitt, W.S. McDonald, Arrangements of ligands giving low electric field gradients, J. Magn. Reson. 58 (1984) 401–412, https://doi.org/10.1016/0022-2364(84)90144-6.

[75] H. Nöth, B. Wrackmeyer, Tables of 11B-NMR data, in: H. Nöth, B. Wrackmeyer (Eds.), Nuclear Magnetic Resonance Spectroscopy of Boron Compounds, Springer Berlin Heidelberg, Berlin, Heidelberg, 1978, pp. 109–429.

[76] P. Kluefers, O. Labisch, Polyol metal complexes. Part 44. Phenylboronic acid esters of the C4 sugar alcohols erythritol and L-threitol, Z. Anorg. Allg. Chem. 629 (2003) 1441–1445, https://doi.org/10.1002/zaac.200300100.

[77] Y. Miyazaki, T. Fujimori, H. Okita, T. Hirano, K. Yoshimura, Thermodynamics of complexation reactions of borate and phenylboronate with diol, triol and tetritol, Dalton Trans. 42 (2013) 10473–10486, https://doi.org/10.1039/c3dt50998b.
[78] T. Burgemeister, R. Grobe-Einsler, R. Grotstollen, A. Mannschreck, G. Wulff, Fast thermal breaking and formation of a B-N bond in 2-(aminomethyl) benzeneboronates 1), Chem. Ber. 114 (1981) 3403–3411, https://doi.org/10.1002/cber.19811141021.
[79] S.X. Cai, J.F.W. Keana, o-Acetamidophenylboronate esters stabilized toward hydrolysis by an intramolecular oxygen-boron interaction: potential linkers for selective bioconjugation via vicinal diol moieties of carbohydrates, Bioconjugate Chem. 2 (1991) 317–322, https://doi.org/10.1021/bc00011a004.
[80] S. Nishitani, Y. Maekawa, T. Sakata, Understanding the molecular structure of the sialic acid-phenylboronic acid complex by using a combined NMR spectroscopy and DFTstudy: Toward sialic acid detection at cell membranes, ChemistryOpen 7 (2018) 513–519, https://doi.org/10.1002/open.201800071.
[81] K. Djanashvili, L. Frullano, J.A. Peters, Molecular recognition of sialic acid end groups by phenylboronates, Chem. Eur. J. 11 (2005) 4010–4018, https://doi.org/10.1002/chem.200401335.
[82] J.A. Peters, K. Djanashvili, Unpublished results.
[83] H. Otsuka, E. Uchimura, H. Koshino, T. Okano, K. Kataoka, Anomalous binding profile of phenylboronic acid with n-acetylneuraminic acid (Neu5Ac) in aqueous solution with varying pH, J. Am. Chem. Soc. 125 (2003) 3493–3502, https://doi.org/10.1021/ja021303r.
[84] A. Matsumoto, A.J. Stephenson-Brown, T. Khan, T. Miyazawa, H. Cabral, K. Kataoka, Y. Miyahara, Heterocyclic boronic acids display sialic acid selective binding in a hypoxic tumor relevant acidic environment, Chem. Sci. 8 (9) (2017) 6165–6170, https://doi.org/10.1039/c7sc01905j.
[85] E. Uchimura, H. Otsuka, T. Okano, Y. Sakurai, K. Kataoka, Totally synthetic polymer with lectin-like function: Induction of killer cells by the copolymer of 3-acrylamidophenylboronic acid with N, N-dimethylacrylamide, Biotechnol. Bioeng. 72 (2001) 307–314, https://doi.org/10.1002/1097-0290(20010205)72:3<307::AID-BIT7>3.0.CO;2-E.
[86] Y. Matsumura, K. Kataoka, Preclinical and clinical studies of anticancer agent-incorporating polymer micelles, Cancer Sci. 100 (2009) 572–579, https://doi.org/10.1111/j.1349-7006.2009.01103.x.
[87] A. Matsumoto, N. Sato, K. Kataoka, Y. Miyahara, Noninvasive sialic acid detection at cell membrane by using phenylboronic acid modified self-assembled monolayer gold electrode, J. Am. Chem. Soc. 131 (2009) 12022–12023, https://doi.org/10.1021/ja902964m.
[88] A. Matsumoto, H. Cabral, N. Sato, K. Kataoka, Y. Miyahara, Assessment of tumor metastasis by the direct determination of cell-membrane sialic acid expression, Angew. Chem. Int. Ed. 49 (2010) 5494–5497, https://doi.org/10.1002/anie.201001220.
[89] A. Matsumoto, N. Sato, H. Cabral, K. Kataoka, Y. Miyahara, Self-assembled molecular gate field effect transistor for label free sialic acid detection at cell membrane, Procedia Eng. 5 (2010) 926–929, https://doi.org/10.1016/j.proeng.2010.09.261.
[90] S. Deshayes, H. Cabral, T. Ishii, Y. Miura, S. Kobayashi, T. Yamashita, A. Matsumoto, Y. Miyahara, N. Nishiyama, K. Kataoka, Phenylboronic acid-installed polymeric micelles for targeting sialylated epitopes in solid tumors, J. Am. Chem. Soc. 135 (2013) 15501–15507, https://doi.org/10.1021/ja406406h.
[91] M. Sanjoh, Y. Miyahara, K. Kataoka, A. Matsumoto, Phenylboronic acids-based diagnostic and therapeutic applications, Anal. Sci. 30 (2014) 111–117, https://doi.org/10.2116/analsci.30.111.
[92] P. Mi, H. Cabral, K. Kataoka, Ligand-installed nanocarriers toward precision therapy, Adv. Mater. 32 (2020) 1902604, https://doi.org/10.1002/adma.201902604.
[93] T. Khan, K. Igarashi, A. Tanabe, T. Miyazawa, S. Fukushima, Y. Miura, Y. Matsumoto, T. Yamasoba, A. Matsumoto, H. Cabral, K. Kataoka, Structural control of boronic acid ligands enhances intratumoral targeting of sialic acid to eradicate cancer stem-like cells, ACS Appl. Bio Mater. 3 (2020) 5030–5039, https://doi.org/10.1021/acsabm.0c00530.
[94] B.E. Collins, S. Sorey, A.E. Hargrove, S.H. Shabbir, V.M. Lynch, E.V. Anslyn, Probing intramolecular B–N interactions in ortho-aminomethyl arylboronic acids, J. Org. Chem. 74 (2009) 4055–4060, https://doi.org/10.1021/jo900187a.
[95] F.C. Fischer, E. Havinga, Thermal and photoinduced deboronations of some pyridine- and benzeneboronate anions, Recl. Trav. Chim. Pays-Bas 93 (1974) 21–24, https://doi.org/10.1002/recl.19740930110.
[96] N. Wellington, S. Macklai, P. Britz-McKibbin, Elucidating the anomalous binding enhancement of isoquinoline boronic acid for sialic acid under acidic conditions: Expanding biorecognition beyond vicinal diols, Chem. - Eur. J. 25 (2019) 15277–15280, https://doi.org/10.1002/chem.201904442.
[97] B.A. Webb, M. Chimenti, M.P. Jacobson, D.L. Barber, Dysregulated pH: a perfect storm for cancer progression, Nat. Rev. Cancer 11 (2011) 671–677, https://doi.org/10.1038/nrc3110.
[98] S. Osawa, A. Matsumoto, Y. Maejima, T. Suzuki, Y. Miyahara, H. Otsuka, Direct observation of cell surface sialylation by atomic force microscopy employing boronic acid–sialic acid reversible interaction, Anal. Chem. 92 (17) (2020) 11714–11720, https://doi.org/10.1021/acs.analchem.0c01705.
[99] Chemical constituents of human blood, in: W.M. Haynes (Ed.) CRC handbook of chemistry and physics, CRC Press, Boca Raton, FL., 2013-2014, pp. 7/45-47.
[100] G. Springsteen, B. Wang, A detailed examination of boronic acid–diol complexation, Tetrahedron 58 (2002) 5291–5300, https://doi.org/10.1016/S0040-4020(02)00489-1.
[101] A. Mahalingam, A.R. Geonnotti, J. Balzarini, P.F. Kiser, Activity and safety of synthetic lectins based on benzoboroxole-functionalized polymers for inhibition of HIV entry, Mol. Pharmaceutics 8 (2011) 2465–2475, https://doi.org/10.1021/mp2002957.
[102] L. Frullano, J. Rohovec, S. Aime, T. Maschmeyer, M.I. Prata, J.J. Pedroso de Lima, C.F.G.C. Geraldes, J.A. Peters, Towards targeted MRI: new MRI contrast agents for sialic acid detection, Chem. Eur. J. 10 (2004) 5205–5217, https://doi.org/10.1002/chem.200400369.
[103] M. Yamamoto, M. Takeuchi, S. Shinkai, Molecular design of a PET-based chemosensor for uronic acids and sialic acids utilizing a cooperative action of boronic acid and metal chelate, Tetrahedron 54 (1998) 3125–3140, https://doi.org/10.1016/S0040-4020(98)00057-X.
[104] M. Regueiro-Figueroa, K. Djanashvili, D. Esteban-Gómez, T. Chauvin, É. Tóth, A. de Blas, T. Rodriguez-Blas, C. Platas-Iglesias, Molecular recognition of sialic acid by lanthanide(III) complexes through cooperative two-site binding, Inorg. Chem. 49 (2010) 4212–4223, https://doi.org/10.1021/ic902461g.
[105] E. Battistini, A. Mortillaro, S. Aime, J.A. Peters, Molecular recognition of sugars by lanthanide (III) complexes of a conjugate of N, N-bis[2-[bis[2-(1,1-dimethylethoxy)-2-oxoethyl]amino]ethyl]glycine and phenylboronic acid, Contrast Media Mol. Imaging 2 (2007) 163–171, https://doi.org/10.1002/cmmi.141.
[106] H. Kobayashi, Y. Masuda, H. Takaya, T. Kubo, K. Otsuka, Separation of glycoproteins based on sugar chains using novel stationary phases modified with poly(ethylene glycol)-conjugated boronic-acid derivatives, Anal. Chem. (Washington, DC, U.S.) 94 (2022) 6882–6892, https://doi.org/10.1021/acs.analchem.2c01002.
[107] T.L. Paál, Investigation of the D-glucose-borate complexing reaction, Acta Chim. Acad. Sci. Hung. 106 (1981) 71–81.
[108] S. Geninatti Crich, D. Alberti, I. Szabo, S. Aime, K. Djanashvili, MRI visualization of melanoma cells by targeting overexpressed sialic acid with a Gd^{III}-dota-en-pba imaging reporter, Angew. Chem., Int. Ed. 54 (2013) 1161–1164, https://doi.org/10.1002/anie.201207131.
[109] P. Pellegatti, L. Raffaghello, G. Bianchi, F. Piccardi, V. Pistoia, F. Di Virgilio, J. El Khoury, Increased level of extracellular ATP at tumor sites: In vivo imaging with plasma membrane luciferase, PLoS One 3 (7) (2008) e2599, https://doi.org/10.1371/journal.pone.0002599.
[110] F. Di Virgilio, Dr. Jekyll/Mr. Hyde: the dual role of extracellular ATP, J. Auton. Nerv. Syst. 81 (2000) 59–63, https://doi.org/10.1016/S0165-1838(00)00114-4.
[111] A. Stubelius, S. Lee, A. Almutairi, The chemistry of boronic acids in nanomaterials for drug delivery, Acc. Chem. Res. 52 (2019) 3108–3119, https://doi.org/10.1021/acs.accounts.9b00292.
[112] L.-L. Huang, Y.-J. Jin, D. Zhao, C. Yu, J. Hao, H.-Y. Xie, A fast and biocompatible living virus labeling method based on sialic acid-phenylboronic acid recognition system, Anal. Bioanal. Chem. 406 (2014) 2687–2693, https://doi.org/10.1007/s00216-014-7651-9.
[113] H. Liu, Y. Li, K. Sun, J. Fan, P. Zhang, J. Meng, S. Wang, L. Jiang, Dual-responsive surfaces modified with phenylboronic acid-containing polymer brush to reversibly capture and release cancer cells, J. Am. Chem. Soc. 135 (2013) 7603–7609, https://doi.org/10.1021/ja401000m.
[114] F. Karimi, J. Collins, D.E. Heath, L.A. Connal, Dynamic covalent hydrogels for triggered cell capture and release, Bioconjugate Chem. 28 (2017) 2235–2240, https://doi.org/10.1021/acs.bioconjchem.7b00360.
[115] A.P. Davis, T.D. James, Carbohydrate receptors, Functional Synthetic Receptors (2005) 45–109, https://doi.org/10.1002/352760572X.ch2.
[116] J. Martinelli, R. Jiménez-Juárez, D. Alberti, S. Geninatti Crich, K. Djanashvili, Solid-phase synthesis and evaluation of tumour-targeting phenylboronate-based MRI contrast agents, Org. Biomol. Chem. 18 (2020) 7899–7906, https://doi.org/10.1039/D0OB01552K.
[117] J. Kim, Y.M. Lee, H. Kim, D. Park, J. Kim, W.J. Kim, Phenylboronic acid-sugar grafted polymer architecture as a dual stimuli-responsive gene carrier for targeted anti-angiogenic tumor therapy, Biomaterials 75 (2016) 102–111, https://doi.org/10.1016/j.biomaterials.2015.10.022.
[118] N. Yoshinaga, J.K. Zhou, C. Xu, C.H. Quek, Y. Zhu, D. Tang, L.Y. Hung, S. A. Najjar, C.Y.A. Shiu, K.G. Margolis, Y.-H. Lao, K.W. Leong, Phenylboronic acid-functionalized polyplexes tailored to oral CRISPR delivery, Nano Lett 23 (3) (2023) 757–764, https://doi.org/10.1021/acs.nanolett.2c02306.
[119] G.A. Ellis, M.J. Palte, R.T. Raines, Boronate-mediated biologic delivery, J. Am. Chem. Soc. 134 (2012) 3631–3634, https://doi.org/10.1021/ja210719s.
[120] G. Wulff, Selective binding to polymers via covalent bonds. The construction of chiral cavities as specific receptor sites, Pure Appl. Chem. 54 (1982) 2093–2102, https://doi.org/10.1351/pac198254112093.
[121] T. Sakata, S. Nishitani, T. Kajisa, Molecularly imprinted polymer-based bioelectrical interfaces with intrinsic molecular charges, RSC Adv. 10 (2020) 16999–17013, https://doi.org/10.1039/d0ra02793f.
[122] A. Kugimiya, J. Matsui, T. Takeuchi, K. Yano, H. Muguruma, A.V. Elgersma, I. Karube, Recognition of sialic acid using molecularly imprinted polymer, Anal. Lett. 28 (1995) 2317–2323, https://doi.org/10.1080/00032719508000375.
[123] A. Kugimiya, T. Takeuchi, Surface plasmon resonance sensor using molecularly imprinted polymer for detection of sialic acid, Biosens. Bioelectron. 16 (2001) 1059–1062, https://doi.org/10.1016/S0956-5663(01)00227-5.
[124] A. Kugimiya, H. Yoneyama, T. Takeuchi, Sialic acid imprinted polymer-coated quartz crystal microbalance, Electroanalysis 12 (2000) 1322–1326, https://doi.org/10.1002/1521-4109(200011)12:16<1322::AID-ELAN1322>3.0.CO;2-J.
[125] A. Kugimiya, J. Matsui, T. Takeuchi, Sialic acid-imprinted polymers using noncovalent interactions, Mater. Sci. Eng., C 4 (1997) 263–266, https://doi.org/10.1016/S0928-4931(97)00010-6.

[126] S. Shinde, Z. El-Schich, A. Malakpour, W. Wan, N. Dizeyi, R. Mohammadi, K. Rurack, A. Gjörloff Wingren, B. Sellergren, Sialic acid imprinted fluorescent core-shell particles for selective labeling of cell surface glycans, J. Am. Chem. Soc. 137 (43) (2015) 13908–13912, https://doi.org/10.1021/jacs.5b08482.
[127] T. Liu, Z. Qiao, J. Wang, P. Zhang, Z. Zhang, D.-S. Guo, X. Yang, Molecular imprinted S-nitrosothiols nanoparticles for nitric oxide control release as cancer target chemotherapy, Colloids Surf., B 173 (2019) 356–365, https://doi.org/10.1016/j.colsurfb.2018.09.078.
[128] R. Liu, Q. Cui, C. Wang, X. Wang, Y. Yang, L. Li, Preparation of sialic acid-imprinted fluorescent conjugated nanoparticles and their application for targeted cancer cell imaging, ACS Appl. Mater. Interfaces 9 (2017) 3006–3015, https://doi.org/10.1021/acsami.6b14320.
[129] F. Huang, B. Zhu, H. Zhang, Y. Gao, C. Ding, H. Tan, J. Li, A glassy carbon electrode modified with molecularly imprinted poly(aniline boronic acid) coated onto carbon nanotubes for potentiometric sensing of sialic acid, Microchim. Acta 186 (2019) 1–11, https://doi.org/10.1007/s00604-019-3387-8.
[130] Y. Zhou, H. Huangfu, J. Yang, H. Dong, L. Liu, M. Xu, Potentiometric analysis of sialic acid with a flexible carbon cloth based on boronate affinity and molecularly imprinted polymers, Analyst 144 (21) (2019) 6432–6437, https://doi.org/10.1039/c9an01600g.
[131] Y. Zhou, H. Dong, L. Liu, J. Liu, M. Xu, A novel potentiometric sensor based on a poly(anilineboronic acid)/graphene modified electrode for probing sialic acid through boronic acid-diol recognition, Biosens. Bioelectron. 60 (2014) 231–236, https://doi.org/10.1016/j.bios.2014.04.012.
[132] D. Yin, S. Wang, Y. He, J. Liu, M. Zhou, J. Ouyang, B. Liu, H.-Y. Chen, Z. Liu, Surface-enhanced Raman scattering imaging of cancer cells and tissues via sialic acid-imprinted nanotags, Chem. Commun. 51 (2015) 17696–17699, https://doi.org/10.1039/C5CC05174F.
[133] S. Wang, Y. Wen, Y. Wang, Y. Ma, Z. Liu, Pattern recognition of cells via multiplexed imaging with monosaccharide-imprinted quantum dots, Anal. Chem. 89 (10) (2017) 5646–5652, https://doi.org/10.1021/acs.analchem.7b00965.
[134] S. Wang, D. Yin, W. Wang, X. Shen, J.-J. Zhu, H.-Y. Chen, Z. Liu, Targeting and imaging of cancer cells via monosaccharide-imprinted fluorescent nanoparticles, Sci. Rep. 6 (2016) 22757, https://doi.org/10.1038/srep22757.
[135] C. Kip, M.C. Demir, D. Yildirim, K.O. Hamaloglu, O. Celikbicak, A. Tuncel, Highly porous, molecularly imprinted core-shell type boronate affinity sorbent with a large surface area for enrichment and detection of sialic acid isomers, J. Inorg. Organomet. Polym. Mater. 31 (2021) 2806–2817, https://doi.org/10.1007/s10904-021-01890-w.
[136] S. Xu, M. Zhao, Z. Gu, H. Lu, Z. Liu, Photothermal therapy of neuroblastoma via polysialic acid-targeting nanomissiles, Small 18 (46) (2022) 2201671, https://doi.org/10.1002/smll.202201671.
[137] S. Patterson, B.D. Smith, R.E. Taylor, Tuning the affinity of a synthetic sialic acid receptor using combinatorial chemistry, Tetrahedron Lett. 39 (1998) 3111–3114, https://doi.org/10.1016/S0040-4039(98)00514-0.
[138] K. Djanashvili, G.A. Koning, A.J.G.M. van der Meer, H.T. Wolterbeek, J.A. Peters, Phenylboronate 160Tb complexes for molecular recognition of glycoproteins expressed on tumor cells, Contrast Media Mol. Imaging 2 (2007) 35–41, https://doi.org/10.1002/cmmi.123.
[139] K. Djanashvili, T.L.M. ten Hagen, R. Blangé, D. Schipper, J.A. Peters, G.A. Koning, Development of a liposomal delivery system for temperature-triggered release of a tumor targeting agent, Ln(III)-DOTA-phenylboronate, Bioorg. Med. Chem. 19 (2011) 1123–1130, https://doi.org/10.1016/j.bmc.2010.06.036.
[140] C. Tsoukalas, S. Geninatti-Crich, A. Gaitanis, T. Tsotakos, M. Paravatou-Petsotas, S. Aime, R. Jiménez-Juárez, C.D. Anagnostopoulos, K. Djanashvili, P. Bouziotis, Tumor targeting via sialic acid: [68Ga]DOTA-en-pba as a new tool for molecular imaging of cancer with PET, Mol. Imaging Biol. 20 (5) (2018) 798–807, https://doi.org/10.1007/s11307-018-1176-0.
[141] J. Martinelli, L. Tei, S. Geninatti Crich, D. Alberti, K. Djanashvili, Towards enhanced MRI performance of tumor-specific dimeric phenylboronic contrast agents, Molecules 26 (2021) 1730, https://doi.org/10.3390/molecules26061730.
[142] P.M. Chaudhary, R.V. Murthy, R. Yadav, R. Kikkeri, A rationally designed peptidomimetic biosensor for sialic acid on cell surfaces, Chem. Commun. 51 (2015) 8112–8115, https://doi.org/10.1039/C5CC01662B.
[143] J. Chen, J. Ding, W. Xu, T. Sun, H. Xiao, X. Zhuang, X. Chen, Receptor and microenvironment dual-recognizable nanogel for targeted chemotherapy of highly metastatic malignancy, Nano Lett. 17 (2017) 4526–4533, https://doi.org/10.1021/acs.nanolett.7b02129.
[144] H.-W. Liu, W.-H.-T. Law, L.-C.-C. Lee, J.-C.-W. Lau, K.-K.-W. Lo, Cyclometalated iridium(iii) bipyridine–phenylboronic acid complexes as bioimaging reagents and luminescent probes for sialic acids, Chem. - Asian J. 12 (2017) 1545–1556, https://doi.org/10.1002/asia.201700359.
[145] S. Renata, N. Verma, Z. Tu, R.-L. Pan, M. Hofmann, C.-H. Lin, Development of a tri-functional nanoprobe for background-free SERS detection of sialic acid on the cell surface, Chemosensors 9 (2021) 92, https://doi.org/10.3390/chemosensors9050092.
[146] M. Takeuchi, M. Yamamoto, S. Shinkai, Fluorescent sensing of uronic acids based on a cooperative action of boronic acid and metal chelate, Chem. Commun. (1997) 1731–1732, https://doi.org/10.1039/A703471G.
[147] E.R. Neil, D. Parker, Selective signalling of sialic acid in solution by circularly polarised luminescence spectroscopy using a dynamically racemic europium(III) complex, RSC Adv. 7 (2017) 4531–4540, https://doi.org/10.1039/C6RA26662B.
[148] W. Yang, H. Fan, X. Gao, S. Gao, V.V.R. Karnati, W. Ni, W.B. Hooks, J. Carson, B. Weston, B. Wang, The first fluorescent diboronic acid sensor specific for hepatocellular carcinoma cells expressing sialyl Lewis X, Chem. Biol. 11 (2004) 439–448, https://doi.org/10.1016/j.chembiol.2004.03.021.
[149] W. Yang, S. Gao, X. Gao, V.V.R. Karnati, W. Ni, B. Wang, W.B. Hooks, J. Carson, B. Weston, Diboronic acids as fluorescent probes for cells expressing sialyl lewis X, Bioorg. Med. Chem. Lett. 12 (2002) 2175–2177, https://doi.org/10.1016/S0960-894X(02)00339-6.
[150] C. Dai, L.H. Cazares, L. Wang, Y. Chu, S.L. Wang, D.A. Troyer, O.J. Semmes, R. R. Drake, B. Wang, Using boronolectin in MALDI-MS imaging for the histological analysis of cancer tissue expressing the sialyl Lewis X antigen, Chem. Commun. 47 (2011) 10338–10340, https://doi.org/10.1039/C1CC11814E.
[151] Y. Chu, D. Wang, K. Wang, Z. Liu, B. Weston, B. Wang, Fluorescent conjugate of sLex-selective bisboronic acid for imaging application, Bioorg. Med. Chem. Lett. 23 (2013) 6307–6309, https://doi.org/10.1016/j.bmcl.2013.09.063.
[152] Y.-E. Wang, R.-X. Rong, H. Chen, M.-Y. Zhu, B.-H. Wang, X.-L. Li, Synthesis of fluorescent bisboronic acid sensors and their recognition of mono-/oligo-saccharides, Chin. Chem. Lett. 28 (2017) 1262–1267, https://doi.org/10.1016/j.cclet.2017.02.013.
[153] S.M. Levonis, M.J. Kiefel, T.a. Houston, Boronolectin with divergent fluorescent response specific for free sialic acid, Chem. Commun. (2009) 2278–2280, https://doi.org/10.1039/b900836p.
[154] M. Regueiro-Figueroa, K. Djanashvili, D. Esteban-Gómez, A. de Blas, C. Platas-Iglesias, T. Rodríguez-Blas, Towards selective recognition of sialic acid through simultaneous binding to its cis-diol and carboxylate functions, Eur. J. Org. Chem. (2010) 3237–3248, https://doi.org/10.1002/ejoc.201000186.
[155] W. Kowalczyk, J. Sanchez, P. Kraaz, O.E. Hutt, D.N. Haylock, P.J. Duggan, The binding of boronated peptides to low affinity mammalian saccharides, Pept. Sci. (Hoboken, NJ, U. S.) (2018) 110, https://doi.org/10.1002/pep2.23101.
[156] P. Zhang, M. Gao, X. Zhang, Functional dendrimer modified ultra-hydrophilic trapping copolymer network towards highly efficient cell capture, Talanta 153 (2016) 366–371, https://doi.org/10.1016/j.talanta.2016.03.044.
[157] J. Yang, J. Zhang, Y. Liu, Z. Shi, H. Han, Q. Li, Phenylboronic acid-modified polyamidoamine-mediated delivery of short GC rich DNA for hepatocarcinoma gene therapy, Biomater. Sci. 7 (2019) 3348–3358, https://doi.org/10.1039/c9bm00394k.
[158] Z. Song, X. Liang, Y. Wang, H. Han, J. Yang, X. Fang, Q. Li, Phenylboronic acid-functionalized polyamidoamine-mediated miR-34a delivery for the treatment of gastric cancer, Biomater. Sci. 7 (2019) 1632–1642, https://doi.org/10.1039/c8bm01385c.
[159] J. Yang, J. Zhang, J. Xing, Z. Shi, H. Han, Q. Li, Inhibition of proliferation and migration of tumor cells through phenylboronic acid-functionalized polyamidoamine-mediated delivery of a therapeutic DNAzyme Dz13, Int. J. Nanomed. 14 (2019) 6371–6385, https://doi.org/10.2147/ijn.s211744.
[160] Y. Hao, Y. Gao, Y. Fan, C. Zhang, M. Zhan, X. Cao, X. Shi, R. Guo, A tumor microenvironment-responsive poly(amidoamine) dendrimer nanoplatform for hypoxia-responsive chemo/chemodynamic therapy, J. Nanobiotechnol. 20 (2022) 43, https://doi.org/10.1186/s12951-022-01247-6.
[161] X. Zhang, Z. Zhang, X. Su, M. Cai, R. Zhuo, Z. Zhong, Phenylboronic acid-functionalized polymeric micelles with a HepG2 cell targetability, Biomaterials 34 (2013) 10296–10304, https://doi.org/10.1016/j.biomaterials.2013.09.042.
[162] Q. Qu, Y. Wang, L. Zhang, X. Zhang, S. Zhou, A nanoplatform with precise control over release of cargo for enhanced cancer therapy, Small 12 (2016) 1378–1390, https://doi.org/10.1002/smll.201503292.
[163] Z. Tang, L. Zhang, Y. Wang, D. Li, Z. Zhong, S. Zhou, Redox-responsive star-shaped magnetic micelles with active-targeted and magnetic-guided functions for cancer therapy, Acta Biomater. 42 (2016) 232–246, https://doi.org/10.1016/j.actbio.2016.06.038.
[164] X. Wei, Y. Wang, X. Xiong, X. Guo, L. Zhang, X. Zhang, S. Zhou, Codelivery of a π–π stacked dual anticancer drug combination with nanocarriers for overcoming multidrug resistance and tumor metastasis, Adv. Funct. Mater. 26 (2016) 8266–8280, https://doi.org/10.1002/adfm.201603336.
[165] Q. Qi, X. Zeng, L. Peng, H. Zhang, M. Zhou, J. Fu, J. Yuan, Tumor-targeting and imaging micelles for pH-triggered anticancer drug release and combined photodynamic therapy, J. Biomater. Sci., Polym. Ed. 31 (2020) 1385–1404, https://doi.org/10.1080/09205063.2020.1760698.
[166] S. Tiwari, J. Sarolia, V. Kansara, N.A. Chudasama, K. Prasad, D. Ray, V.K. Aswal, P. Bahadur, Synthesis, colloidal characterization and targetability of phenylboronic acid functionalized α-tocopheryl polyethylene glycol succinate in cancer cells, Polymers (Basel, Switz.), 12 (2020) 2258, doi:10.3390/polym12102258.
[167] A.K. Jangid, R. Solanki, M. Jadav, S. Bora, S. Patel, D. Pooja, H. Kulhari, Phenyl boronic acid -PEG-stearic acid biomaterial-based and sialic acid targeted nanomicelles for colon cancer treatment, Colloids Surf., A 656 (2023), 130445, https://doi.org/10.1016/j.colsurfa.2022.130445.
[168] H. Chun, M. Yeom, H.-O. Kim, J.-W. Lim, W. Na, G. Park, C. Park, A. Kang, D. Yun, J. Kim, D. Song, S. Haam, Efficient antiviral co-delivery using polymersomes by controlling the surface density of cell-targeting groups for influenza A virus treatment, Polym. Chem. 9 (2018) 2116–2123, https://doi.org/10.1039/C8PY00116B.
[169] D.-E. Wang, J. Yan, J. Jiang, X. Liu, C. Tian, J. Xu, M.-S. Yuan, X. Han, J. Wang, Polydiacetylene liposomes with phenylboronic acid tags: a fluorescence turn-on sensor for sialic acid detection and cell-surface glycan imaging, Nanoscale 10 (2018) 4570–4578, https://doi.org/10.1039/C7NR08557E.
[170] W.L.A. Brooks, B.S. Sumerlin, Synthesis and applications of boronic acid-containing polymers: From materials to medicine, Chem. Rev. 116 (2016) 1375–1397, https://doi.org/10.1021/acs.chemrev.5b00300.
[171] X. Wang, H. Tang, C. Wang, J. Zhang, W. Wu, X. Jiang, Phenylboronic acid-mediated tumor targeting of chitosan nanoparticles, Theranostics 6 (2016) 1378–1392, https://doi.org/10.7150/thno.15156.

[172] X. Wang, B. Wei, X.u. Cheng, J. Wang, R. Tang, Phenylboronic acid-decorated gelatin nanoparticles for enhanced tumor targeting and penetration, Nanotechnology 27 (38) (2016), 385101, https://doi.org/10.1088/0957-4484/27/38/385101.
[173] Y. Zhang, W. Chen, C. Yang, Q. Fan, W. Wu, X. Jiang, Enhancing tumor penetration and targeting using size-minimized and zwitterionic nanomedicines, J. Controlled Release 237 (2016) 115–124, https://doi.org/10.1016/j.jconrel.2016.07.011.
[174] W. Chen, S. Ji, X. Qian, Y. Zhang, C. Li, W. Wu, F. Wang, X. Jiang, Phenylboronic acid-incorporated elastin-like polypeptide nanoparticle drug delivery systems, Polym. Chem. 8 (2017) 2105–2114, https://doi.org/10.1039/C7PY00330G.
[175] X. Wang, B. Wei, X. Cheng, J. Wang, R. Tang, 3-Carboxyphenylboronic acid-modified carboxymethyl chitosan nanoparticles for improved tumor targeting and inhibitory, Eur. J. Pharm. Biopharm. 113 (2017) 168–177, https://doi.org/10.1016/j.ejpb.2016.12.034.
[176] M.M. Elgohary, M.W. Helmy, E.-Z.-A. Abdelfattah, D.M. Ragab, S.M. Mortada, J.-Y. Fang, A.O. Elzoghby, Targeting sialic acid residues on lung cancer cells by inhalable boronic acid-decorated albumin nanocomposites for combined chemo/herbal therapy, J. Controlled Release 285 (2018) 230–243, https://doi.org/10.1016/j.jconrel.2018.07.014.
[177] L. Lei, Z. Xu, X. Hu, Y. Lai, J. Xu, B. Hou, Y. Wang, H. Yu, Y. Tian, W. Zhang, Bioinspired multivalent peptide nanotubes for sialic acid targeting and imaging-guided treatment of metastatic melanoma, Small 15 (2019) 1900157, https://doi.org/10.1002/smll.201900157.
[178] X. Qian, L. Ge, K. Yuan, C. Li, X. Zhen, W. Cai, R. Cheng, X. Jiang, Targeting and microenvironment-improving of phenylboronic acid-decorated soy protein nanoparticles with different sizes to tumor, Theranostics 9 (2019) 7417–7430, https://doi.org/10.7150/thno.33470.
[179] R. Feng, W. Wang, L. Zhu, H. Xu, S. Chen, Z. Song, Phenylboronic acid-functionalized F127-oligochitosan conjugate micelles for doxorubicin encapsulation, J. Biomed. Mater. Res., Part B 108 (2020) 3345–3355, https://doi.org/10.1002/jbm.b.34670.
[180] Y. Long, Z. Lu, S. Xu, M. Li, X. Wang, Z. Zhang, Q. He, Self-delivery micellar nanoparticles prevent premetastatic niche formation by interfering with the early recruitment and vascular destruction of granulocytic myeloid-derived suppressor cells, Nano Lett. 20 (2020) 2219–2229, https://doi.org/10.1021/acs.nanolett.9b03883.
[181] L. Peng, X. Zeng, Q. Qi, H. Zhang, J. Fu, M. Zhou, J. Yuan, Sialic acid-targeted drug delivery and imaging system for pH- and glutathione-triggered multiple anticancer drug release and enhanced oxidative stress, J. Bioact. Compat. Polym. 35 (2020) 254–269, https://doi.org/10.1177/0883911520913913.
[182] C. Zheng, Q. Guo, Z. Wu, L. Sun, Z. Zhang, C. Li, X. Zhang, Amphiphilic glycopolymer nanoparticles as vehicles for nasal delivery of peptides and proteins, Eur. J. Pharm. Sci. 49 (2013) 474–482, https://doi.org/10.1016/j.ejps.2013.04.027.
[183] Y. Lu, Z. Bie, Y. Liu, Z. Liu, Fine-tuning the specificity of boronate affinity monoliths toward glycoproteins through pH manipulation, Analyst 138 (1) (2013) 290–298, https://doi.org/10.1039/C2AN36048A.
[184] K. Ishihara, M. Abe, K. Fukazawa, T. Konno, Control of cell-substrate binding related to cell proliferation cycle status using a cytocompatible phospholipid polymer bearing phenylboronic acid groups, Macromol. Biosci. 21 (2021) 2000341, https://doi.org/10.1002/mabi.202000341.
[185] Q.i. Cao, Y.u. Peng, Q. Yu, Z. Shi, Q. Jia, Post synthetic modification of Zr-MOF with phenylboronic acid: Fluorescence sensing of sialic acid, Dyes and Pigments 197 (2022) 109839, https://doi.org/10.1016/j.dyepig.2021.109839.
[186] H. Yu, Y. Li, A. Huang, Detection of sialic acid using boronic-acid-functionalized metal organic framework UiO-66-NH(2)@B(OH)(2), Talanta 232 (2021), 122434, https://doi.org/10.1016/j.talanta.2021.122434.
[187] L. Cheng, X. Zhang, Z. Zhang, H. Chen, S. Zhang, J. Kong, Multifunctional phenylboronic acid-tagged fluorescent silica nanoparticles via thiol-ene click reaction for imaging sialic acid expressed on living cells, Talanta 115 (2013) 823–829, https://doi.org/10.1016/j.talanta.2013.06.060.
[188] L. Wu, Y. Yan, P. Gao, S. Huang, Recognition of MCF-7 human breast carcinoma cells using silica-encapsulated fluorescent nanoparticles modified with aminophenylboronic acid, Microchim. Acta (2016) 1–8, https://doi.org/10.1007/s00604-015-1736-9.
[189] Y. Chen, H. Liu, Y. Xiong, H. Ju, Quantitative screening of cell-surface gangliosides by nondestructive extraction and hydrophobic collection, Angew. Chem., Int. Ed. 57 (2018) 785–789, https://doi.org/10.1002/anie.201710984.
[190] R. Jin, J. Wang, M. Gao, X. Zhang, Aminophenylboronic acid-functionalized thorny-trap-shaped monolayer microarray for efficient capture and release of circulating tumor cells, Anal. Chem. 92 (2020) 3403–3408, https://doi.org/10.1021/acs.analchem.9b05486.
[191] Y. Qu, Y. Zheng, L. Yu, Y. Zhou, Y. Wang, Y. Zhang, Q. Yu, H. Chen, A universal platform for high-efficiency “engineering” living cells: Integration of cell capture, intracellular delivery of biomolecules, and cell harvesting functions, Adv. Funct. Mater. 30 (2020) 1906362, https://doi.org/10.1002/adfm.201906362.
[192] Y. Xiong, Y. Chen, L. Ding, X. Liu, H. Ju, Fluorescent visual quantitation of cell-secreted sialoglycoconjugates by chemoselective recognition and hybridization chain reaction, Analyst 144 (15) (2019) 4545–4551, https://doi.org/10.1039/c9an00572b.
[193] M. Kundu, P. Sadhukhan, N. Ghosh, S. Chatterjee, P. Manna, J. Das, P.C. Sil, pH-responsive and targeted delivery of curcumin via phenylboronic acid-functionalized ZnO nanoparticles for breast cancer therapy, J. Adv. Res. 18 (2019) 161–172, https://doi.org/10.1016/j.jare.2019.02.036.
[194] P. Sadhukhan, M. Kundu, S. Chatterjee, N. Ghosh, P. Manna, J. Das, P.C. Sil, Targeted delivery of quercetin via pH-responsive zinc oxide nanoparticles for breast cancer therapy, Mater. Sci. Eng. C 100 (2019) 129–140, https://doi.org/10.1016/j.msec.2019.02.096.
[195] X. Hao, Q. Zhang, L. Li, L. Zhou, Rapid spectral detection of sialic acid using phenylboronic acid functionalized rGO, Mater. Lett. 227 (2018) 165–168, https://doi.org/10.1016/j.matlet.2018.05.002.
[196] L. Chen, N. Wang, J. Wu, F. Yan, H. Ju, Organic electrochemical transistor for sensing of sialic acid in serum samples, Anal. Chim. Acta 1128 (2021) 231–237, https://doi.org/10.1016/j.aca.2020.07.006.
[197] V. Rathod, R. Tripathi, P. Joshi, P.K. Jha, P. Bahadur, S. Tiwari, Paclitaxel encapsulation into dual-functionalized multi-walled carbon nanotubes, AAPS PharmSciTech 20 (2019) 51, https://doi.org/10.1208/s12249-018-1218-6.
[198] L. Thoo, M.Z. Fahmi, I.N. Zulkipli, N. Keasberry, A. Idris, Interaction and cellular uptake of surface-modified carbon dot nanoparticles by J774.1 macrophages, Cent. Eur. J. Immunol. 42 (2017) 324–330, https://doi.org/10.5114/ceji.2017.70978.
[199] S. Xu, S. Che, P. Ma, F. Zhang, L. Xu, X. Liu, X. Wang, D. Song, Y. Sun, One-step fabrication of boronic-acid-functionalized carbon dots for the detection of sialic acid, Talanta 197 (2019) 548–552, https://doi.org/10.1016/j.talanta.2019.01.074.
[200] W. Hai, S. Pu, X. Wang, L. Bao, N. Han, L. Duan, J. Liu, T. Goda, W. Wu, Poly(3,4-ethylenedioxythiophene) bearing pyridylboronic acid group for specific recognition of sialic acid, Langmuir 36 (2020) 546–553, https://doi.org/10.1021/acs.langmuir.9b03442.
[201] X. Guo, J. Liu, F. Liu, F. She, Q. Zheng, H. Tang, M. Ma, S. Yao, Label-free and sensitive sialic acid biosensor based on organic electrochemical transistors, Sens. Actuators, B 240 (2017) 1075–1082, https://doi.org/10.1016/j.snb.2016.09.099.
[202] M. Dervisevic, M. Senel, T. Sagir, S. Isik, Highly sensitive detection of cancer cells with an electrochemical cytosensor based on boronic acid functional polythiophene, Biosens. Bioelectron. 90 (2017) 6–12, https://doi.org/10.1016/j.bios.2016.10.100.
[203] A. Liu, S. Peng, J.C. Soo, M. Kuang, P. Chen, H. Duan, Quantum dots with phenylboronic acid tags for specific labeling of sialic acids on living cells, Anal. Chem. 83 (2011) 1124–1130, https://doi.org/10.1021/ac1028853.
[204] J.-T. Cao, P.-H. Zhang, Y.-M. Liu, E.S. Abdel-Halim, J.-J. Zhu, Versatile microfluidic platform for the assessment of sialic acid expression on cancer cells using quantum dots with phenylboronic acid tags, ACS Appl. Mater. Interfaces 7 (2015) 14878–14884, https://doi.org/10.1021/acsami.5b03519.
[205] J. Vinayagam, G.-R. Chen, T.-Y. Huang, J.-H. Ho, Y.-C. Ling, K.-L. Ou, J.-Y. Chang, Aqueous synthesis of CuInZnS/ZnS quantum dots by using dual stabilizers: A targeting nanoprobe for cell imaging, Mater. Lett. 173 (2016) 242–247, https://doi.org/10.1016/j.matlet.2016.03.041.
[206] J. Wang, G. Xu, F. Wei, J. Yang, P. Zhou, Q. Hu, A novel Fe3O4/CdTe fluorescence probe for sialic acid detection based on a phenylboronic acid–sialic acid recognition system, RSC Adv. 6 (2016) 481–488, https://doi.org/10.1039/C5RA17171G.
[207] C.A.P. Monteiro, R.C. Silva, L.G. Assis, G. Pereira, G.A.L. Pereira, B.S. Santos, P. E. Cabral Filho, A. Fontes, Quantum dots functionalized with 3-mercaptophenylboronic acids as novel nanoplatforms to evaluate sialic acid content on cell membranes, Colloids Surf., B: Biointerfaces 193 (2020) 111142, https://doi.org/10.1016/j.colsurfb.2020.111142.
[208] M. Zhang, Q. Wang, Y. Xu, L. Guo, Z. Lai, Z. Li, Graphitic carbon nitride quantum dots as analytical probe for viewing sialic acid on the surface of cells and tissues, Anal. Chim. Acta 1095 (2020) 204–211, https://doi.org/10.1016/j.aca.2019.10.031.
[209] B. Shashni, Y. Horiguchi, K. Kurosu, H. Furusho, Y. Nagasaki, Application of surface enhanced Raman spectroscopy as a diagnostic system for hypersialylated metastatic cancers, Biomaterials 134 (2017) 143–153, https://doi.org/10.1016/j.biomaterials.2017.04.038.
[210] X. Yang, L. Zhou, Y. Hao, B. Zhou, P. Yang, Erythrocytes-based quartz crystal microbalance cytosensor for in situ detection of cell surface sialic acid, Analyst (Cambridge U. K.), 142 (2017) 2169–2176, https://doi.org/10.1039/c7an00073a.
[211] G. Broncova, P. Matejka, Z. Nemeckova, V. Vrkoslav, T.V. Shishkanova, Electrochemical detection of sialic acid using phenylboronic acid-modified poly (diaminobenzoic acid) electrodes, Electroanalysis 30 (2018) 672–680, https://doi.org/10.1002/elan.201700634.
[212] R. Deng, J. Yue, H. Qu, L. Liang, D. Sun, J. Zhang, C. Liang, W. Xu, S. Xu, Glucose-bridged silver nanoparticle assemblies for highly sensitive molecular recognition of sialic acid on cancer cells via surface-enhanced raman scattering spectroscopy, Talanta 179 (2018) 200–206, https://doi.org/10.1016/j.talanta.2017.11.006.
[213] D. Dutta, S.K. Sailapu, A. Chattopadhyay, S.S. Ghosh, Phenylboronic acid templated gold nanoclusters for mucin detection using a smartphone-based device and targeted cancer cell theranostics, ACS Appl. Mater. Interfaces 10 (2018) 3210–3218, https://doi.org/10.1021/acsami.7b13782.
[214] S. Li, J. Liu, Y. Lu, L. Zhu, C. Li, L. Hu, J. Li, J. Jiang, S. Low, Q. Liu, Mutual promotion of electrochemical-localized surface plasmon resonance on nanochip for sensitive sialic acid detection, Biosens. Bioelectron. 117 (2018) 32–39, https://doi.org/10.1016/j.bios.2018.05.062.
[215] L. Liang, Y. Shen, J. Zhang, S. Xu, W. Xu, C. Liang, B. Han, Identification of breast cancer through spectroscopic analysis of cell-membrane sialic acid expression, Anal. Chim. Acta 1033 (2018) 148–155, https://doi.org/10.1016/j.aca.2018.04.072.
[216] L. Cong, L. Liang, F. Cao, D. Sun, J. Yue, W. Xu, C. Liang, S. Xu, Distinguishing cancer cell lines at a single living cell level via detection of sialic acid by dual-

channel plasmonic imaging and by using a SERS-microfluidic droplet platform, Microchim. Acta 186 (2019) 1–10, https://doi.org/10.1007/s00604-019-3480-z.
[217] F. Hu, J. Xu, Y.i. Chen, Sensing ultra-trace dopamine by restoration of fluorescence on locally acidified gold nanoparticles, Analyst 144 (15) (2019) 4477–4482, https://doi.org/10.1039/c9an00712a.
[218] Y. Chen, L. Ding, H. Ju, In situ tracing of cell surface sialic acid by chemoselective recognition to unload gold nanocluster probe from density tunable dendrimeric array, Chem. Commun. 49 (2013) 862–864, https://doi.org/10.1039/C2CC37761F.
[219] S. Sankoh, C. Thammakhet, A. Numnuam, W. Limbut, P. Kanatharana, P. Thavarungkul, 4-mercaptophenylboronic acid functionalized gold nanoparticles for colorimetric sialic acid detection, Biosens. Bioelectron. 85 (2016) 743–750, https://doi.org/10.1016/j.bios.2016.05.083.
[220] W. Song, L. Ding, Y. Chen, H. Ju, Plasmonic coupling of dual gold nanoprobes for SERS imaging of sialic acids on living cells, Chem. Commun. 52 (2016) 10640–10643, https://doi.org/10.1039/C6CC04147G.
[221] L. Liang, H. Qu, B. Zhang, J. Zhang, R. Deng, Y. Shen, S. Xu, C. Liang, W. Xu, Tracing sialoglycans on cell membrane via surface-enhanced Raman scattering spectroscopy with a phenylboronic acid-based nanosensor in molecular recognition, Biosens. Bioelectron. 94 (2017) 148–154, https://doi.org/10.1016/j.bios.2017.02.043.
[222] L. Zhang, C. Yu, R. Gao, Y. Niu, Y. Li, J. Chen, J. He, An impedimetric biosensor for the diagnosis of renal cell carcinoma based on the interaction between 3-aminophenyl boronic acid and sialic acid, Biosens. Bioelectron. 92 (2017) 434–441, https://doi.org/10.1016/j.bios.2016.10.083.
[223] B.S. Kwak, H.O. Kim, J.H. Kim, S. Lee, H.-I. Jung, Quantitative analysis of sialic acid on erythrocyte membranes using a photothermal biosensor, Biosens. Bioelectron. 35 (2012) 484–488, https://doi.org/10.1016/j.bios.2012.03.008.
[224] H. Di, H. Liu, M. Li, J. Li, D. Liu, High-precision profiling of sialic acid expression in cancer cells and tissues using background-free surface-enhanced Raman scattering tags, Anal. Chem. 89 (2017) 5874–5881, https://doi.org/10.1021/acs.analchem.7b00199.
[225] T. Gong, Y. Cui, D. Goh, K.K. Voon, P.P. Shum, G. Humbert, J.-L. Auguste, X.-Q. Dinh, K.-T. Yong, M. Olivo, Highly sensitive SERS detection and quantification of sialic acid on single cell using photonic-crystal fiber with gold nanoparticles, Biosens. Bioelectron. 64 (2015) 227–233, https://doi.org/10.1016/j.bios.2014.08.077.
[226] X. Zhang, B. Chen, M. He, Y. Zhang, L. Peng, B. Hu, Boronic acid recognition based-gold nanoparticle-labeling strategy for the assay of sialic acid expression on cancer cell surface by inductively coupled plasma mass spectrometry, Analyst 141 (2016) 1286–1299, https://doi.org/10.1039/C5AN02402A.
[227] T.J. Jayeoye, W. Cheewasedtham, C. Putson, T. Rujiralai, Colorimetric determination of sialic acid based on boronic acid-mediated aggregation of gold nanoparticles, Microchim. Acta 185 (2018) 409, https://doi.org/10.1007/s00604-018-2951-y.
[228] R. Qian, L. Ding, L. Yan, H. Ju, Fluorescence imaging for in situ detection of cell surface sialic acid by competitive binding of 3-(dansylamino)phenylboronic acid, Anal. Chim. Acta 894 (2015) 85–90, https://doi.org/10.1016/j.aca.2015.08.054.
[229] M. Mammen, S.-K. Choi, G.M. Whitesides, Polyvalent interactions in biological systems: Implications for design and use of multivalent ligands and inhibitors, Angew. Chem. Int. Ed. 37 (1998) 2754–2794, https://doi.org/10.1002/(SICI)1521-3773(19981102)37:20<2754::AID-ANIE2754>3.0.CO;2-3.
[230] J. Huskens, A. Mulder, T. Auletta, C.A. Nijhuis, M.J.W. Ludden, D.N. Reinhoudt, A model for describing the thermodynamics of multivalent host–guest interactions at interfaces, J. Am. Chem. Soc. 126 (2004) 6784–6797, https://doi.org/10.1021/ja049085k.
[231] R.S. Kane, Thermodynamics of multivalent interactions: influence of the linker, Langmuir 26 (2010) 8636–8640, https://doi.org/10.1021/la9047193.
[232] J. Huskens, Models and methods in multivalent systems, in: Multivalency, 2018, pp. 23-74, doi:10.1002/9781119143505.ch2.
[233] T. Curk, J. Dobnikar, D. Frenkel, Design principles for super selectivity using multivalent interactions, in: Multivalency, 2018, pp. 75-101, doi:10.1002/9781119143505.ch3.
[234] G. Morgese, B.F.M. de Waal, S. Varela-Aramburu, A.R.A. Palmans, L. Albertazzi, E.W. Meijer, Anchoring supramolecular polymers to human red blood cells by combining dynamic covalent and non-covalent chemistries, Angew. Chem., Int. Ed. 59 (2020) 17229–17233, https://doi.org/10.1002/anie.202006381.
[235] Y. Horiguchi, K. Barthelmes, Y. Miyahara, A. Matsumoto, pH-responsive adsorption and dissociation of sialic acid expressed protein on boronic acid immobilized surface, Chem. Lett. 50 (2021) 1467–1469, https://doi.org/10.1246/cl.210229.
[236] X.-D. Xu, H. Cheng, W.-H. Chen, S.-X. Cheng, R.-X. Zhuo, X.-Z. Zhang, In situ recognition of cell-surface glycans and targeted imaging of cancer cells, Sci. Rep. 3 (2013) 2679, https://doi.org/10.1038/srep02679.
[237] J. Wang, Z. Zhang, X. Wang, W. Wu, X. Jiang, Size- and pathotropism-driven targeting and washout-resistant effects of boronic acid-rich protein nanoparticles for liver cancer regression, J. Controlled Release 168 (2013) 1–9, https://doi.org/10.1016/j.jconrel.2013.02.019.
[238] J. Wang, W. Wu, Y. Zhang, X. Wang, H. Qian, B. Liu, X. Jiang, The combined effects of size and surface chemistry on the accumulation of boronic acid-rich protein nanoparticles in tumors, Biomaterials 35 (2014) 866–878, https://doi.org/10.1016/j.biomaterials.2013.10.028.
[239] J.-Y. Lee, S.-J. Chung, H.-J. Cho, D.-D. Kim, Phenylboronic acid-decorated chondroitin sulfate a-based theranostic nanoparticles for enhanced tumor targeting and penetration, Adv. Funct. Mater. 25 (2015) 3705–3717, https://doi.org/10.1002/adfm.201500680.
[240] J.Y. Jeong, E.-H. Hong, S.Y. Lee, J.-Y. Lee, J.-H. Song, S.-H. Ko, J.-S. Shim, S. Choe, D.-D. Kim, H.-J. Ko, H.-J. Cho, Boronic acid-tethered amphiphilic hyaluronic acid derivative-based nanoassemblies for tumor targeting and penetration, Acta Biomater. 53 (2017) 414–426, https://doi.org/10.1016/j.actbio.2017.02.030.
[241] L. Su, T. Chen, T. Xue, A. Sheng, L. Cheng, J. Zhang, Fabrication of pH-adjusted boronic acid-aptamer conjugate for electrochemical analysis of conjugated N-glycolylneuraminic acid, ACS Appl. Mater. Interfaces 12 (2020) 7650–7657, https://doi.org/10.1021/acsami.9b23029.
[242] A.R. Lippert, G.C. Van de Bittner, C.J. Chang, Boronate oxidation as a bioorthogonal reaction approach for studying the chemistry of hydrogen peroxide in living systems, Acc. Chem. Res. 44 (2011) 793–804, https://doi.org/10.1021/ar200126t.
[243] Z. Guo, I. Shin, J. Yoon, Recognition and sensing of various species using boronic acid derivatives, Chem. Commun. 48 (2012) 5956–5967, https://doi.org/10.1039/C2CC31985C.
[244] E.W. Miller, A.E. Albers, A. Pralle, E.Y. Isacoff, C.J. Chang, Boronate-based fluorescent probes for imaging cellular hydrogen peroxide, J. Am. Chem. Soc. 127 (2005) 16652–16659, https://doi.org/10.1021/ja054474f.
[245] H. Li, C.-H. Lee, I. Shin, Preparation of a multiple-targeting nir-based fluorogenic probe and its application for selective cancer cell imaging, Org. Lett. 21 (2019) 4628–4631, https://doi.org/10.1021/acs.orglett.9b01530.
[246] W. Chen, X. Zhen, W. Wu, X. Jiang, Responsive boron biomaterials and their biomedical applications, Sci. China: Chem. 63 (2020) 648–664, https://doi.org/10.1007/s11426-019-9699-3.
[247] S. Ulrich, Growing prospects of dynamic covalent chemistry in delivery applications, Acc. Chem. Res. 52 (2019) 510–519, https://doi.org/10.1021/acs.accounts.8b00591.
[248] T. Lan, Q. Guo, Phenylboronic acid-decorated polymeric nanomaterials for advanced bio-application, Nanotechnol. Rev. 8 (2019) 548–561, https://doi.org/10.1515/ntrev-2019-0049.
[249] J. Whited, X. Zhang, H. Nie, D. Wang, Y. Li, X.-L. Sun, Recent chemical biology approaches for profiling cell surface sialylation status, ACS Chem. Biol. 13 (2018) 2364–2374, https://doi.org/10.1021/acschembio.8b00456.
[250] G. Fang, H. Wang, Z. Bian, J. Sun, A. Liu, H. Fang, B. Liu, Q. Yao, Z. Wu, Recent development of boronic acid-based fluorescent sensors, RSC Adv. 8 (2018) 29400–29427, https://doi.org/10.1039/C8RA04503H.
[251] R.P. Brannigan, V.V. Khutoryanskiy, Progress and current trends in the synthesis of novel polymers with enhanced mucoadhesive properties, Macromol. Biosci. 19 (2019) 1900194, https://doi.org/10.1002/mabi.201900194.
[252] S. Liu, C.N. Chang, M.S. Verma, D. Hileeto, A. Muntz, U. Stahl, J. Woods, L. W. Jones, F.X. Gu, Phenylboronic acid modified mucoadhesive nanoparticle drug carriers facilitate weekly treatment of experimentallyinduced dry eye syndrome, Nano Res. 8 (2015) 621–635, https://doi.org/10.1007/s12274-014-0547-3.
[253] S. Liu, M.D. Dozois, C.N. Chang, A. Ahmad, D.L.T. Ng, D. Hileeto, H. Liang, M.-M. Reyad, S. Boyd, L.W. Jones, F.X. Gu, Prolonged ocular retention of mucoadhesive nanoparticle eye drop formulation enables treatment of eye diseases using significantly reduced dosage, Mol. Pharmaceutics 13 (2016) 2897–2905, https://doi.org/10.1021/acs.molpharmaceut.6b00445.
[254] G. Prosperi-Porta, S. Kedzior, B. Muirhead, H. Sheardown, Phenylboronic-acid-based polymeric micelles for mucoadhesive anterior segment ocular drug delivery, Biomacromolecules 17 (2016) 1449–1457, https://doi.org/10.1021/acs.biomac.6b00054.
[255] G. Tan, J. Li, Y. Song, Y. Yu, D. Liu, W. Pan, Phenylboronic acid-tethered chondroitin sulfate-based mucoadhesive nanostructured lipid carriers for the treatment of dry eye syndrome, Acta Biomater. 99 (2019) 350–362, https://doi.org/10.1016/j.actbio.2019.08.035.
[256] Z. Gong, M. Chen, Y.-W. Wang, B.-S. Huang, Y.-J. Chen, K.-H. Nan, J.-J. Wang, Anchoring polyethylene glycol to the ocular surface by phenylboronic acid functionalization: Implications for fabrication of long-acting artificial tears, Colloid Interface Sci. Commun. 42 (2021), 100429, https://doi.org/10.1016/j.colcom.2021.100429.
[257] X. Zhang, Y. Wang, C. Zheng, C. Li, Phenylboronic acid-functionalized glycopolymeric nanoparticles for biomacromolecules delivery across nasal respiratory, Eur. J. Pharm. Biopharm. 82 (2012) 76–84, https://doi.org/10.1016/j.ejpb.2012.05.013.
[258] C. Li, Z. Liu, X. Yan, W. Lu, Y. Liu, Mucin-controlled drug release from mucoadhesive phenylboronic acid-rich nanoparticles, Int. J. Pharm. 479 (2015) 261–264, https://doi.org/10.1016/j.ijpharm.2014.12.011.
[259] C.Y. Li, Z.G. Huang, Z.S. Liu, L.Q. Ci, Z.P. Liu, Y. Liu, X.Y. Yan, W.Y. Lu, Sulfonate-modified phenylboronic acid-rich nanoparticles as a novel mucoadhesive drug delivery system for vaginal administration of protein therapeutics: improved stability, mucin-dependent release and effective intravaginal placement, Int. J. Nanomed. 11 (2016) 5917–5930, https://doi.org/10.2147/IJN.S113658.
[260] J.W. Kong, Z. Lam, R. Ganguly, R.D. Webster, Z.X. Wong, W.K. Leong, K.H. Chan, L.-J.-Y. Joey, L.-H. Loo, L.-H. Loo, Group viii metal carbonyl cluster-boronic acid conjugates: Cytotoxicity and mode of action studies, ACS Omega 6 (2021) 29045–29053, https://doi.org/10.1021/acsomega.1c04116.
[261] H. Lage, An overview of cancer multidrug resistance: a still unsolved problem, Cell. Mol. Life Sci. 65 (20) (2008) 3145–3167, https://doi.org/10.1007/s00018-008-8111-5.
[262] H.R. Mellor, R. Callaghan, Resistance to chemotherapy in cancer: A complex and integrated cellular response, Pharmacology 81 (2008) 275–300, https://doi.org/10.1159/000115967.

[263] C. Holohan, S. Van Schaeybroeck, D.B. Longley, P.G. Johnston, Cancer drug resistance: an evolving paradigm, Nat. Rev. Cancer 13 (2013) 714–726, https://doi.org/10.1038/nrc3599.
[264] M. Kartal-Yandim, A. Adan-Gokbulut, Y. Baran, Molecular mechanisms of drug resistance and its reversal in cancer, Crit. Rev. Biotechnol. 36 (2016) 716–726, https://doi.org/10.3109/07388551.2015.1015957.
[265] M.S. Singh, S.N. Tammam, M.A. Shetab Boushehri, A. Lamprecht, MDR in cancer: Addressing the underlying cellular alterations with the use of nanocarriers, Pharmacol. Res. 126 (2017) 2–30, https://doi.org/10.1016/j.phrs.2017.07.023.
[266] K. Bukowski, M. Kciuk, R. Kontek, Mechanisms of multidrug resistance in cancer chemotherapy, Int. J. Mol. Sci. 21 (9) (2020) 3233, https://doi.org/10.3390/ijms21093233.
[267] Q. Sun, Z. Zhou, N. Qiu, Y. Shen, Rational design of cancer nanomedicine: Nanoproperty integration and synchronization, Adv. Mater. 29 (14) (2017) 1606628, https://doi.org/10.1002/adma.201606628.
[268] Y. Xu, Y. Lu, L. Wang, W. Lu, J. Huang, B. Muir, J. Yu, Nanomicelles based on a boronate ester-linked diblock copolymer as the carrier of doxorubicin with enhanced cellular uptake, Colloids Surf., B 141 (2016) 318–326, https://doi.org/10.1016/j.colsurfb.2016.01.044.
[269] L. Zhang, Y. Wang, X. Zhang, X. Wei, X. Xiong, S. Zhou, Enzyme and redox dual-triggered intracellular release from actively targeted polymeric micelles, ACS Appl. Mater. Interfaces 9 (2017) 3388–3399, https://doi.org/10.1021/acsami.6b14078.
[270] Y. Xu, Y. Huang, W. Lu, S. Liu, Y. Xiao, J. Yu, 4-Carboxyphenylboronic acid-decorated, redox-sensitive rod-shaped nano-micelles fabricated through co-assembling strategy for active targeting and synergistic co-delivery of camptothecin and gemcitabine, Eur. J. Pharm. Biopharm. 144 (2019) 193–206, https://doi.org/10.1016/j.ejpb.2019.09.019.
[271] Y. Huang, Y. He, X. Xia, H. Quan, J. Yu, Phenylboronic acid-functionalized co-delivery micelles with synergistic effect and down-regulation of HIF-1alpha to overcome multidrug resistance, J. Drug Delivery Sci. Technol. 62 (2021), 102346, https://doi.org/10.1016/j.jddst.2021.102346.
[272] Y. Huang, Y. Gao, T. Chen, Y. Xu, W. Lu, J. Yu, Y. Xiao, S. Liu, Reduction-triggered release of CPT from acid-degradable polymeric prodrug micelles bearing boronate ester bonds with enhanced cellular uptake, ACS Biomater. Sci. Eng. 3 (2017) 3364–3375, https://doi.org/10.1021/acsbiomaterials.7b00618.
[273] H.S. Choi, W. Liu, P. Misra, E. Tanaka, J.P. Zimmer, B. Itty Ipe, M.G. Bawendi, J. V. Frangioni, Renal clearance of quantum dots, Nat. Biotechnol. 25 (2007) 1165–1170, https://doi.org/10.1038/nbt1340.
[274] H. Maeda, Tumor-selective delivery of macromolecular drugs via the EPR effect: Background and future prospects, Bioconjugate Chem. 21 (2010) 797–802, https://doi.org/10.1021/bc100070g.
[275] V. Torchilin, Tumor delivery of macromolecular drugs based on the EPR effect, Adv. Drug Delivery Rev. 63 (2011) 131–135, https://doi.org/10.1016/j.addr.2010.03.011.
[276] H. Maeda, K. Tsukigawa, J. Fang, A retrospective 30 years after discovery of the enhanced permeability and retention effect of solid tumors: Next-generation chemotherapeutics and photodynamic therapy—problems, solutions, and prospects, Microcirculation 23 (2016) 173–182, https://doi.org/10.1111/micc.12228.
[277] M.A. Subhan, S.S. Yalamarty, N. Filipczak, F. Parveen, V.P. Torchilin, J. Pers. Med. (2021), https://doi.org/10.3390/jpm11060571.
[278] R. Sun, J. Xiang, Q. Zhou, Y. Piao, J. Tang, S. Shao, Z. Zhou, Y.H. Bae, Y. Shen, The tumor EPR effect for cancer drug delivery: current status, limitations, and alternatives, Adv. Drug Deliv. Rev. 191 (2022), 114614, https://doi.org/10.1016/j.addr.2022.114614.
[279] S.D. Perrault, C. Walkey, T. Jennings, H.C. Fischer, W.C. Chan, Mediating tumor targeting efficiency of nanoparticles through design, Nano Lett 9 (2009) 1909–1915, https://doi.org/10.1021/nl900031y.
[280] F.-X. Theillet, A. Binolfi, T. Frembgen-Kesner, K. Hingorani, M. Sarkar, C. Kyne, C. Li, P.B. Crowley, L. Gierasch, G.J. Pielak, A.H. Elcock, A. Gershenson, P. Selenko, Physicochemical properties of cells and their effects on intrinsically disordered proteins (IDPs), Chem. Rev. 114 (2014) 6661–6714, https://doi.org/10.1021/cr400695p.
[281] L. Ma, Q. Ouyang, G.C. Werthmann, H.M. Thompson, E.M. Morrow, Live-cell microscopy and fluorescence-based measurement of luminal pH in intracellular organelles, Front. Cell Dev. Biol. 5 (2017), https://doi.org/10.3389/fcell.2017.00071.
[282] K.A. White, B.K. Grillo-Hill, D.L. Barber, Cancer cell behaviors mediated by dysregulated pH dynamics at a glance, J. Cell Sci. 130 (2017) 663–669, https://doi.org/10.1242/jcs.195297.
[283] M. Constantin, S. Bucatariu, I. Popescu, B. Cosman, P. Ascenzi, G. Fundueanu, Intelligent micro-vehicles for drug transport and controlled release to cancer cells, React. Funct. Polym. 165 (2021), 104961, https://doi.org/10.1016/j.reactfunctpolym.2021.104961.
[284] J.R. Casey, S. Grinstein, J. Orlowski, Sensors and regulators of intracellular pH, Nat. Rev. Mol. Cell Biol. 11 (2010) 50–61, https://doi.org/10.1038/nrm2820.
[285] C. Qian, Y. Chen, S. Zhu, J. Yu, L. Zhang, P. Feng, X. Tang, Q. Hu, W. Sun, Y. Lu, X. Xiao, Q.-D. Shen, Z. Gu, ATP-responsive and near-infrared-emissive nanocarriers for anticancer drug delivery and real-time imaging, Theranostics 6 (2016) 1053–1064, https://doi.org/10.7150/thno.14843.
[286] J. Wang, Y. Bi, H. Ruan, G. Sun, X. Cui, X. Yang, C. Qin, Hollow S-nitrosothiols nanoparticle with polymeric brushes for nitric oxide (NO)-releasing as tumor targeted chemotherapy, J. Biomater. Sci., Polym. Ed. 30 (2019) 122–136, https://doi.org/10.1080/09205063.2018.1556852.
[287] J. Lee, J. Kim, Y.M. Lee, D. Park, S. Im, E.H. Song, H. Park, W.J. Kim, Self-assembled nanocomplex between polymerized phenylboronic acid and doxorubicin for efficient tumor-targeted chemotherapy, Acta Pharmacol. Sin. 38 (2017) 848–858, https://doi.org/10.1038/aps.2017.16.
[288] Q. Sun, X. Sun, X. Ma, Z. Zhou, E. Jin, B. Zhang, Y. Shen, E.A. Van Kirk, W. J. Murdoch, J.R. Lott, T.P. Lodge, M. Radosz, Y. Zhao, Integration of nanoassembly functions for an effective delivery cascade for cancer drugs, Adv. Mater. 26 (2014) 7615–7621, https://doi.org/10.1002/adma.201401554.
[289] H. Cabral, Y. Matsumoto, K. Mizuno, Q. Chen, M. Murakami, M. Kimura, Y. Terada, M.R. Kano, K. Miyazono, M. Uesaka, N. Nishiyama, K. Kataoka, Accumulation of sub-100 nm polymeric micelles in poorly permeable tumours depends on size, Nat. Nanotechnol. 6 (2011) 815–823, https://doi.org/10.1038/nnano.2011.166.
[290] T. Miyazaki, T. Khan, Y. Tachihara, M. Itoh, T. Miyazawa, T. Suganami, Y. Miyahara, H. Cabral, A. Matsumoto, Boronic acid ligands can target multiple subpopulations of pancreatic cancer stem cells via pH-dependent glycan-terminal sialic acid recognition, ACS Appl. Bio Mater. 4 (9) (2021) 6647–6651, https://doi.org/10.1021/acsabm.1c00383.
[291] S. Liu, J. Pan, J. Liu, Y. Ma, F. Qiu, L. Mei, X. Zeng, G. Pan, Dynamically PEGylated and borate-coordination-polymer-coated polydopamine nanoparticles for synergetic tumor-targeted, chemo-photothermal combination therapy, Small 14 (2018) 1703968, https://doi.org/10.1002/smll.201703968.
[292] D. Wu, X. Shi, F. Zhao, S.T.F. Chilengue, L. Deng, A. Dong, D. Kong, W. Wang, J. Zhang, An injectable and tumor-specific responsive hydrogel with tissue-adhesive and nanomedicine-releasing abilities for precise locoregional chemotherapy, Acta Biomater. 96 (2019) 123–136, https://doi.org/10.1016/j.actbio.2019.06.033.
[293] J. Xu, T. Hu, M. Zhang, P. Feng, X. Wang, X. Cheng, R. Tang, A sequentially responsive nanogel via Pt(IV) crosslinking for overcoming GSH-mediated platinum resistance, J. Colloid Interface Sci. 601 (2021) 85–97, https://doi.org/10.1016/j.jcis.2021.05.107.
[294] D. Zhao, J.-Q. Xu, X.-Q. Yi, Q. Zhang, S.-X. Cheng, R.-X. Zhuo, F. Li, pH-activated targeting drug delivery system based on the selective binding of phenylboronic acid, ACS Appl. Mater. Interfaces 8 (2016) 14845–14854, https://doi.org/10.1021/acsami.6b04737.
[295] Y. Long, Z. Lu, L. Mei, M. Li, K. Ren, X. Wang, J. Tang, Z. Zhang, Q. He, Enhanced melanoma-targeted therapy by "Fru-blocked" phenyboronic acid-modified multiphase antimetastatic micellar nanoparticles, Adv. Sci. 5 (2018) 1800229, https://doi.org/10.1002/advs.201800229.
[296] H. Lu, Y. Xu, R. Qiao, Z. Lu, P. Wang, X. Zhang, A. Chen, L. Zou, Z. Wang, A novel clustered SPIO nanoplatform with enhanced magnetic resonance T2 relaxation rate for micro-tumor detection and photothermal synergistic therapy, Nano Res. 13 (2020) 2216–2225, https://doi.org/10.1007/s12274-020-2839-0.
[297] A. Lopalco, R.M. Iacobazzi, N. Denora, V.J. Stella, Bortezomib aqueous solubility in the presence and absence of d-mannitol: A clarification with formulation implications, J. Pharm. Sci. 110 (2021) 543–547, https://doi.org/10.1016/j.xphs.2020.10.012.
[298] M. Liu, X. Tang, J. Ding, M. Liu, B. Zhao, Y. Deng, Y. Song, A sialylated-bortezomib prodrug strategy based on a highly expressed selectin target for the treatment of leukemia or solid tumors, Pharm. Res. 36 (2019) 176, https://doi.org/10.1007/s11095-019-2714-4.
[299] D. Zhong, H. Wu, Y. Wu, Y. Li, J. Yang, Q. Gong, K. Luo, Z. Gu, Redox dual-responsive dendrimeric nanoparticles for mutually synergistic chemo-photodynamic therapy to overcome drug resistance, J. Controlled Release 329 (2021) 1210–1221, https://doi.org/10.1016/j.jconrel.2020.10.048.
[300] J. Cao, X. Gao, M. Cheng, X. Niu, X. Li, Y. Zhang, Y. Liu, W. Wang, Z. Yuan, Reversible shielding between dual ligands for enhanced tumor accumulation of ZnPc-loaded micelles, Nano Lett. 19 (2019) 1665–1674, https://doi.org/10.1021/acs.nanolett.8b04645.
[301] Y. Hao, C. Zheng, L. Wang, Y. Hu, H. Guo, Q. Song, H. Zhang, Z. Zhang, Y. Zhang, Covalent self-assembled nanoparticles with pH-dependent enhanced tumor retention and drug release for improving tumor therapeutic efficiency, J. Mater. Chem. B 5 (2017) 2133–2144, https://doi.org/10.1039/C6TB02833K.
[302] H. Cheng, H. Zhang, G. Xu, J. Peng, Z. Wang, B. Sun, D. Aouameur, Z. Fan, W. Jiang, J. Zhou, Y. Ding, A combinative assembly strategy inspired reversibly borate-bridged polymeric micelles for lesion-specific rapid release of anti-coccidial drugs, Nano-Micro Lett. 12 (2020) 155, https://doi.org/10.1007/s40820-020-00495-1.
[303] L. Fang, Z. Zhao, J. Wang, P. Zhang, Y. Ding, Y. Jiang, D. Wang, Y. Li, Engineering autologous tumor cell vaccine to locally mobilize antitumor immunity in tumor surgical bed, Sci. Adv. 6 (25) (2020) eaba4024, https://doi.org/10.1126/sciadv.aba4024.
[304] B. Fan, L. Kang, L. Chen, P. Sun, M. Jin, Q. Wang, Y.H. Bae, W. Huang, Z. Gao, Systemic siRNA delivery with a dual pH-responsive and tumor-targeted nanovector for inhibiting tumor growth and spontaneous metastasis in orthotopic murine model of breast carcinoma, Theranostics 7 (2017) 357–376, https://doi.org/10.7150/thno.16855.
[305] M. Ji, P. Li, N. Sheng, L. Liu, H. Pan, C. Wang, L. Cai, Y. Ma, Sialic acid-targeted nanovectors with phenylboronic acid-grafted polyethylenimine robustly enhance sirna-based cancer therapy, ACS Appl. Mater. Interfaces 8 (2016) 9565–9576, https://doi.org/10.1021/acsami.5b11866.
[306] X. Tang, Q. Sheng, C. Xu, M. Li, J. Rao, X. Wang, Y. Long, Y. Tao, X. He, Z. Zhang, Q. He, pH/ATP cascade-responsive nano-courier with efficient tumor targeting and siRNA unloading for photothermal-immunotherapy, Nano Today 37 (2021), 101083, https://doi.org/10.1016/j.nantod.2021.101083.

[307] D. Wu, J. Yang, Z. Xing, H. Han, T. Wang, A. Zhang, Y. Yang, Q. Li, Phenylboronic acid-functionalized polyamidoamine-mediated Bcl-2 siRNA delivery for inhibiting the cell proliferation, Colloids Surf., B 146 (2016) 318–325, https://doi.org/10.1016/j.colsurfb.2016.06.034.

[308] Q. Tang, J. Liu, Y. Jiang, M. Zhang, L. Mao, M. Wang, Cell-selective messenger RNA delivery and CRISPR/Cas9 genome editing by modulating the interface of phenylboronic acid-derived lipid nanoparticles and cellular surface sialic acid, ACS Appl. Mater. Interfaces 11 (2019) 46585–46590, https://doi.org/10.1021/acsami.9b17749.

[309] M. Naito, T. Ishii, A. Matsumoto, K. Miyata, Y. Miyahara, K. Kataoka, A phenylboronate-functionalized polyion complex micelle for ATP-triggered release of siRNA, Angew. Chem. Int. Ed. 51 (2012) 10751–10755, https://doi.org/10.1002/anie.201203360.

[310] J. Wang, W. Wu, X. Jiang, Nanoscaled boron-containing delivery systems and therapeutic agents for cancer treatment, Nanomedicine 10 (2015) 1149–1163, https://doi.org/10.2217/nnm.14.213.

[311] A. Kim, M. Suzuki, Y. Matsumoto, N. Fukumitsu, Y. Nagasaki, Non-isotope enriched phenylboronic acid-decorated dual-functional nano-assembles for an actively targeting BNCT drug, Biomaterials 268 (2021), 120551, https://doi.org/10.1016/j.biomaterials.2020.120551.

[312] K. Takahashi, H. Nakamura, S. Furumoto, K. Yamamoto, H. Fukuda, A. Matsumura, Y. Yamamoto, Synthesis and in vivo biodistribution of BPA–Gd–DTPA complex as a potential MRI contrast carrier for neutron capture therapy, Bioorg. Med. Chem. 13 (2005) 735–743, https://doi.org/10.1016/j.bmc.2004.10.046.

[313] M. Liu, J. Zhang, X. Li, C. Cai, X. Cao, X. Shi, R. Guo, A polydopamine-coated LAPONITE-stabilized iron oxide nanoplatform for targeted multimodal imaging-guided photothermal cancer therapy, J. Mater. Chem. B 7 (2019) 3856–3864, https://doi.org/10.1039/c9tb00398c.

[314] Y. Cao, S. Han, H. Zhang, J. Wang, Q.-Y. Jiang, Y. Zhou, Y.-J. Yu, J. Wang, F. Chen, D.K.P. Ng, Detection of cell-surface sialic acids and photodynamic eradication of cancer cells using dye-modified polydopamine-coated gold nanobipyramids, J. Mater. Chem. B 9 (29) (2021) 5780–5784, https://doi.org/10.1039/d1tb01274f.

[315] X. Sun, Y. Cai, Z. Xu, D. Zhu, Preparation and properties of tumor-targeting MRI contrast agent based on linear polylysine derivatives, Molecules 24 (2019) 1477, https://doi.org/10.3390/molecules24081477.

[316] T. Li, Y. Liu, Self-assembled nanorods of phenylboronic acid functionalized pyrene for in situ two-photon imaging of cell surface sialic acids and photodynamic therapy, Anal. Chem. 93 (2021) 7029–7036, https://doi.org/10.1021/acs.analchem.1c00118.